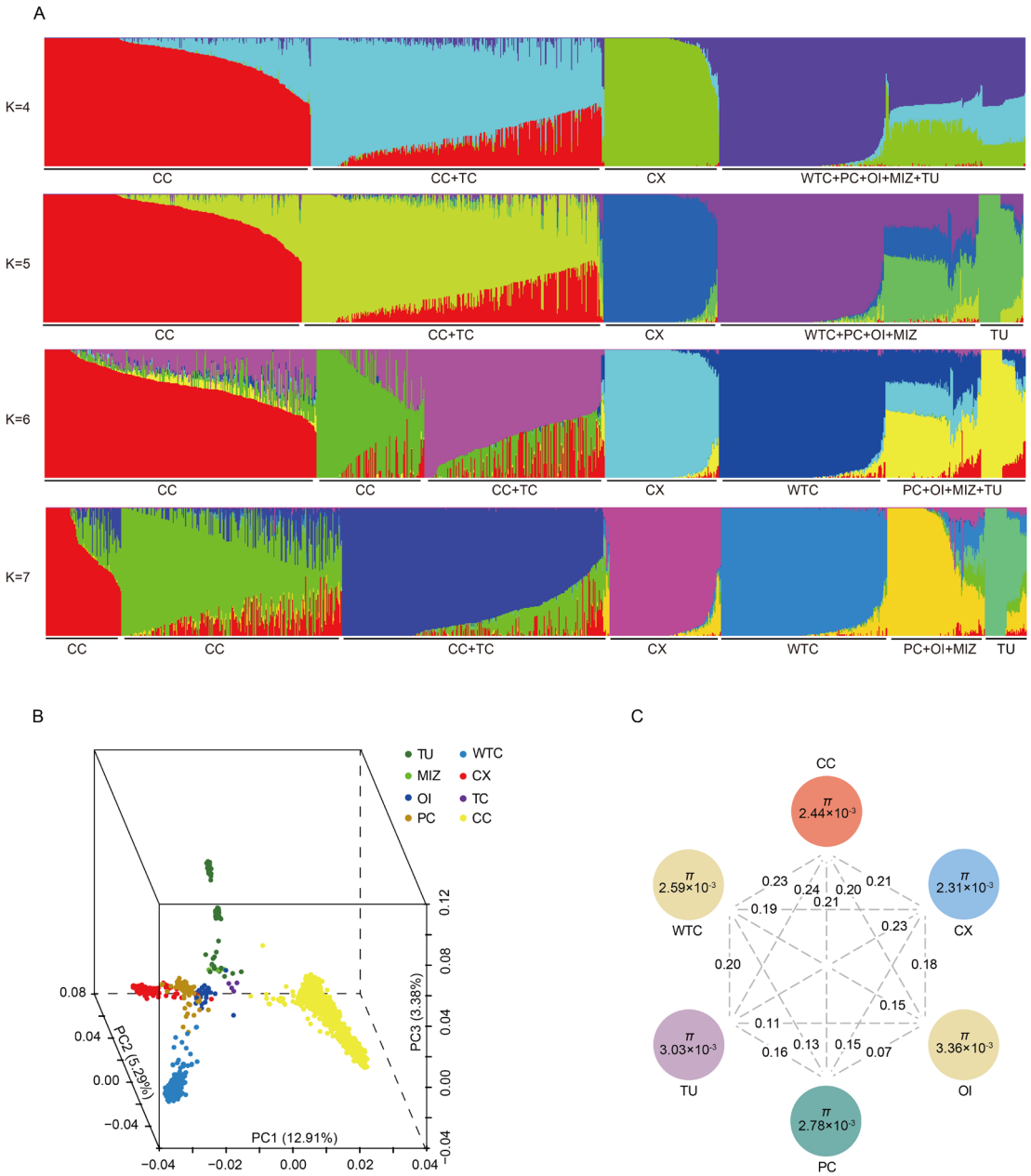

fig. S1. Population structure and genomic diversity of 1,720 *B. rapa* accessions based on SNPs.

(**A**) Structure of 1,720 *B. rapa* accessions based on SNPs. Bar-plots showing the inferred ancestral components at K = 4 to 7. Each vertical bar represents a group of accessions. Colored segments within each bar indicate the proportional contributions from different ancestral population clusters. (**B**) Three-dimensional PCA of *B. rapa* accessions based on SNPs. Each dot represents a group colored by morphotypes, including Turnip (TU), Mizuna (MIZ), Oilseed (OI), Pak choi (PC), Wutacai (WTC), Caixin (CX), Taicai (TC), and Chinese cabbage (CC). PC1, PC2, and PC3 show 12.91%, 5.29%, and 3.38% of the total genetic variation, respectively. (**C**) Nucleotide diversity (π) and population divergence (F_{ST}) across the six morphotypes (accession number >20). The value in each circle represents a measure of π for each morphotype and values on each line indicate F_{ST} between two morphotypes.

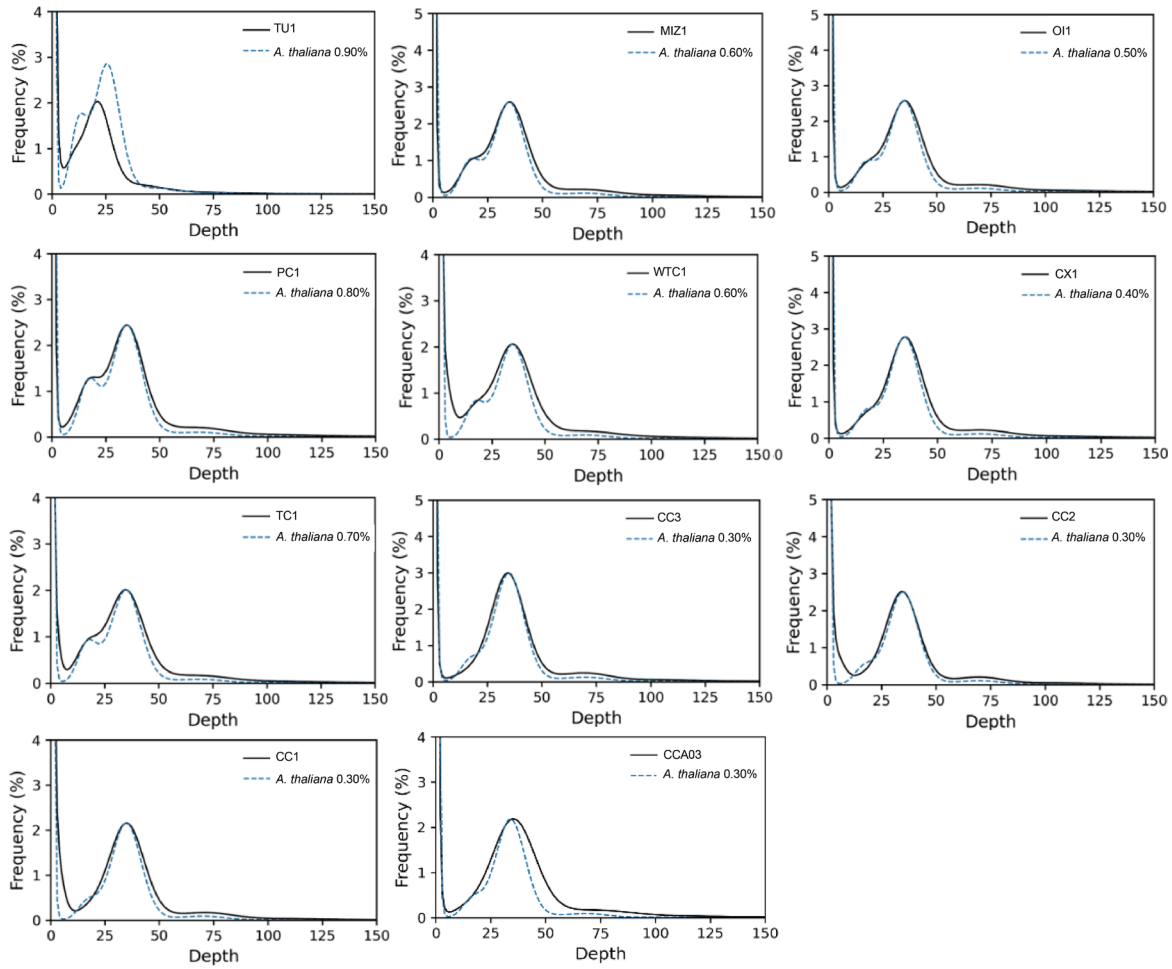

fig. S2. K-mer depth-frequence distribution in 11 *B. rapa* genomes.

Each graph represents one of 11 gapless genome assemblies, including Turnip (TU1), Mizuna (MIZ1), Oilseed (OI1), Pak choi (PC1), Wutacai (WTC1), Caixin (CX1), Taicai (TC1) and Chinese cabbage (CC1, CC2, CC3, CCA03). X- and Y-axis show k-mer (k=21) depth and k-mer frequency, respectively. Heterozygosity values below 0.3% were set to 0.3%.

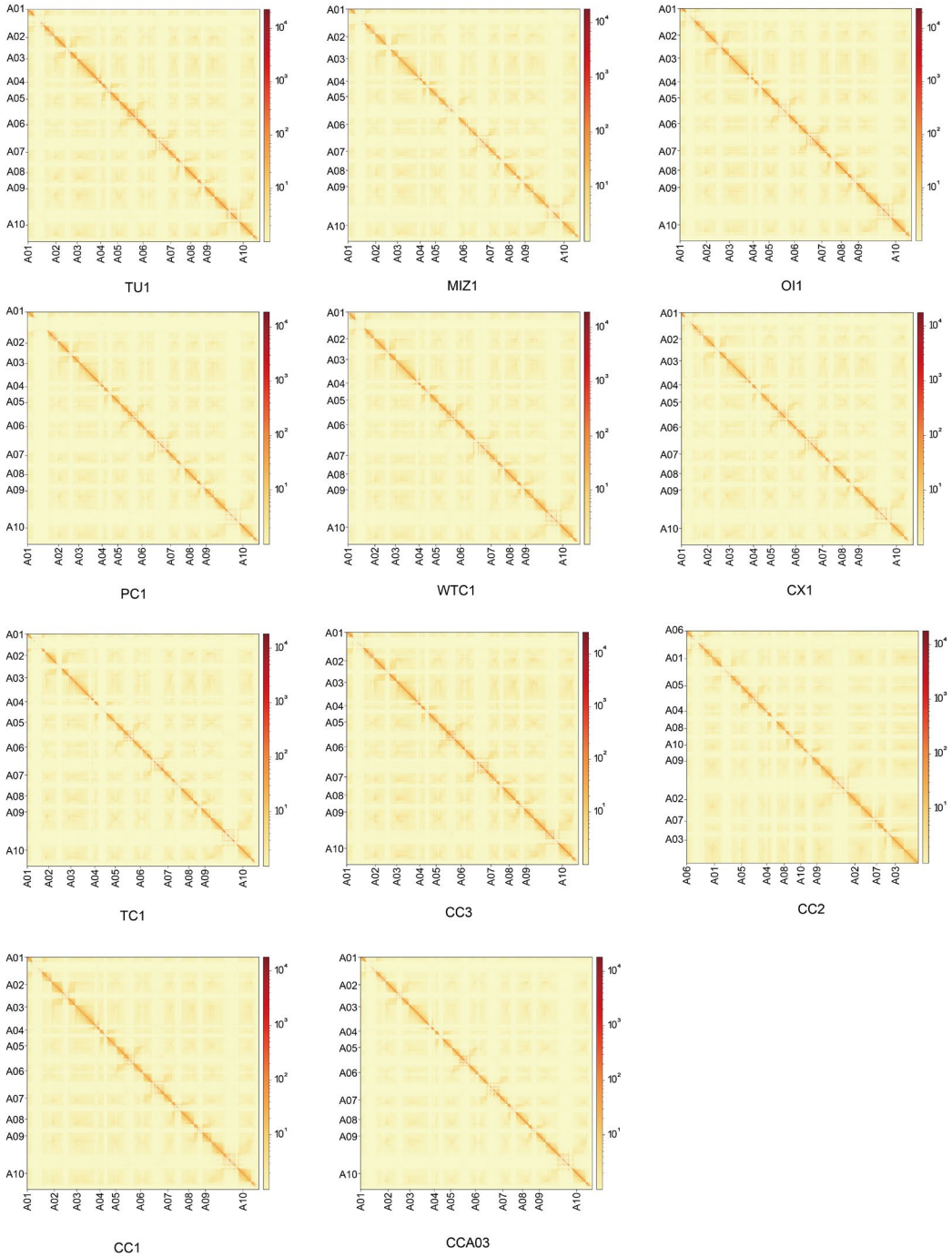

fig. S3. Interaction heatmap of 11 *B. rapa* genomes at 100-kb resolution based on Hi-C analysis.

The heatmaps visualize the Hi-C contact matrices at a resolution of 100-kb window, providing a comprehensive overview of the chromatin interactions across the genomes. Within each accession, interactions along the diagonal exhibit higher intensity compared to off-diagonal positions, indicating that in the Hi-C assembled chromosomes, proximal sequences (diagonal positions) have stronger interaction frequencies while distal sequences (off-diagonal positions) display weaker interaction signals. The level of Hi-C interaction strength is indicated by the color scale. This observation aligns with the principles of Hi-

C-assisted genome assembly. The absence of significant noise (strong interaction intensities) outside the diagonal regions further substantiates the high quality of the genome assembly. Each graph represents one of 11 assemblies, including Turnip (TU1), Mizuna (MIZ1), Oilseed (OI1), Pak choi (PC1), Wutacai (WTC1), Caixin (CX1), Taicai (TC1) and Chinese cabbage (CC1, CC2, CC3, CCA03).

A Comprehensive map on chromosomes A01-A10 of TU1

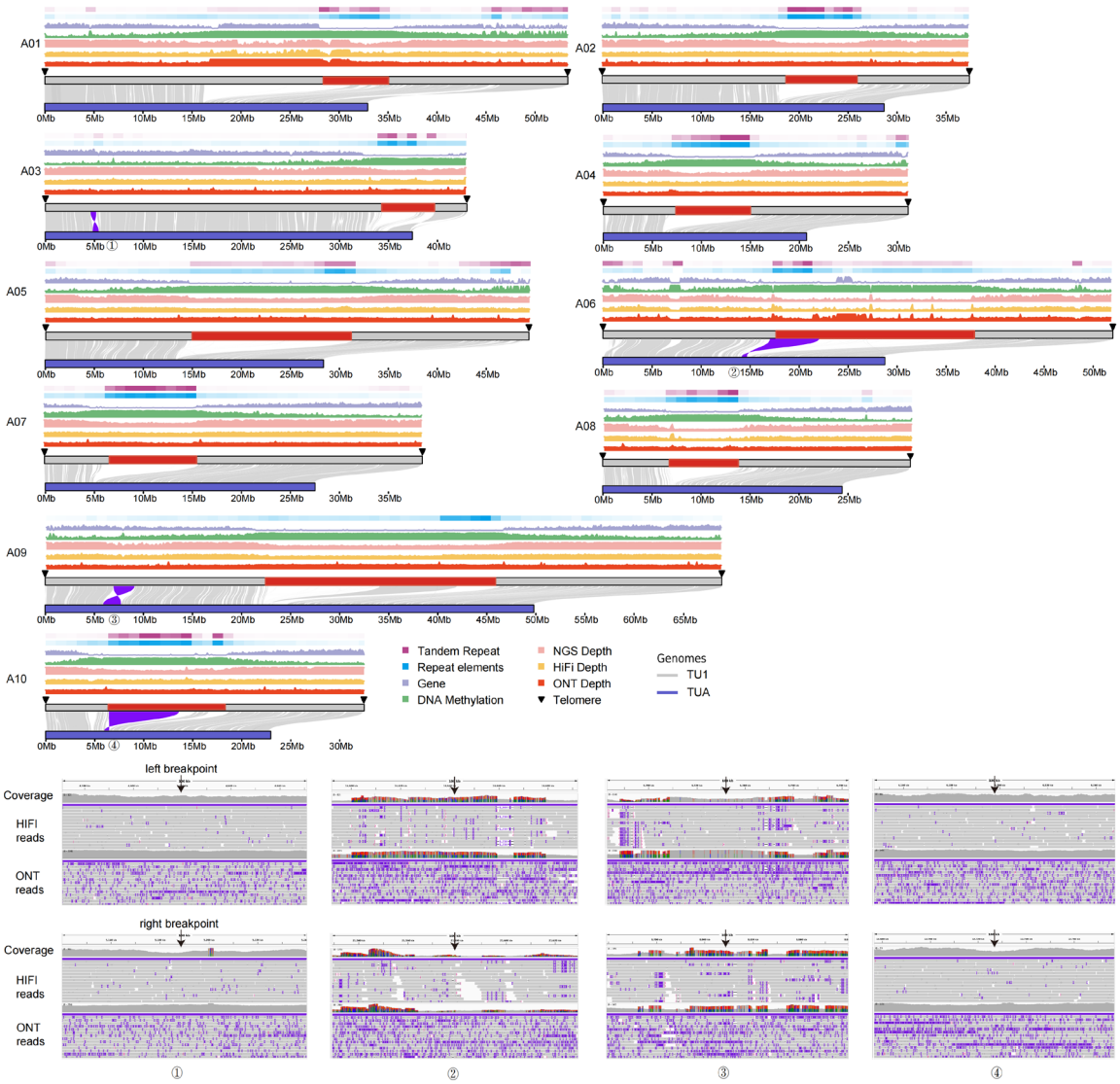

B Comprehensive map on chromosomes A01-A10 of MIZ1

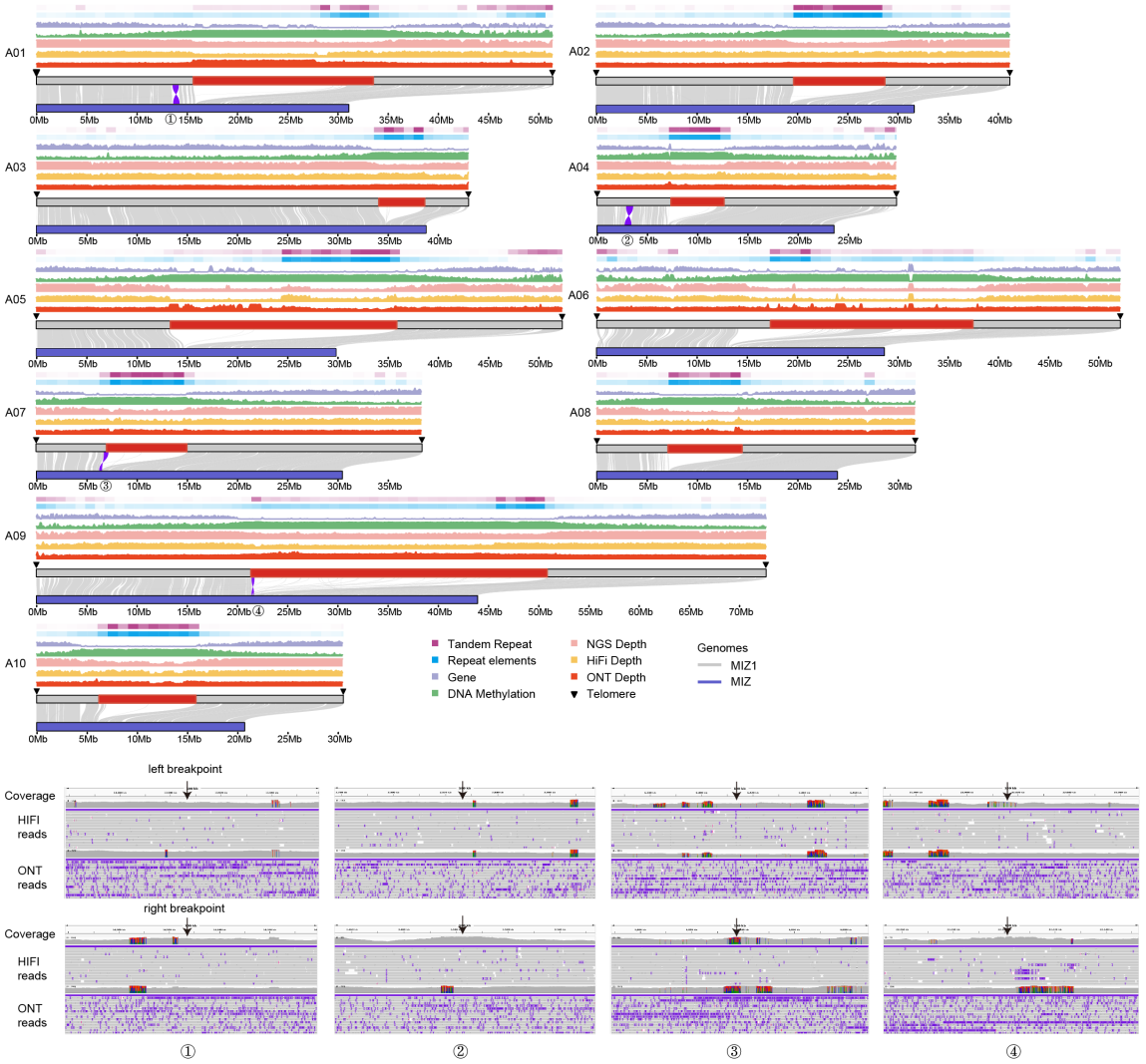

C Comprehensive map on chromosomes A01-A10 of OI1

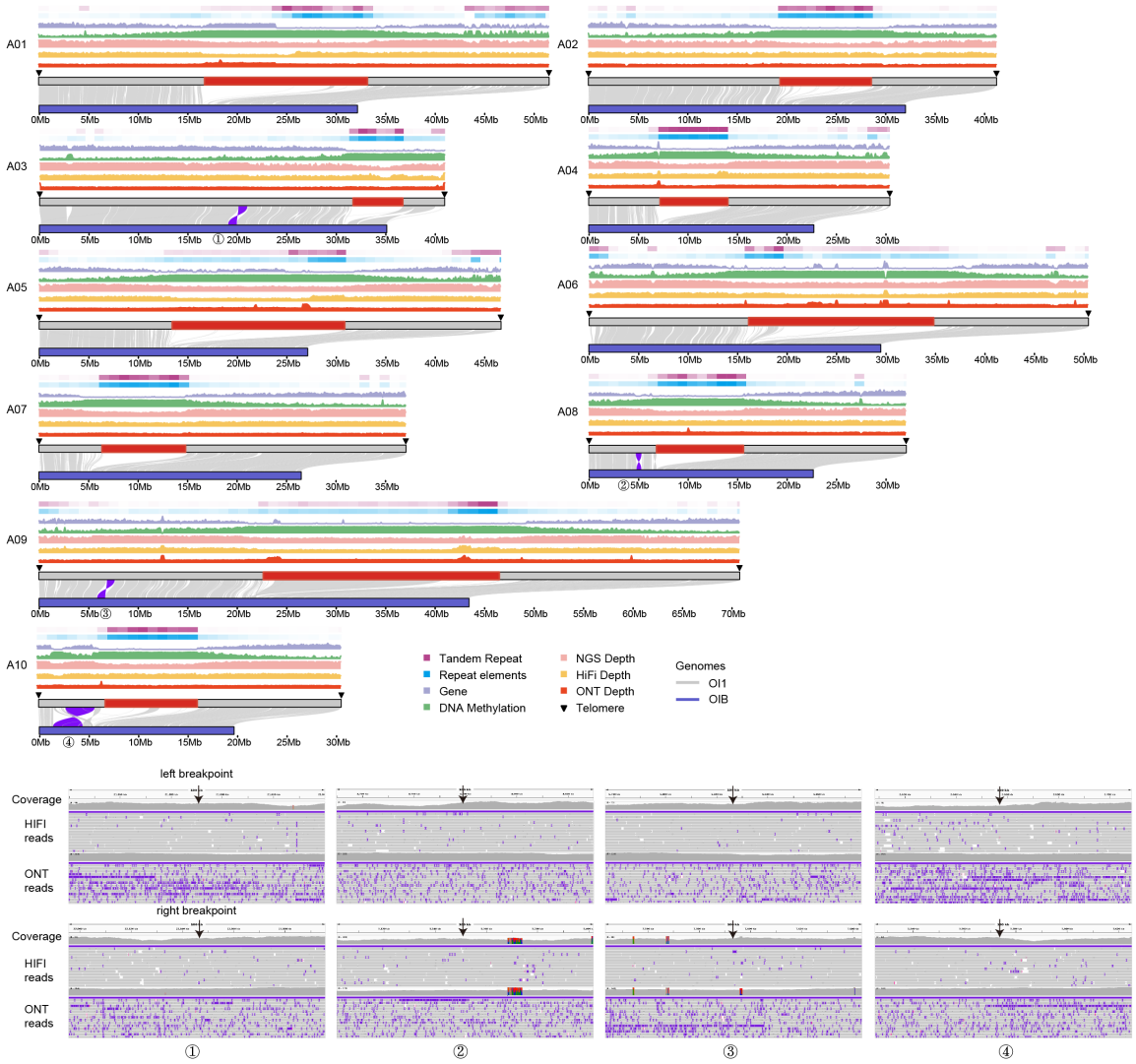

D Comprehensive map on chromosomes A01-A10 of PC1

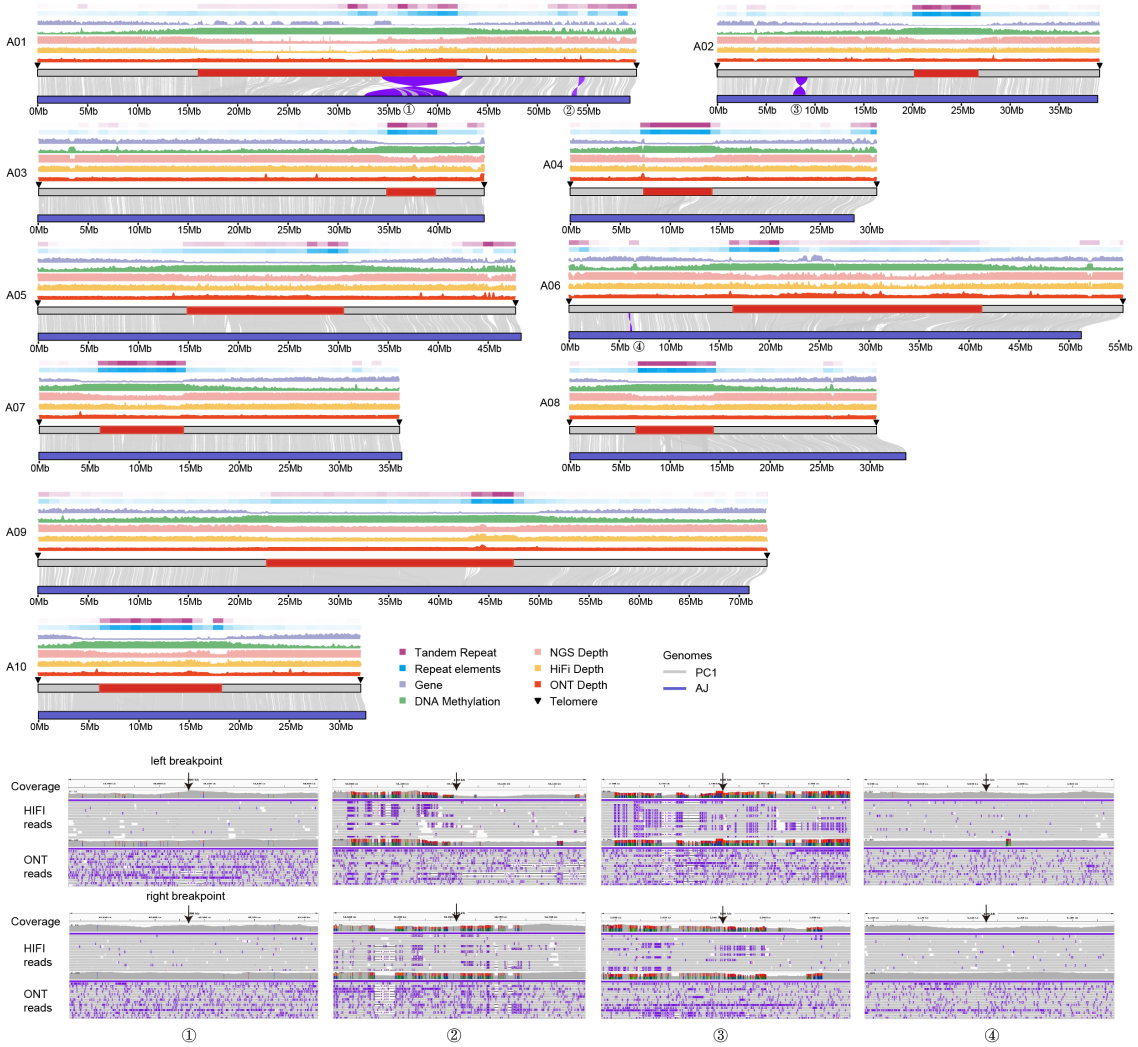

E Comprehensive map on chromosomes A01-A10 of WTC1

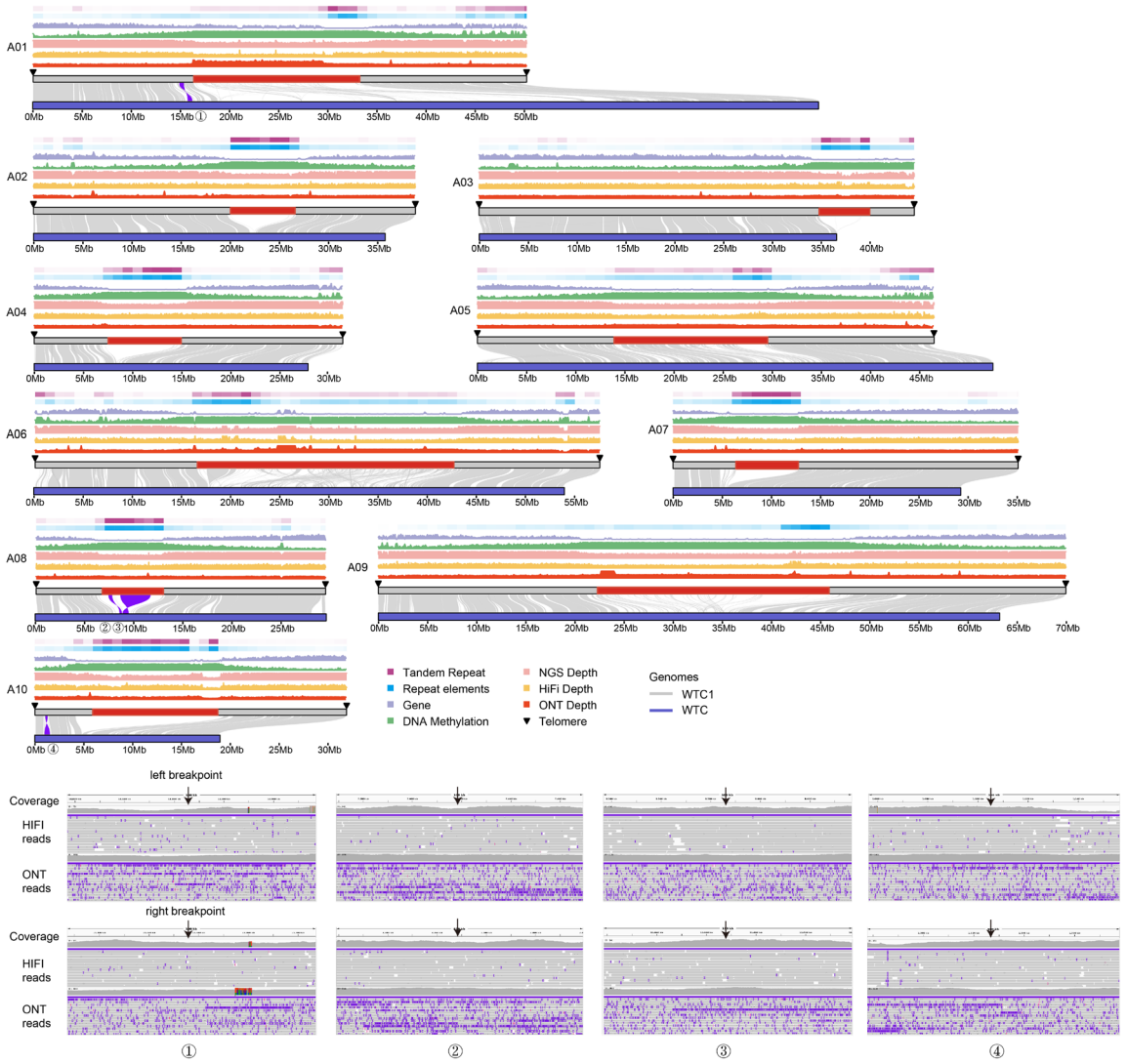

F Comprehensive map on chromosomes A01-A10 of CX1

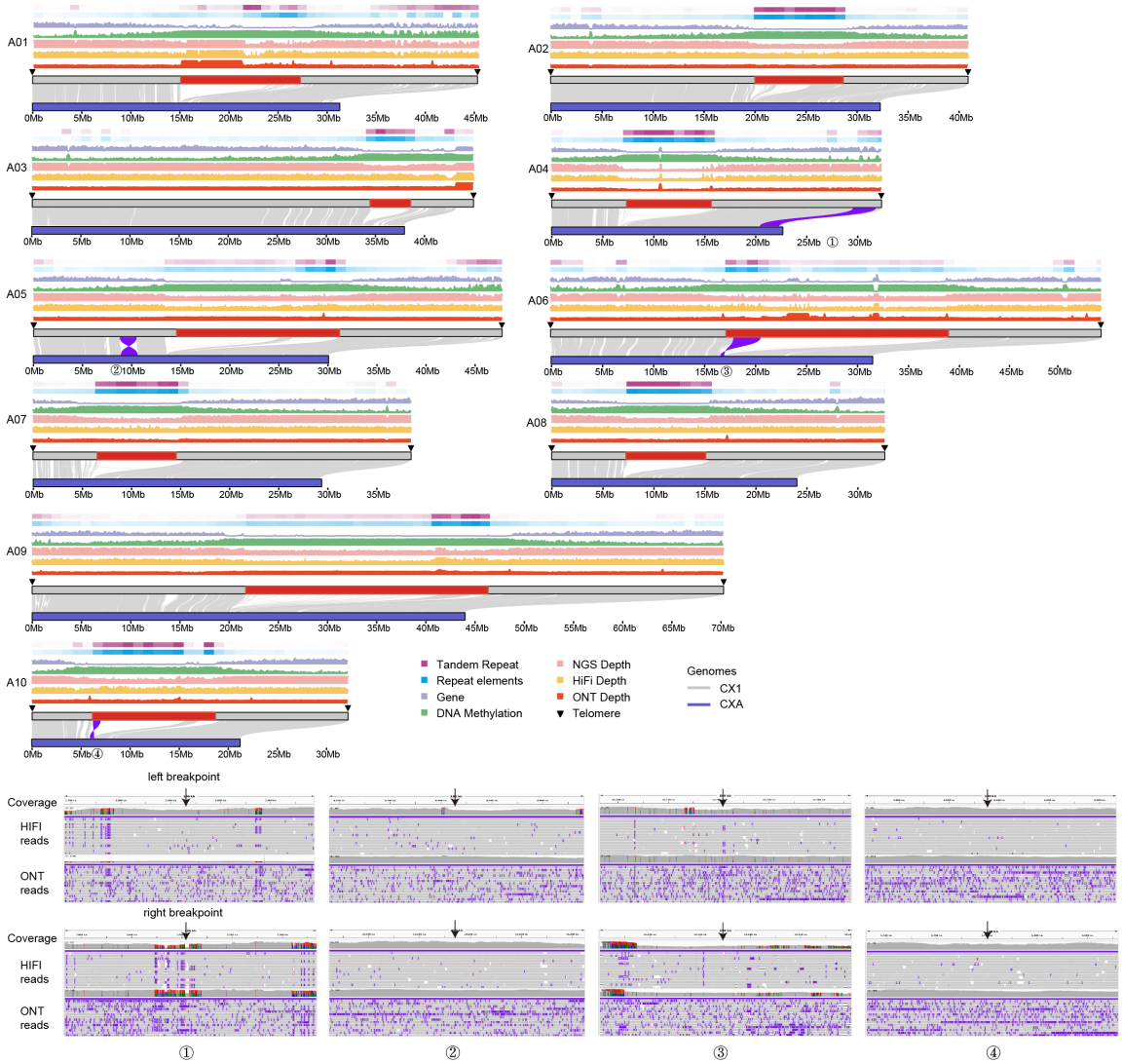

G Comprehensive map on chromosomes A01-A10 of TC1

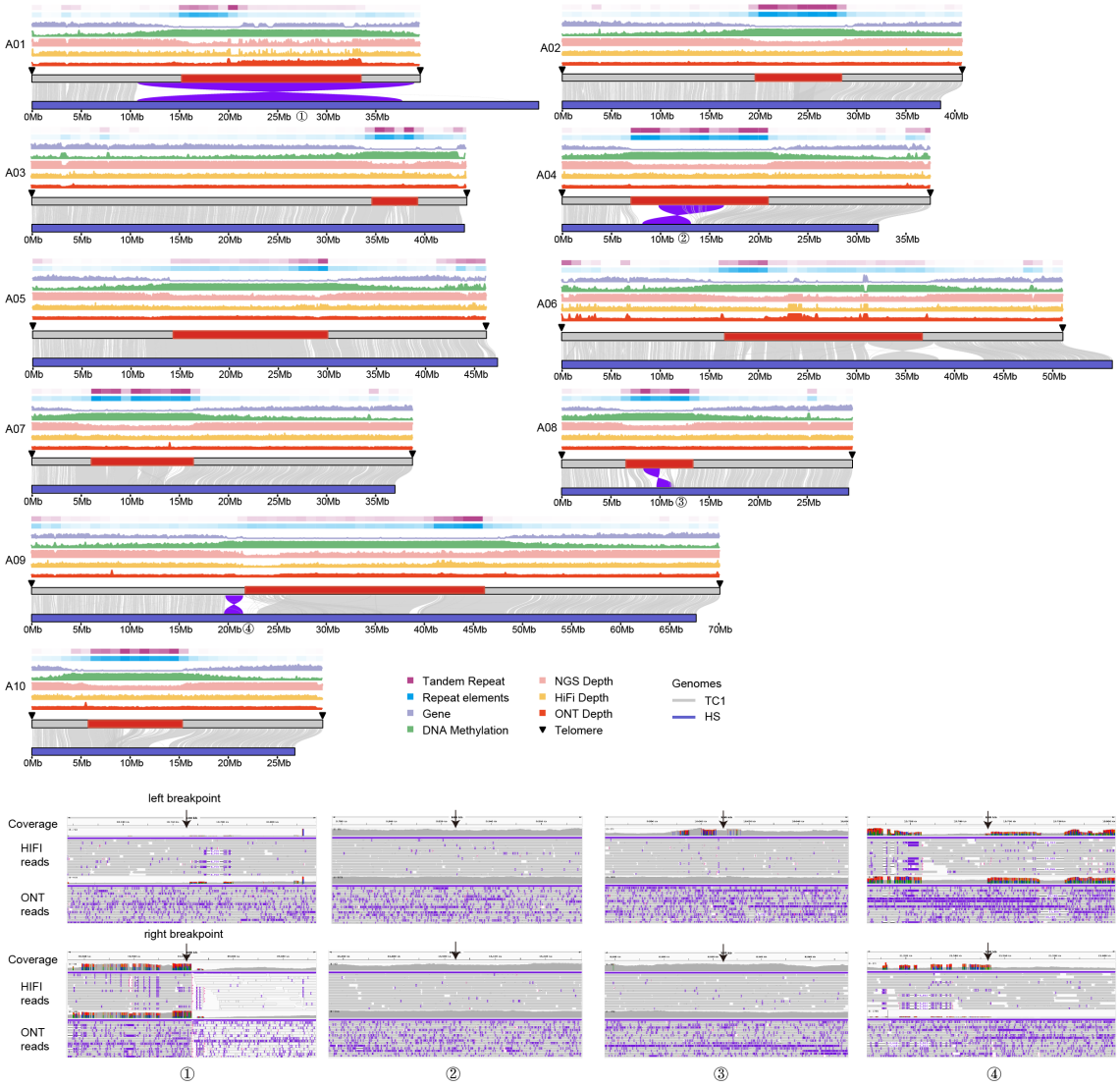

H Comprehensive map on chromosomes A01-A10 of CC3

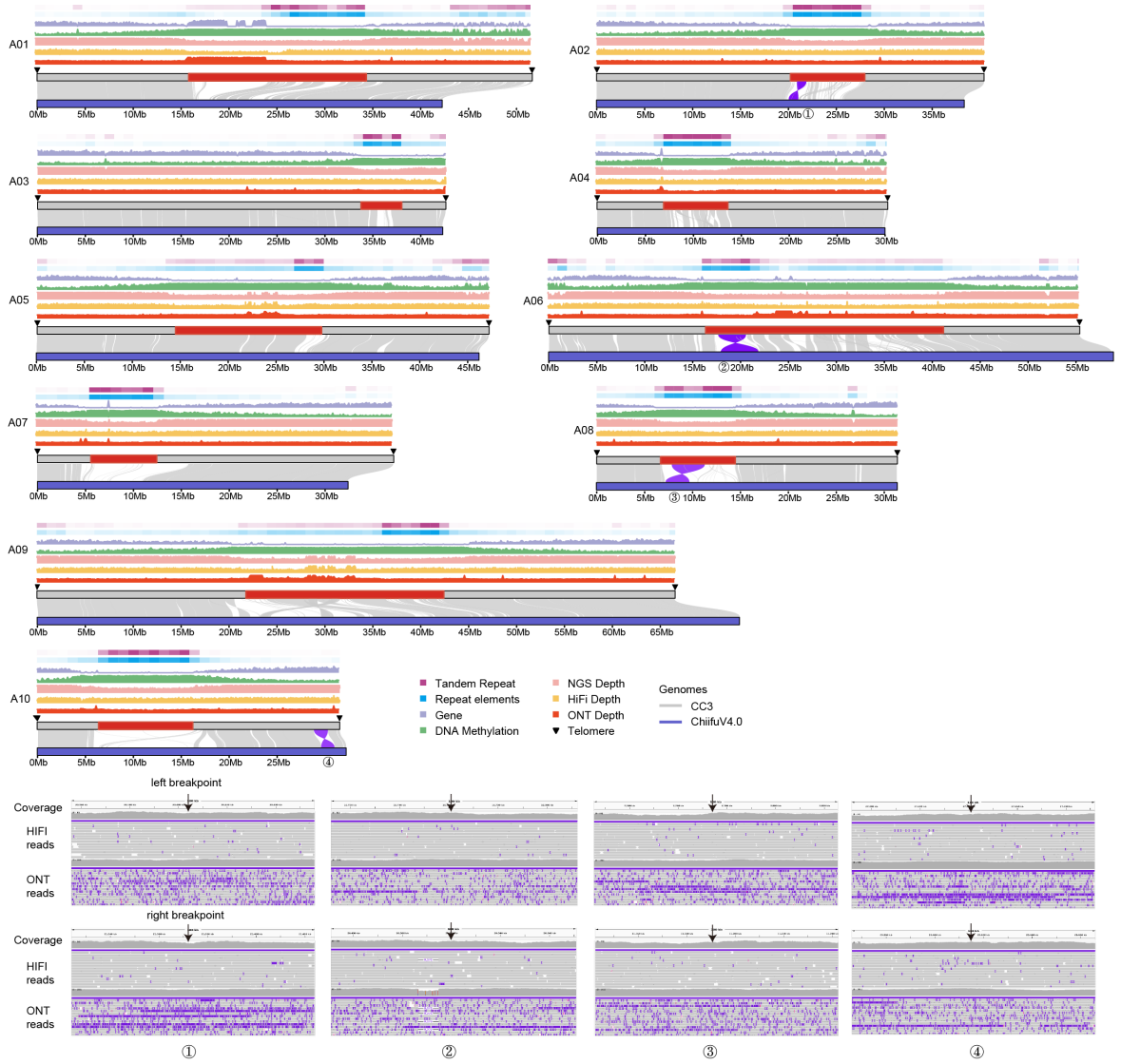

I Comprehensive map on chromosomes A01-A10 of CC2

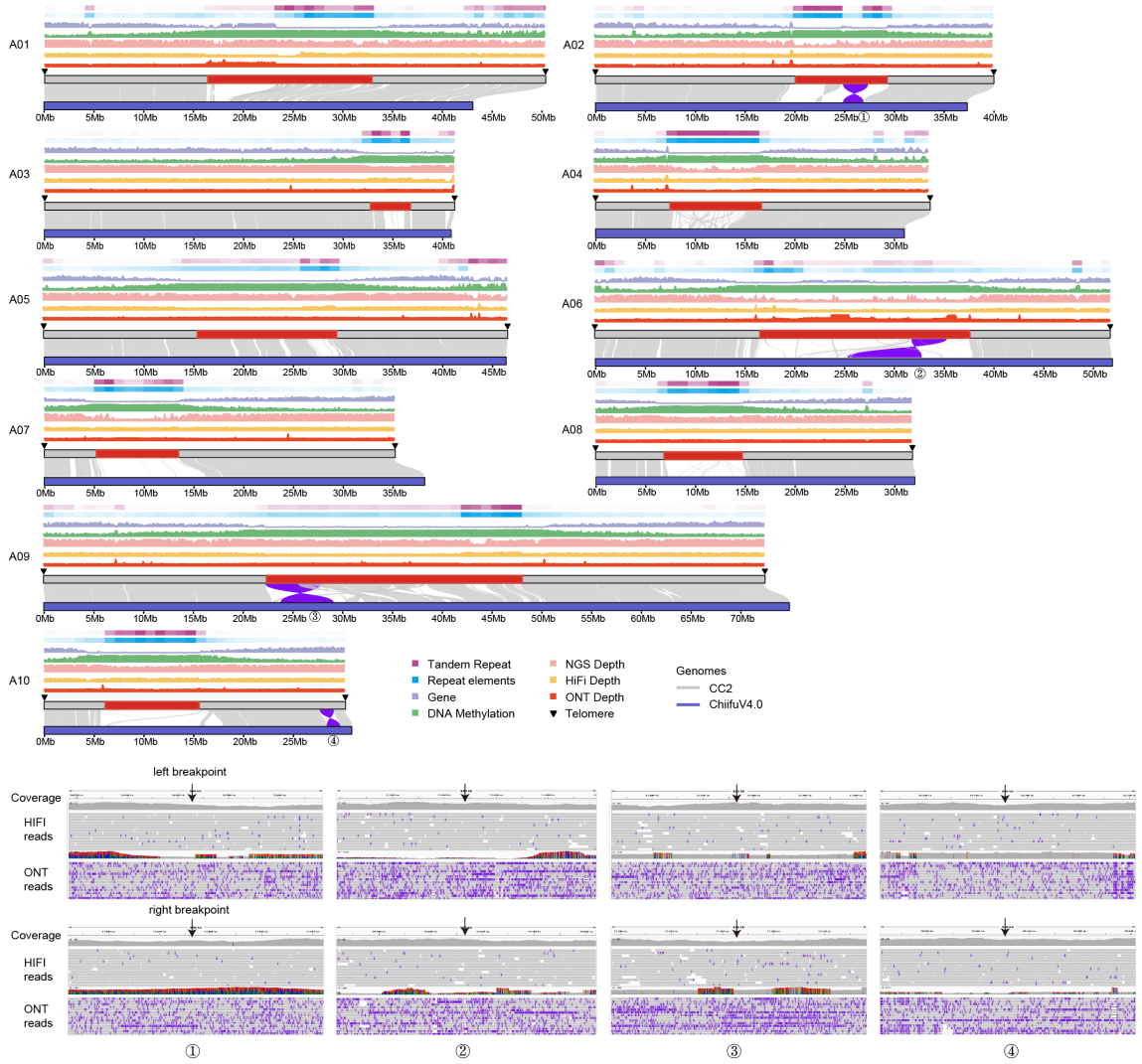

J Comprehensive map on chromosomes A01-A10 of CC1

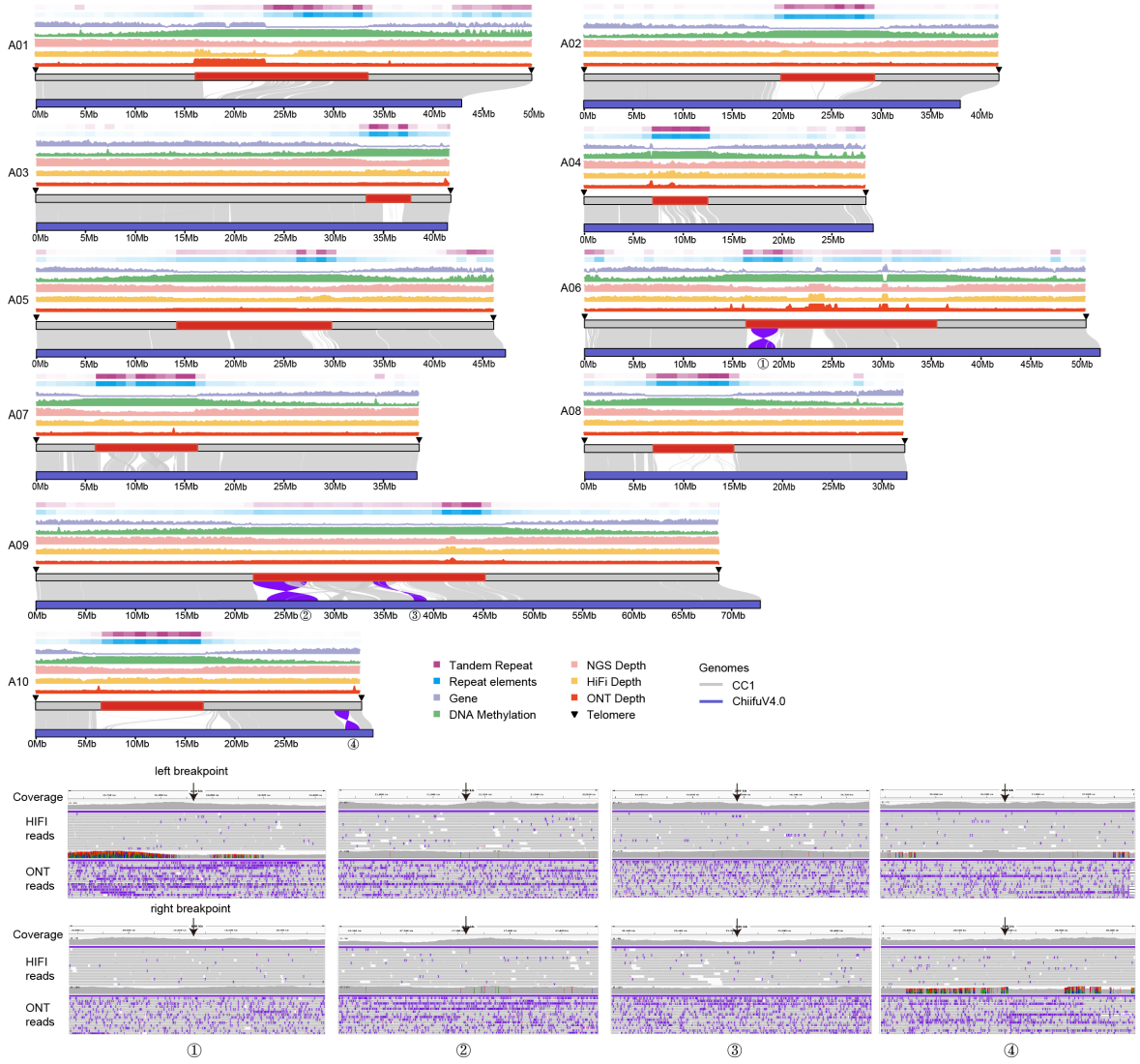

K Comprehensive map on chromosomes A01-A10 of CCA03

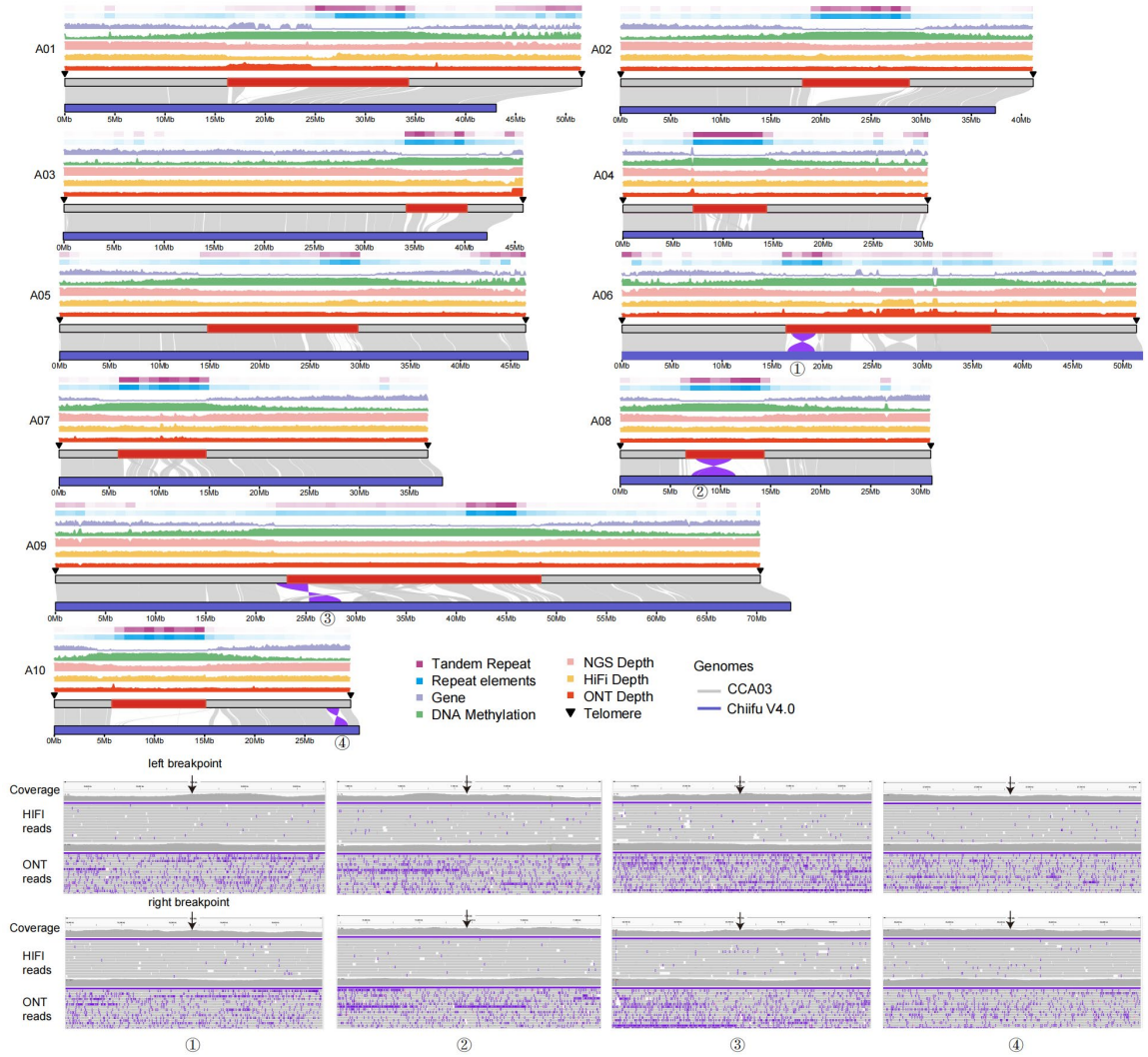

fig. S4. Comprehensive map on chromosomes of 11 *B. rapa* genomes.
(**A**-**K**) Genome-wide distribution of Tandem Repeats Density, Repeat elements Density, Gene Density, DNA Methylation Density, NGS Depth, HiFi Depth, ONT Depth, Telomere (solid triangle) from top to bottom in chromosomes A01-A10 of each accession as indicated. The gray regions in each of the chromosome map shows the syntenic alignment between CCA03 and the latest Chinese cabbage reference genome Chiifu V4.0. The two IGV graphs in panels A-K show manual validation of four large inversions marked ① to ④ on relevant chromosome(s), based on mapping the ONT reads and HIFI reads to the CCA03 genome assembly. Accessions include TU1 (**A**), MIZ1 (**B**), OI1 (**C**), PC1 (**D**), WTC1 (**E**), CX1 (**F**), TC1 (**G**), CC3 (**H**), CC2 (**I**), CC1 (**J**), and CCA03 (**K**).

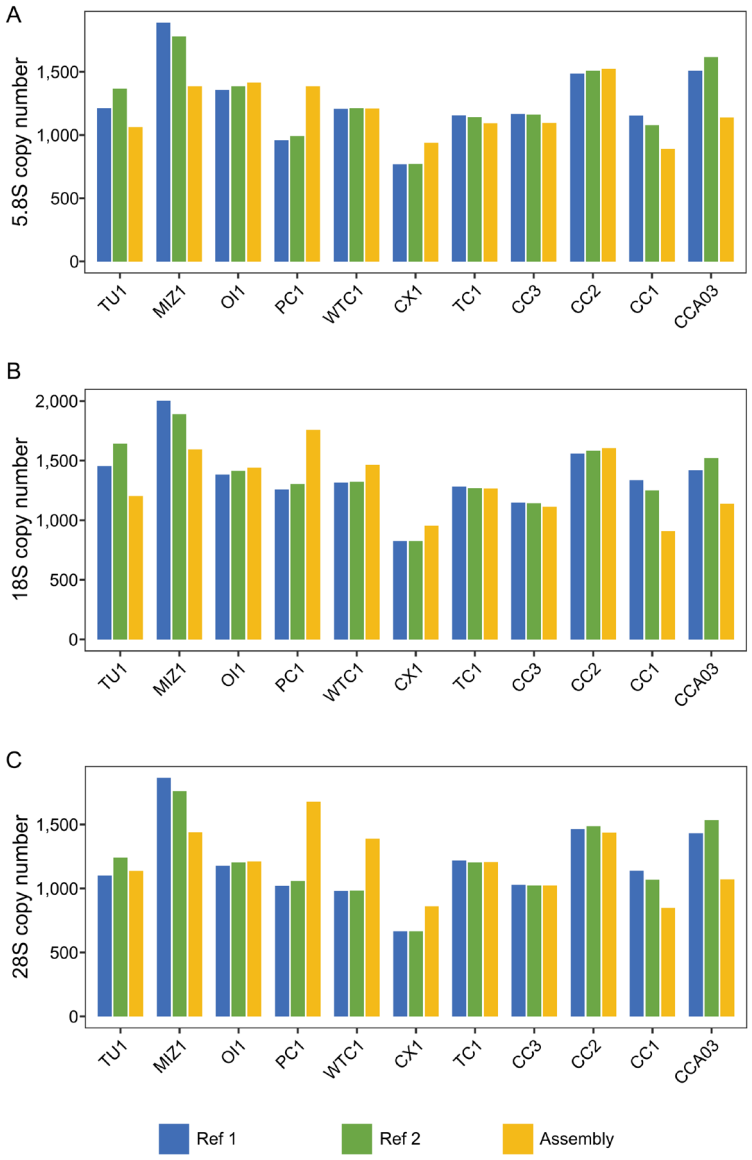

fig. S5. Copy number of 45S rDNAs by digital PCR in 11 *B. rapa* genomes.
Comparison of the copy number of (**A**) 5.8S, (**B**) 18S, (**C**) 28S rDNAs in the assemblies. Copy number was estimated from data of digital PCR-based assays with two single copy genes as reference (Ref 1 and Ref 2). Information about Ref 1 and Ref 2 is presented in table S26.

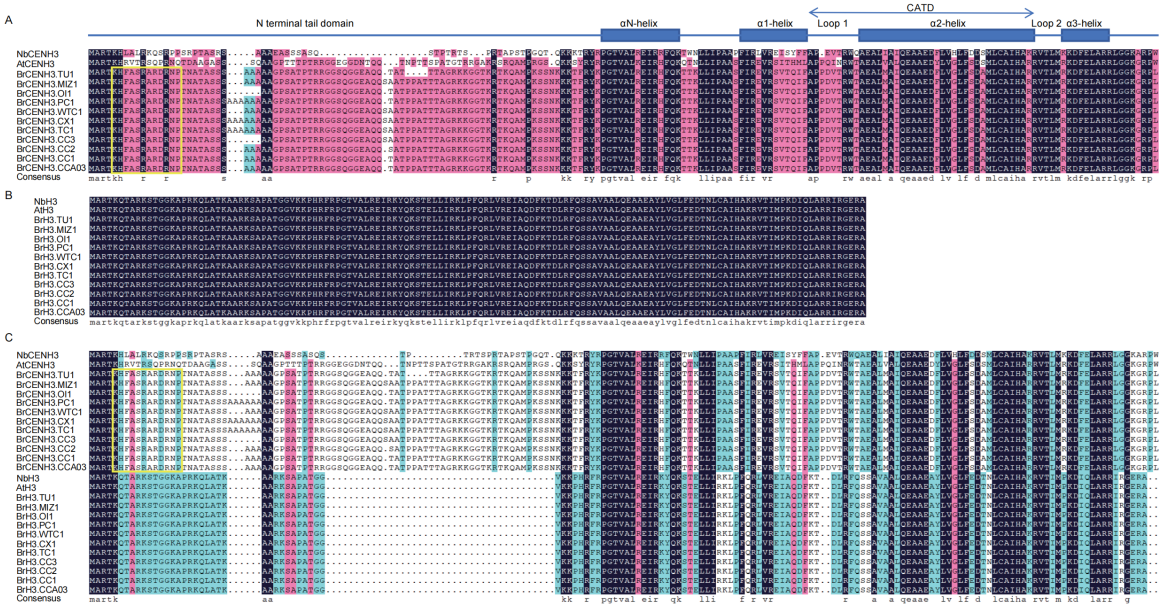

fig. S6. Antigenic peptide designing for production of anti-BrCENH3 antibody.

(**A**) Multiple amino-acid sequence alignment of CENH3 proteins. Domains and structures are shown. (**B**) Multiple amino-acid sequence alignment of H3 proteins. (**C**) Comparisons among H3 and CENH3s. The BrCENH3-specific dodecapeptide used as an antigen to generate anti-BrCENH3 antibody is boxed in panel A and C.

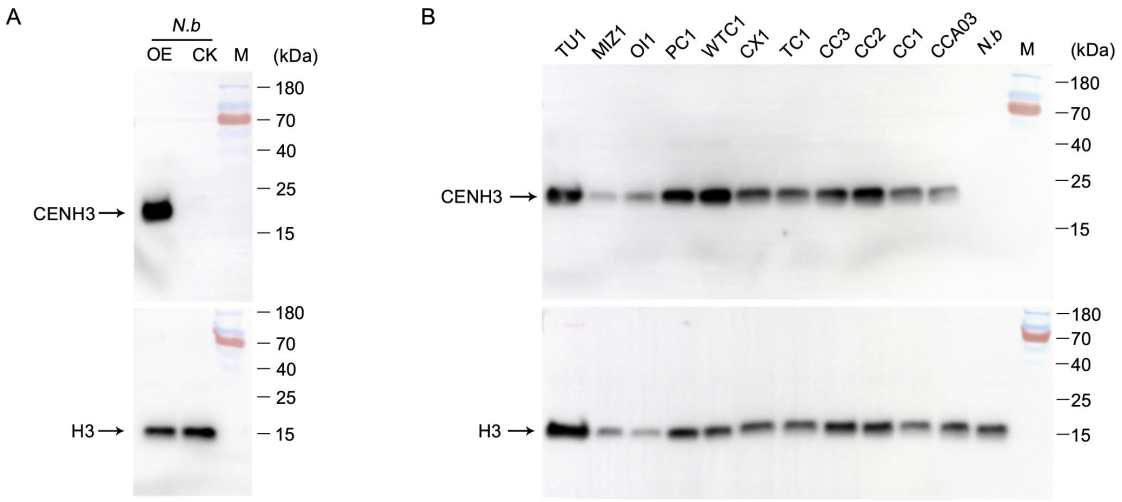

fig. S7. Western blot detection of BrCENH3.

(**A**) Transient assay. A CaMV 35S promoter-controlled BraCENH3 expression cassette 35S::BrCENH3 was constructed and cloned into *Agrobacterium tumefaciens* GV3101. Young leaves of *Nicotinana benthimiana* (*N.b*) were agroinfiltrated with *A. tumefaciens* GV3101 carrying 35S:BrCENH3. At 4 days post-agroinfiltration, total protein was extracted from these infiltrated leaf tissues (OE) and analyzed by western blot using the anti-BrCENH3 (upper panel) or anti-H3 (Lower panel) antibody. Protein samples extracted from leaf tissues agroinfiltrated with *A. tumefaciens* GV3101 carrying the empty gene expression vector was used as the negative control (CK). (**B**) Western detection of BrCENH3s and BrH3s in *B. rapa*. Total protein was extracted from leaf tissues of the eleven *B. rapa* subspecies/morphotypes as well as *N. benthimiana* (*N.b*) and analyzed by western blot using the anti-BrCENH3 (upper panel) or anti-H3 (Lower panel) antibody. Sizes (kDa) and positions of protein markers and positions of CENH3 and H3 are indicated.

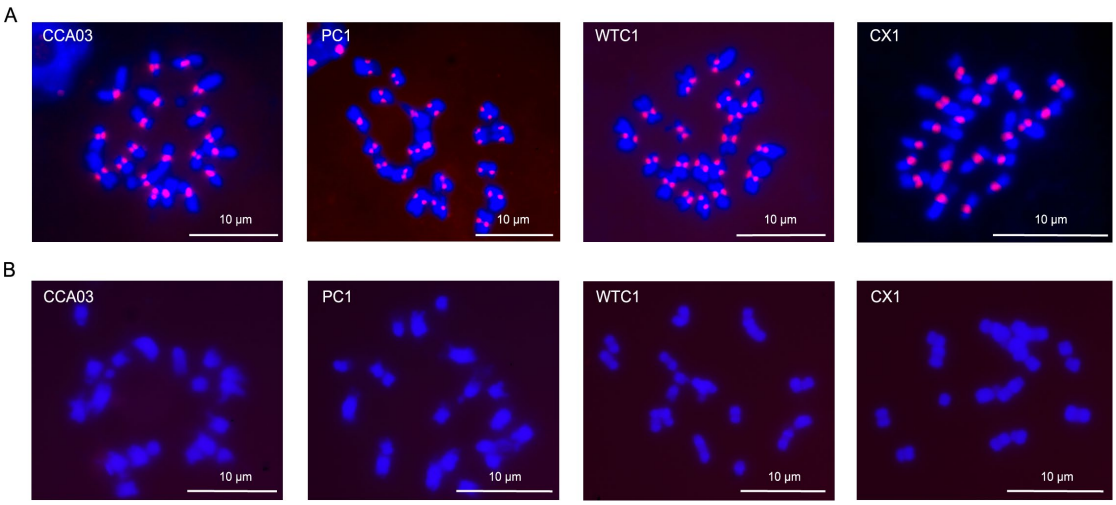

fig. S8. Immunostaining of chromosomes with anti-BrCENH3 antibodies.
Immunostaining was performed on sections of CCA03, PC1, WTC1 and CX1 root tips with the antibody specifically raised against BrCENH3. Chromosomes at metaphase (blue) were stained with 4′,6-diamidino-2-phenylindole (DAPI). Red fluorescence signals are visible at the primary constrictions of the chromosomes stained with the anti-BrCENH3 antibody (**A**), but not with the antisera purified from rabbits immunized with the carrier protein alone (**B**). Scale bar = 10 um.

A Characterization of the (peri)centromeres A01-A10 in TU1

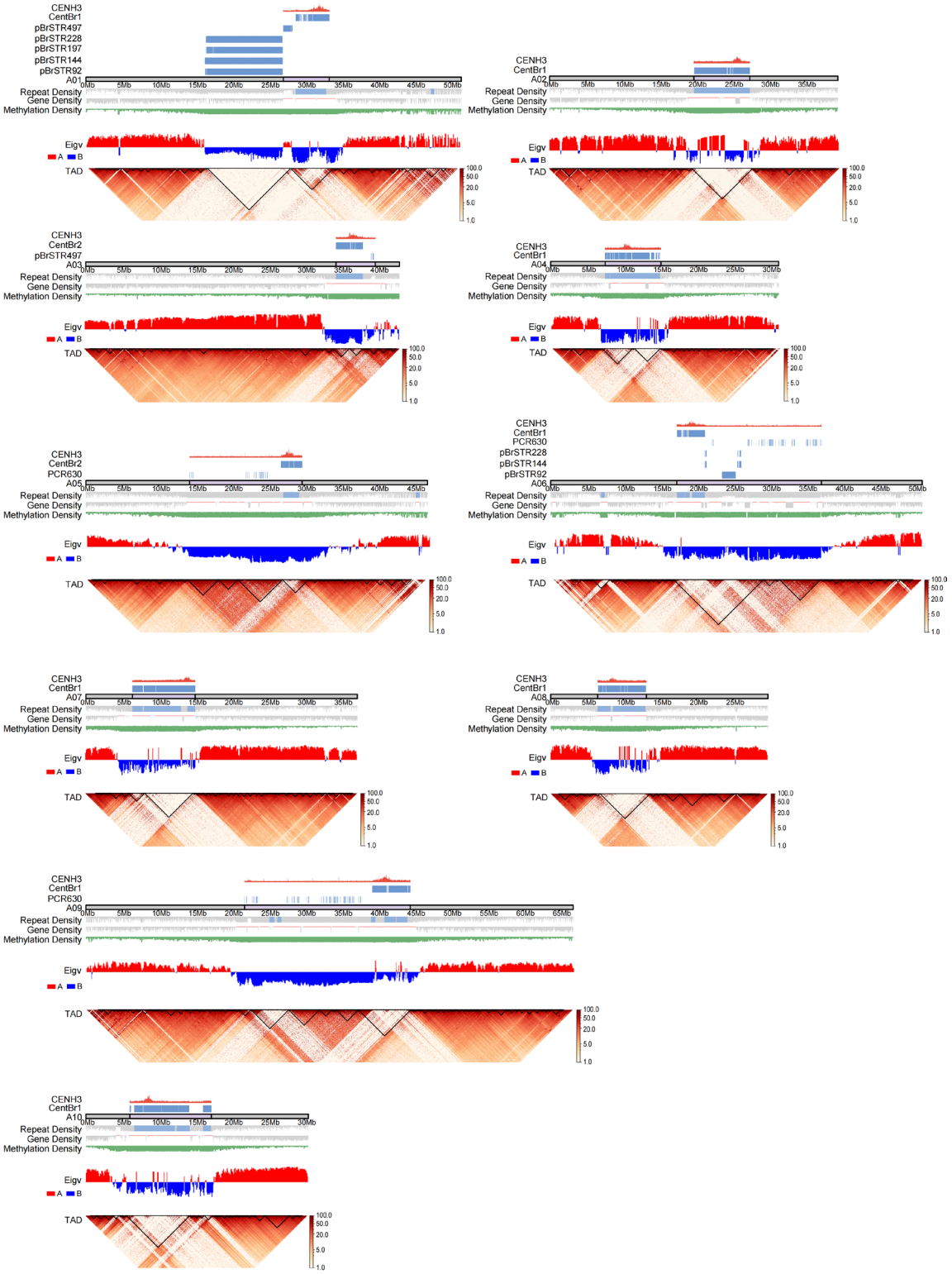

B Characterization of the (peri)centromeres A01-A10 in MIZ1

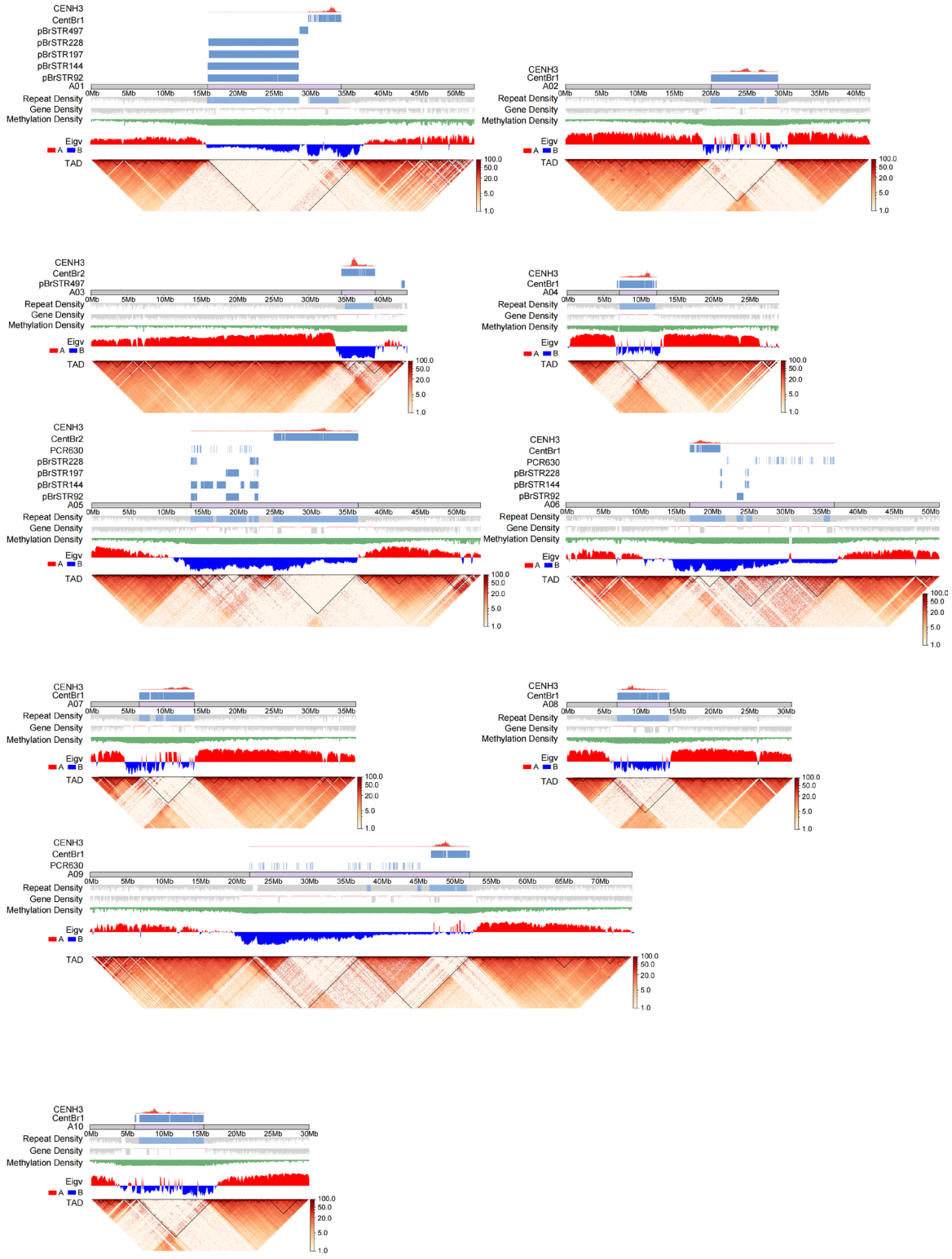

C Characterization of the (peri)centromeres A01-A10 in OI1

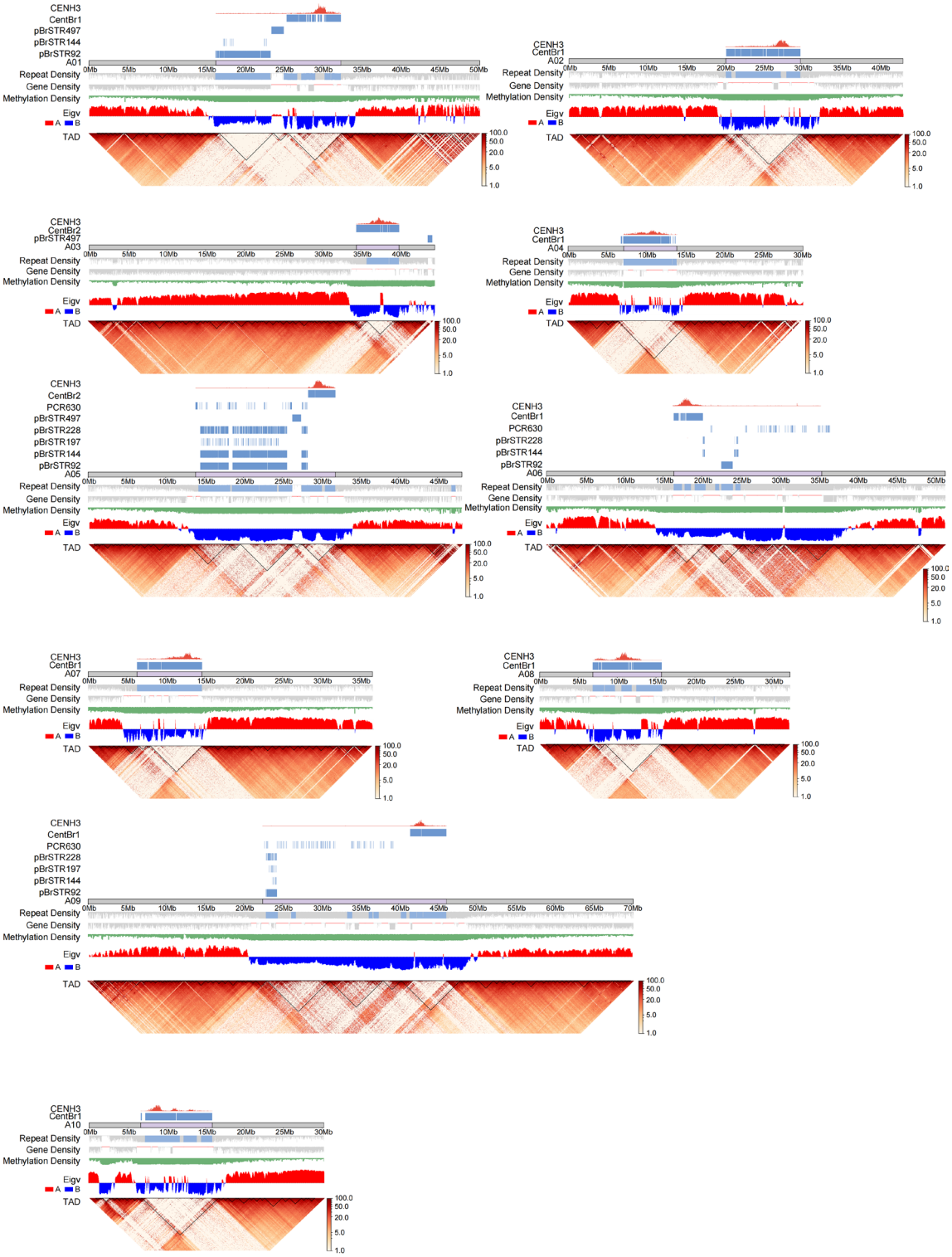

D Characterization of the (peri)centromeres A01-A10 in PC1

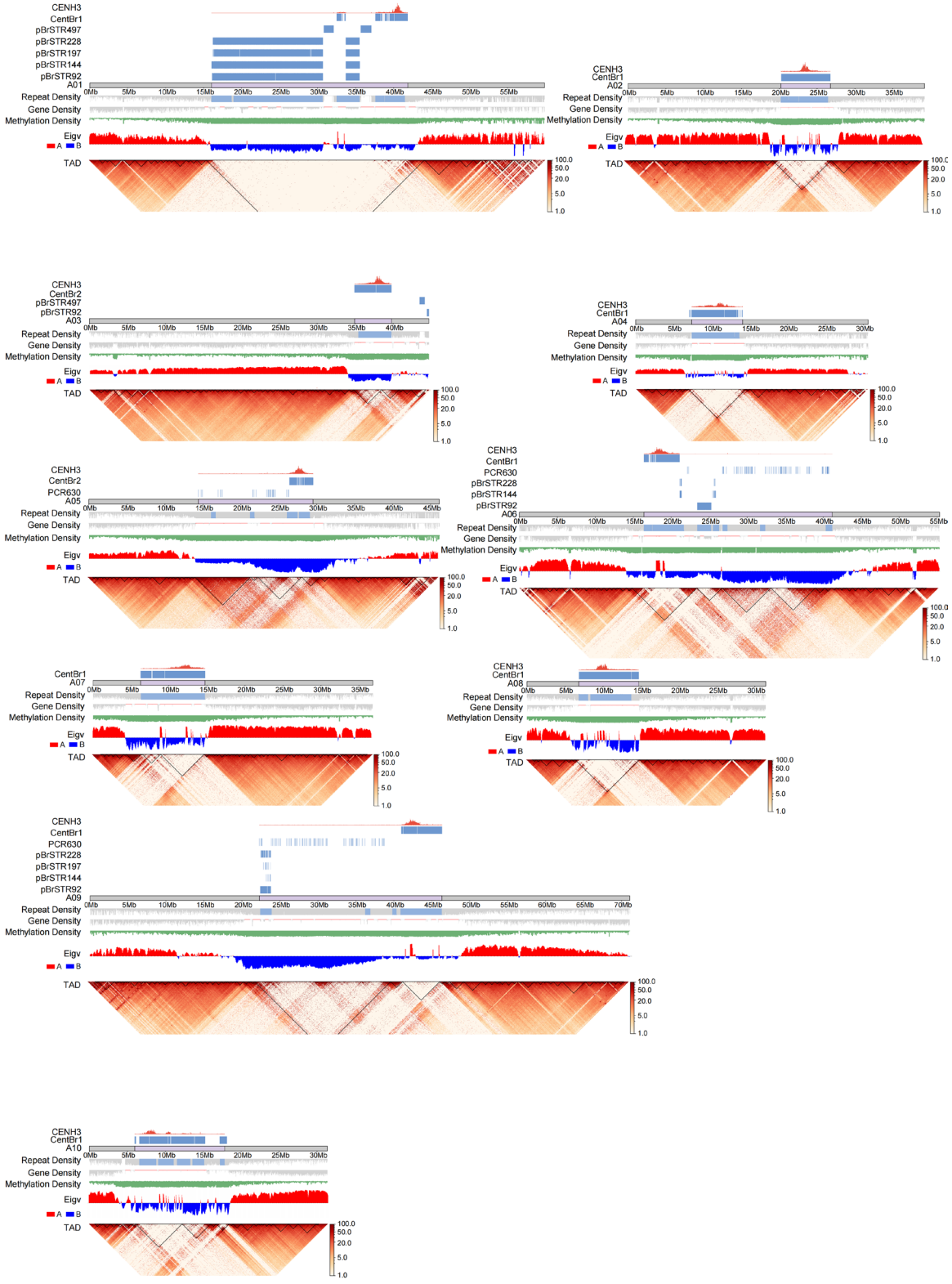

E Characterization of the (peri)centromeres in A01-A10 WTC1

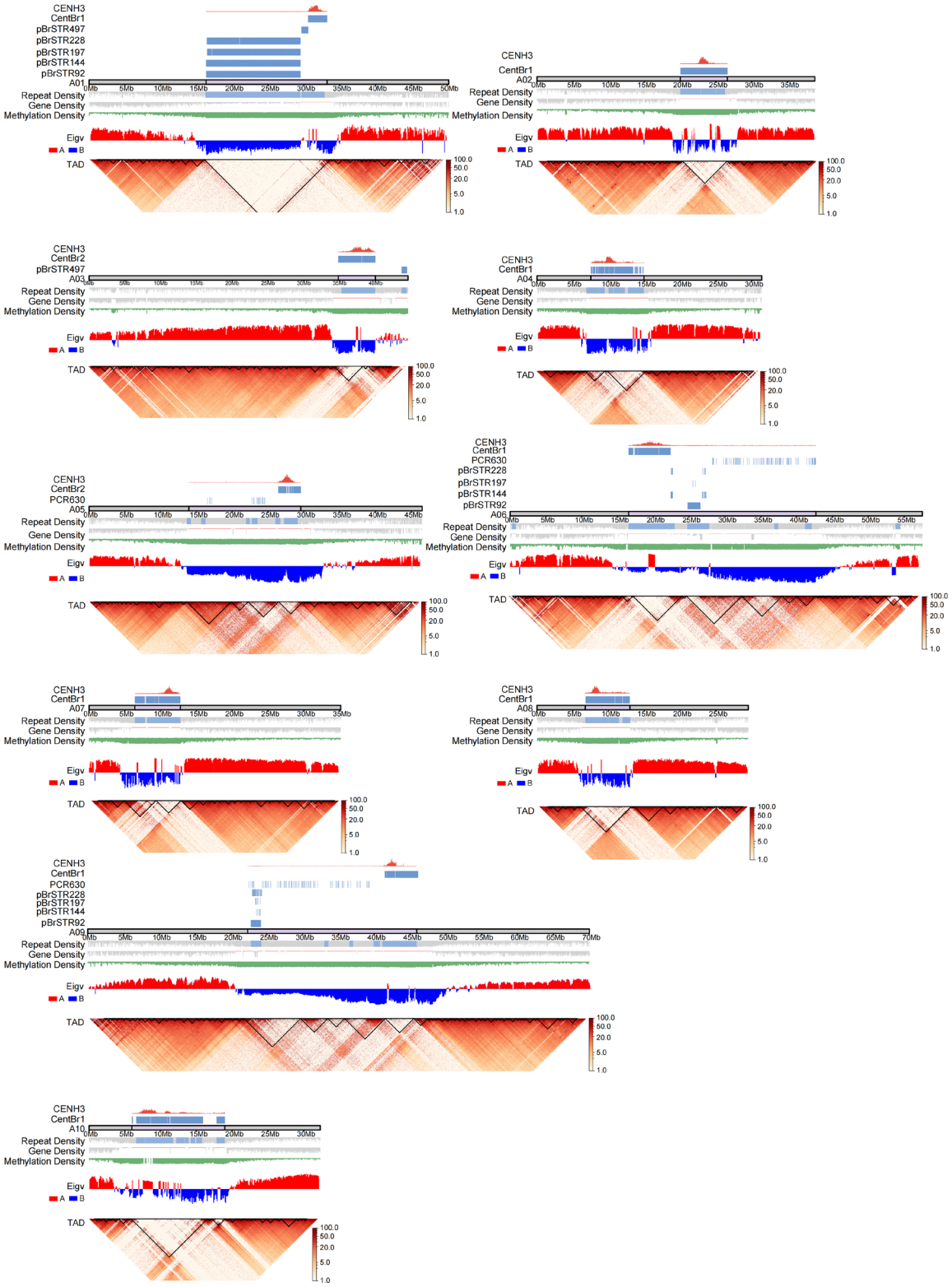

F Characterization of the (peri)centromeres A01-A10 in CX1

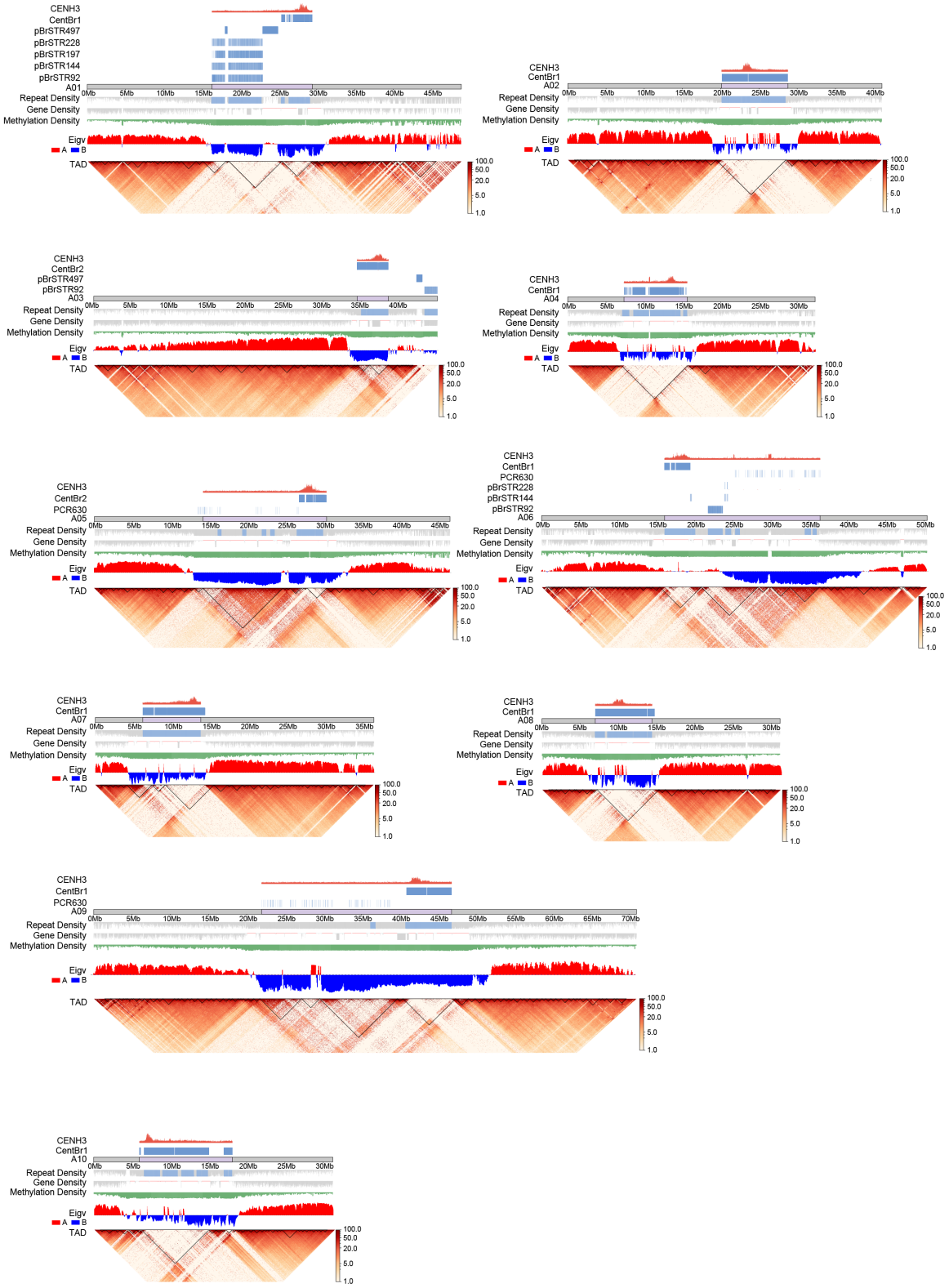

G Characterization of the (peri)centromeres A01-A10 in TC1

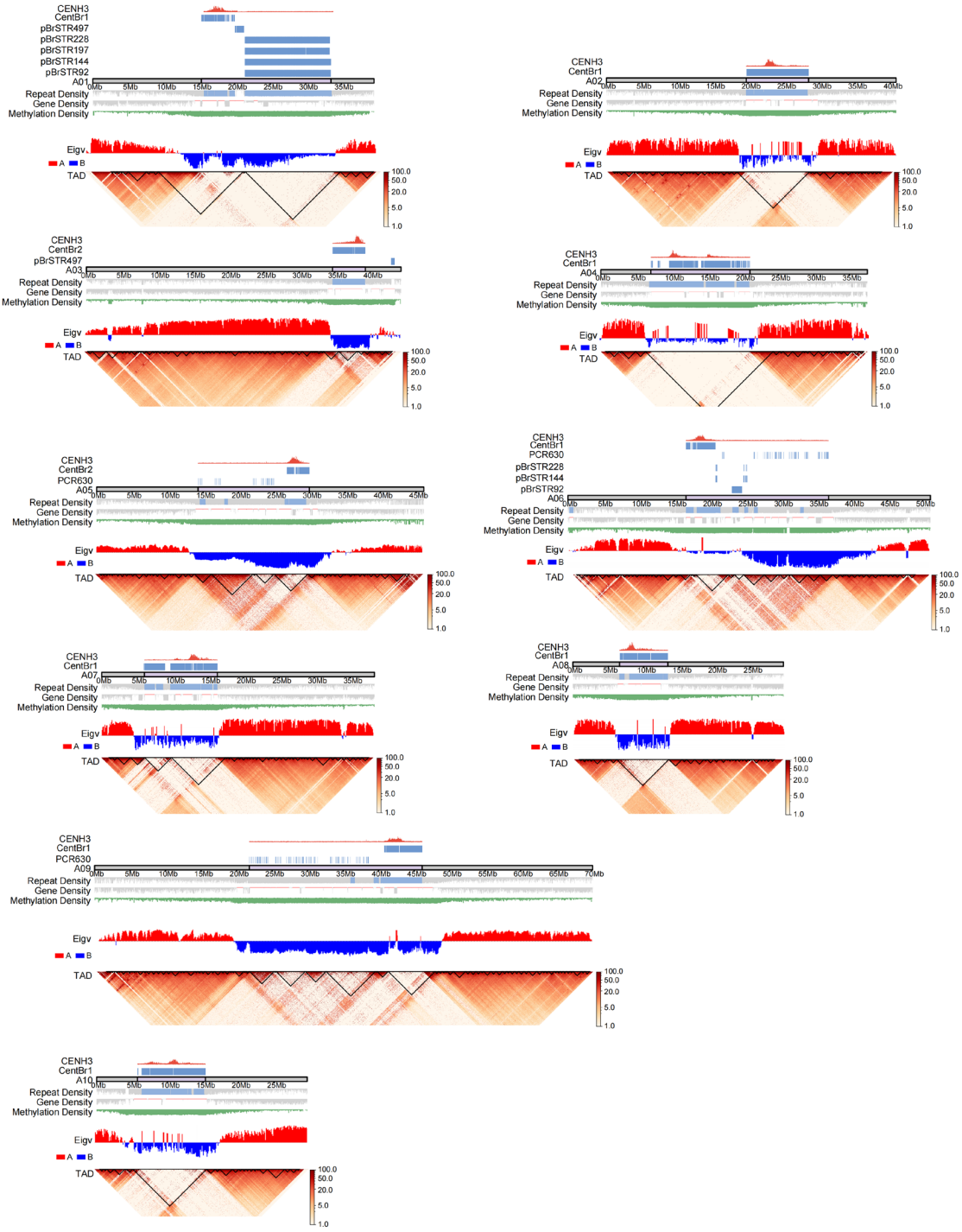

H Characterization of the (peri)centromeres A01-A10 in CC3

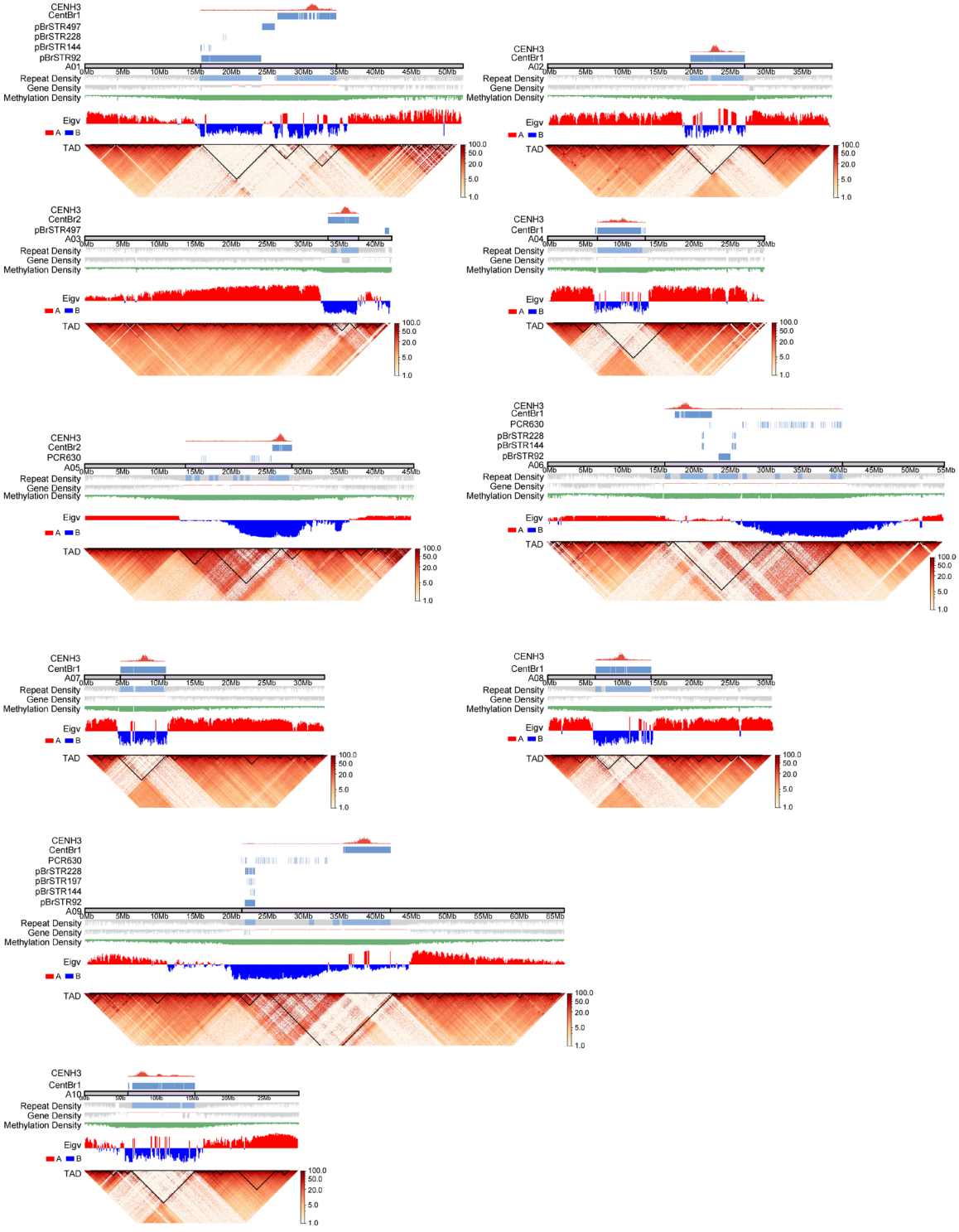

I Characterization of the (peri)centromeres A01-A10 in CC2

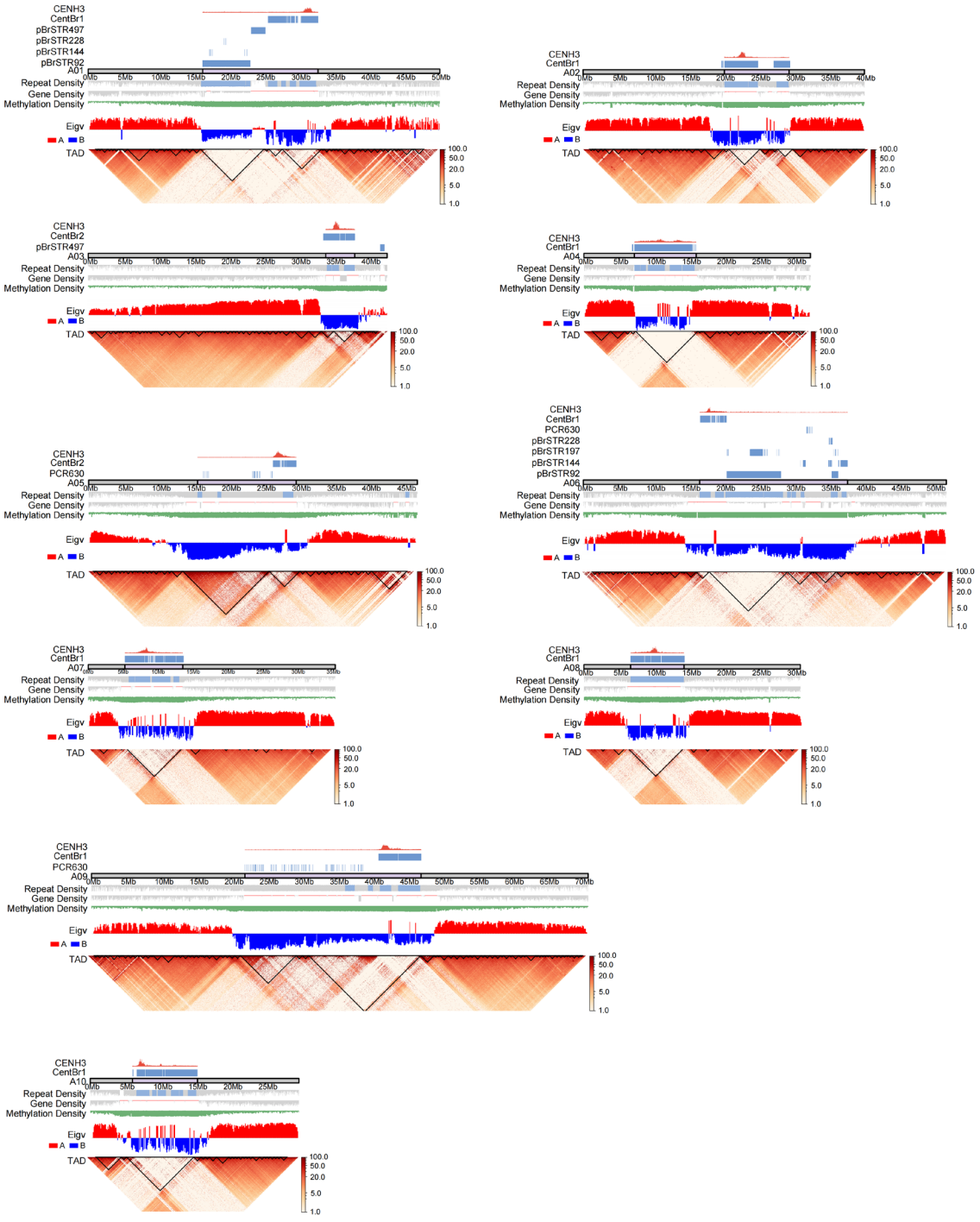

J Characterization of the (peri)centromeres A01-A10 in CC1

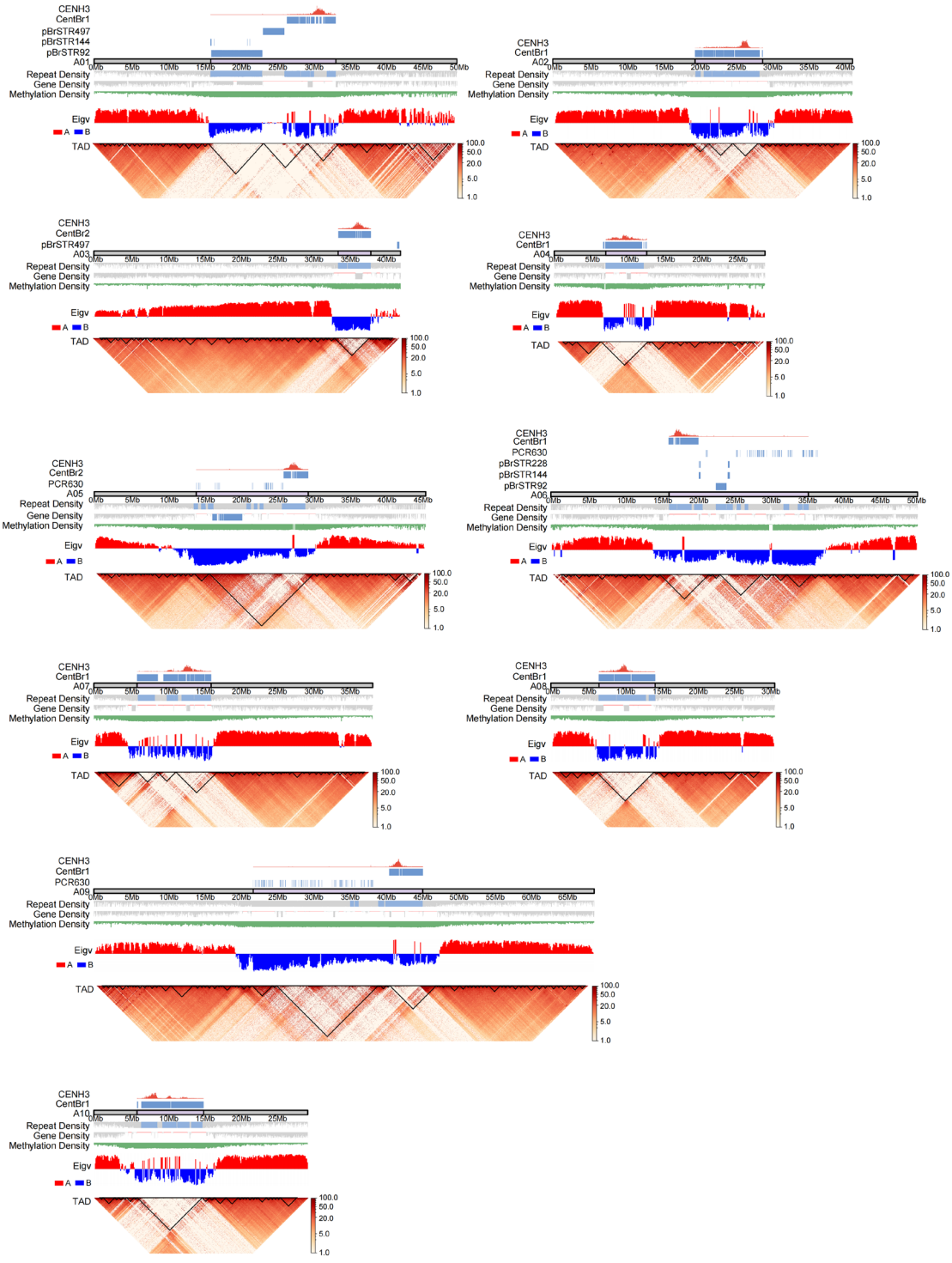

K Characterization of the (peri)centromeres A01-A10 in CCA03

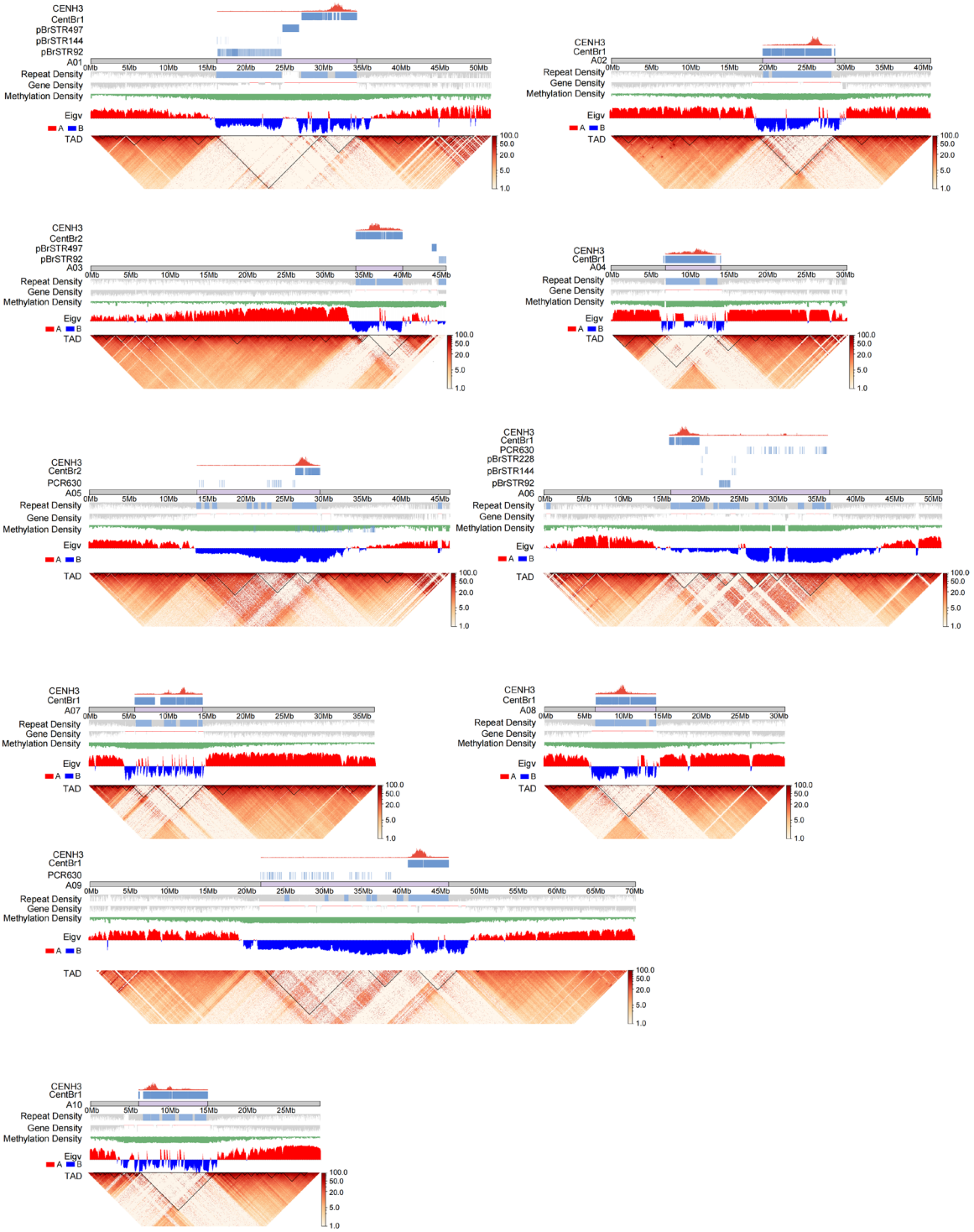

fig. S9. Characterization of the (peri)centromeres in 11 *B. rapa* genomes.
(**A**-**K**) CENH3 Coverage, CENH3 Density, satellite coverage, repeat elements density, gene density, DNA methylation density and A/B compartment in chromosomes A01-A10 of each *B. rapa* accession as indicated. Trapezoid heatmap displays the topologically associating domain (TAD) within the chromatin interaction map. Eigv, eigenvector value of correlation matrix. CENH3-rich region of per chromosome was centromere and pericentromere with high satellite coverage, high repeat elements density and low gene density was shown with

purple block. Accessions include TU1 (**A**), MIZ1 (**B**), OI1 (**C**), PC1 (**D**), WTC1 (**E**), CX1 (**F**), TC1 (**G**), CC3 (**H**), CC2 (**I**), CC1 (**J**), and CCA03 (**K**).

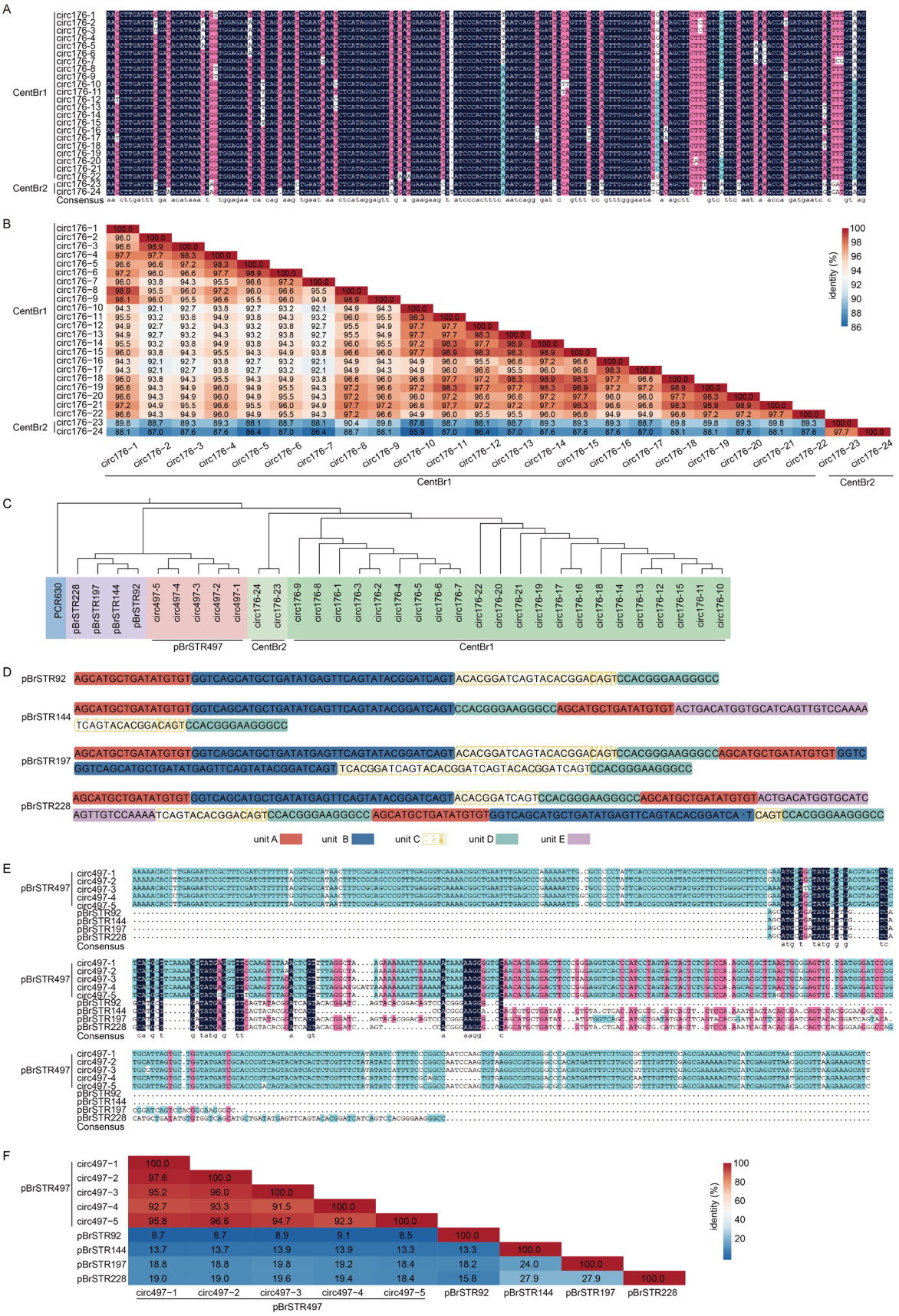

fig. S10. Phylogenetic analysis and classification of satellites at monomeric nucleotide sequence level.

(**A**) Multiple sequence alignments of CentBr satellites. Sequences of twenty-two variants circ176-1 – circ176-22 of CentBr1 and two variants circ176-23 and circ176-24 of CentBr2 are shown. (**B**) Percentages of pairwise sequence identities among variants within and between CentBr1 and CentBr2 showed in panel A. (**C**) Phylogenetic relationship among seven types of satellites across 11 B. rapa genomes. Satellites within the same clades are shown in the same colors. The sequence of PCR630 used in this analysis is shown in table S17. (**D**) Monomeric satellite sequences of pBrSTR92, pBrSTR144, pBrSTR197 and pBrSTR228. Units A-E in each satellite are shown with different colors (also see Fig. 2B). Unit C consists of three subunits which are framed by boxes with different patterns. (**E**) Multiple sequence alignments of pBrSTR497, pBrSTR92, pBrSTR144, pBrSTR197 and pBrSTR228. (**F**) Percentages of pairwise sequence identities among pBrSTR497, pBrSTR92, pBrSTR144, pBrSTR197, and pBrSTR228 showed in panel E.

Based on the monomeric nucleotide length (base-pairs, bp), degree of sequence repeats, and the chromosomal locations, satellite DNAs are generally classified into (i) microsatellites (2-6 bp, short tandem repeats, and telomeric regions); (ii) minisatellites (approximate 15 bp, variable tandem repeats, and euchromatic regions); (iii) satellites (tens to hundred bp, high tandem repeats, and centromeric, pericentromeric and subtelomeric regions); and (iv) macrosatellites (up to several kilobase-pairs, dozens to hundred tandem repeats, and chromosomal arms as well as subtelomeric regions) (*108*). The five satellites pBrSTR497, pBrSTR92, pBrSTR144, pBrSTR197, and pBrSTR228 have a monomeric length of 497, 92, 144, 197, and 228 bp, respectively. These satellites are highly enriched in the centromeric and pericentromeric heterochromatin regions (Fig. 2; fig. S10 and S15). Thus by definition，they should be classified as the classic centromeric “satellites”, rather than microsatellites, minisatellites or macrosatellites.

The monomeric sequence of pBrSTR497 (497-bp) differs completely from that of pBrSTR92, pBrSTR144, pBrSTR197, and pBrSTR228, sharing 8.5-19.8% nucleotide identities (fig. S10E). The latter four satellites possess some related sequences since they were formed from different arrangements of the five units A-E (Fig. 2B, fig. S10D). However, pBrSTR92, pBrSTR144, pBrSTR197, and pBrSTR228 are not high-order repeats of any of the five units A-E, and they are four distinct satellites because of marked differences in their lengths (92 to 228 bp) and very low overall nucleotide identities (13.3-27.9%) at the entire monomeric sequence level (fig. S10F).

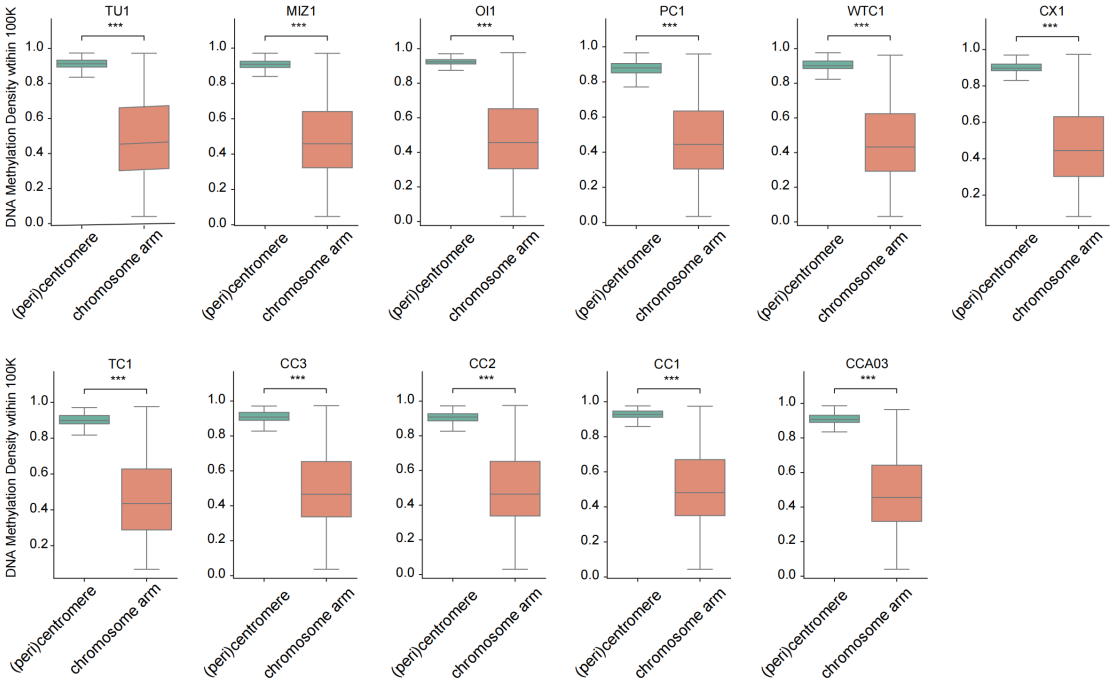

fig. S11. DNA methylation level between (peri)centromeres and chromosomal arms in 11 *B. rapa* subspecies/morphotypes.

Statistical significance of pairwise comparisons between chromosomal regions was assessed by Mann-Whitney U tests, with *** indicating $P < 0.001$.

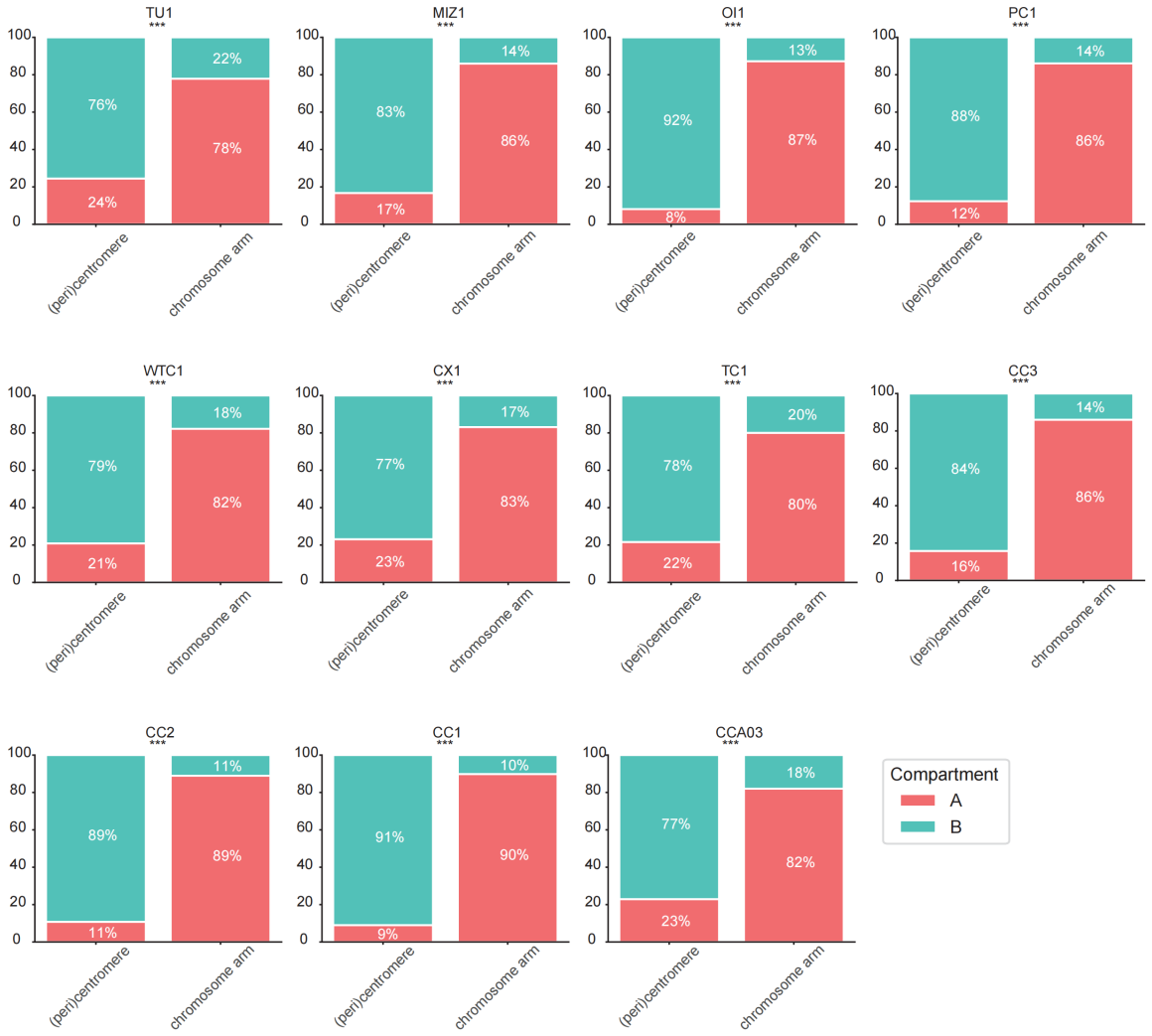

fig. S12. Distribution of A (red) and B compartment (blue) in (peri)centromeric regions and chromosomal arms in 11 *B. rapa* subspecies/morphotypes.

Statistical significance of pairwise comparisons between chromosomal regions was assessed by Mann-Whitney U tests, with *** indicating $P < 0.001$.

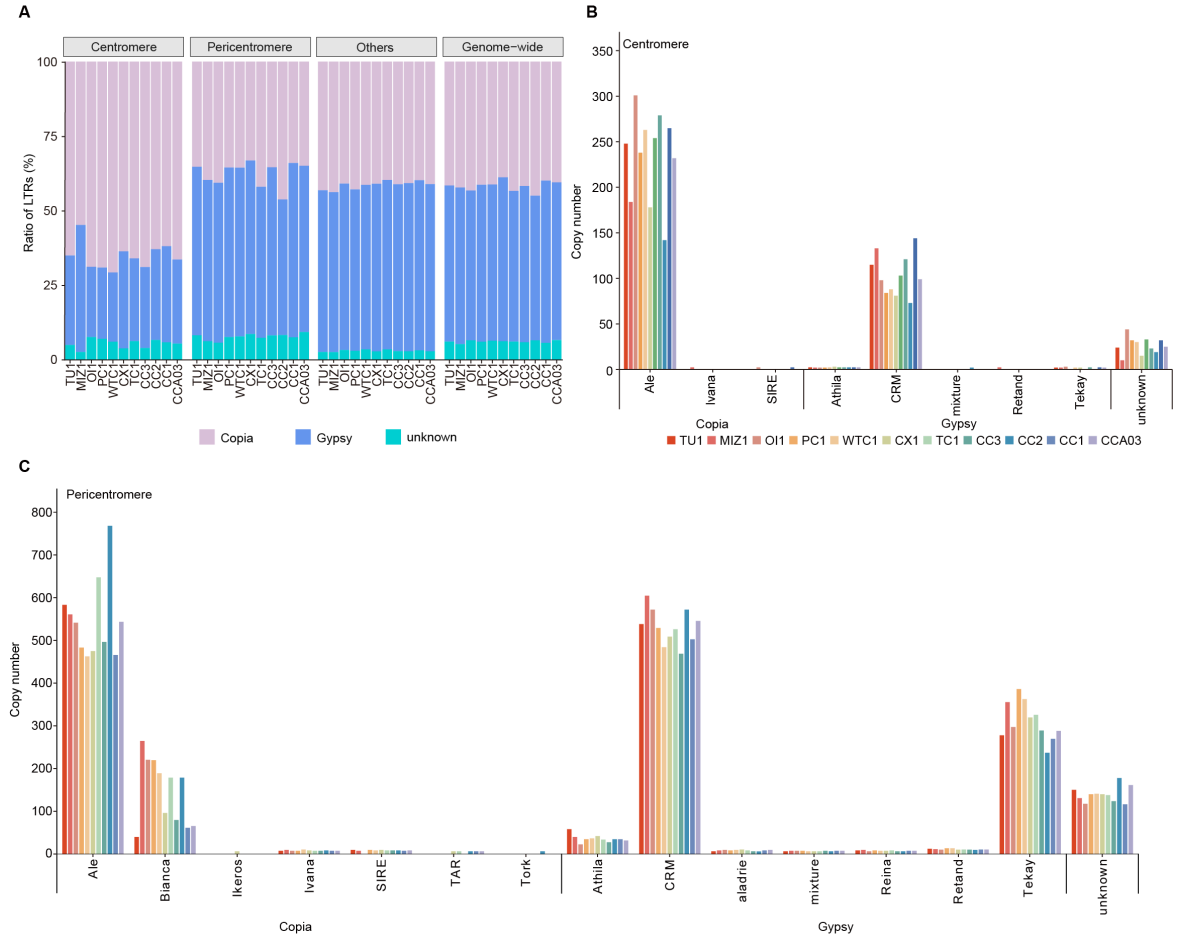

fig. S13. Annotation of LTRs in 11 *B. rapa* genomes.

(**A**) Percentage of LTRs in Centromere, Pericentromere, other genomic regions (Others), and Genome-wide. (**B**) Copy numbers of FL-LTR-RTs in centromere regions of 11 *B. rapa* genomes. (**C**) Copy numbers of FL-LTR-RT families in pericentromeric regions of 11 *B. rapa* genomes.

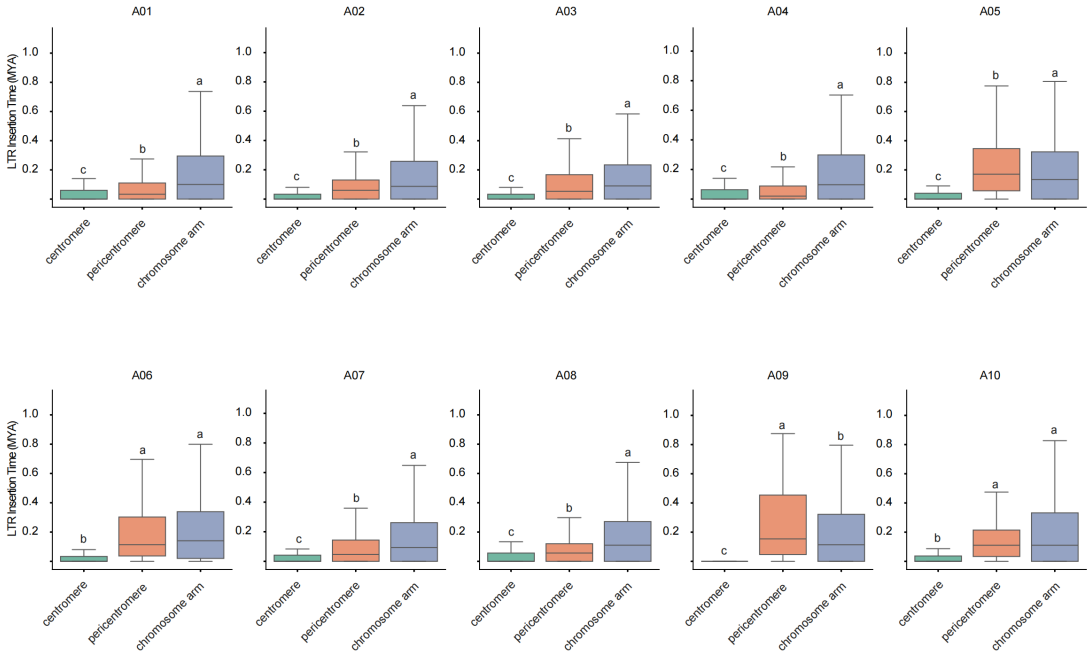

fig. S14. LTR retrotransposon insertion ages across chromosomal regions (A01-A10) in *B. rapa*.

Ages in million years ago (MYA) of LTR-retrotransposon insertions in centromeres, pericentromeres, and chromosome arms of 11 *B. rapa* accessions. Significance testing between chromosomal regions were performed using Mann-Whitney U tests. The different lowercase letters above the box plots represent significant differences ($P < 0.05$).

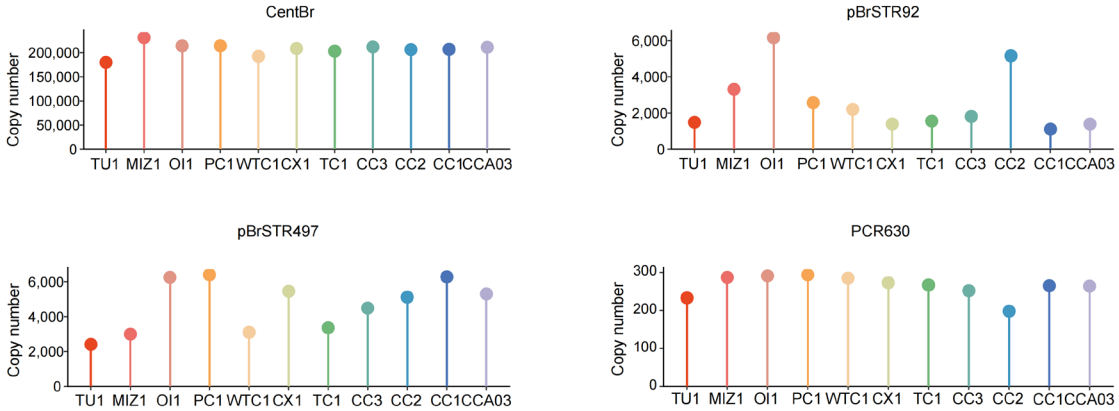

fig. S15. Copy numbers of satellites in 11 *B. rapa* genomes.

Copy numbers of four satellite repeats (CentBr, pBrSTR92, pBrSTR497, and PCR630) are shown across 11 *Brassica rapa* genomes. Bars are color-coded by subspecies/morphotype, as indicated on the x-axis.

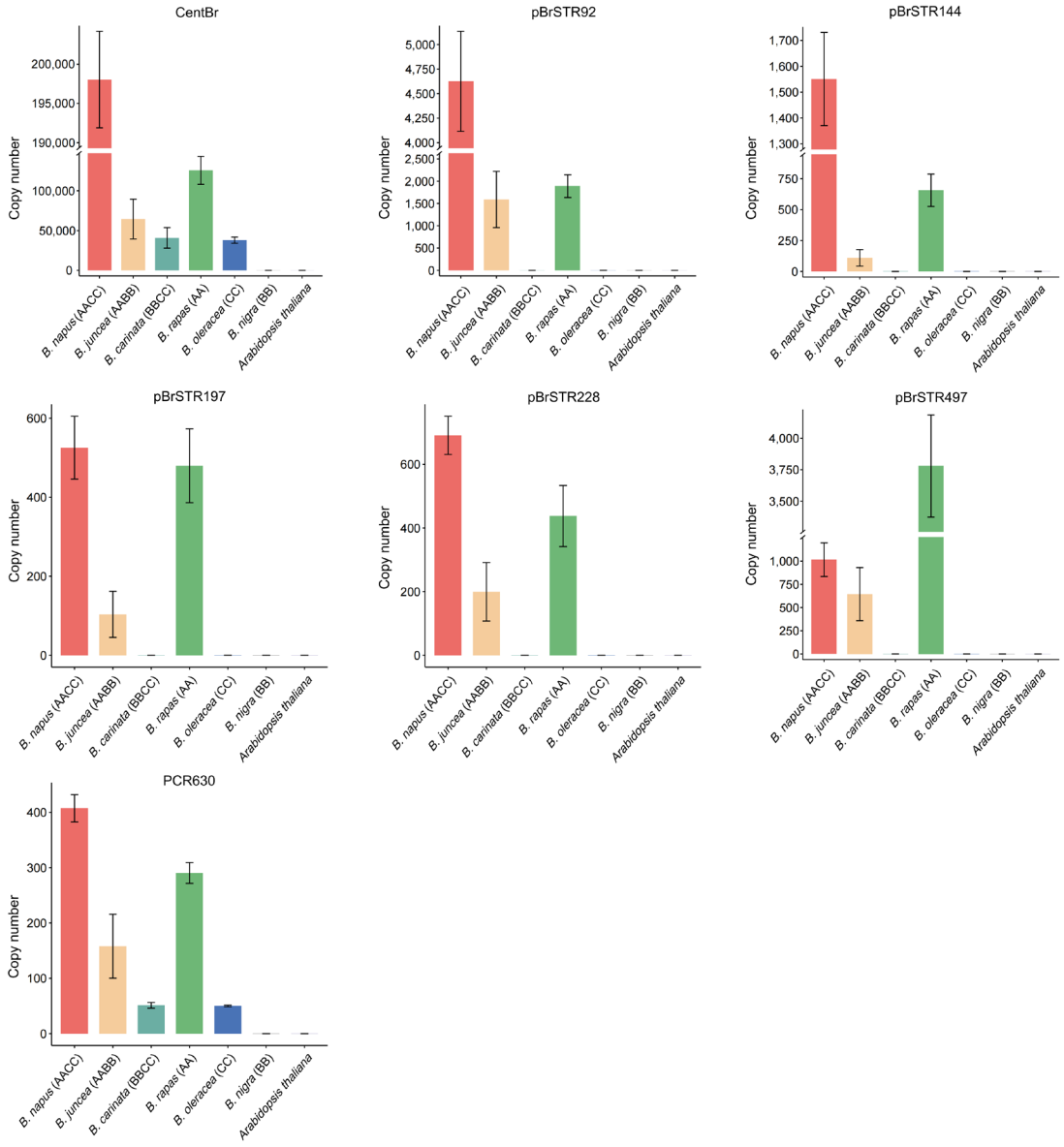

fig. S16. Copy numbers of 5 newly characterized and 2 known satellites across 6 *Brassica* sp., three diploids (AA, BB, CC) and three allotetraploids (AABB, AACC, BBCC) as well as *Arabidopsis thaliana*.

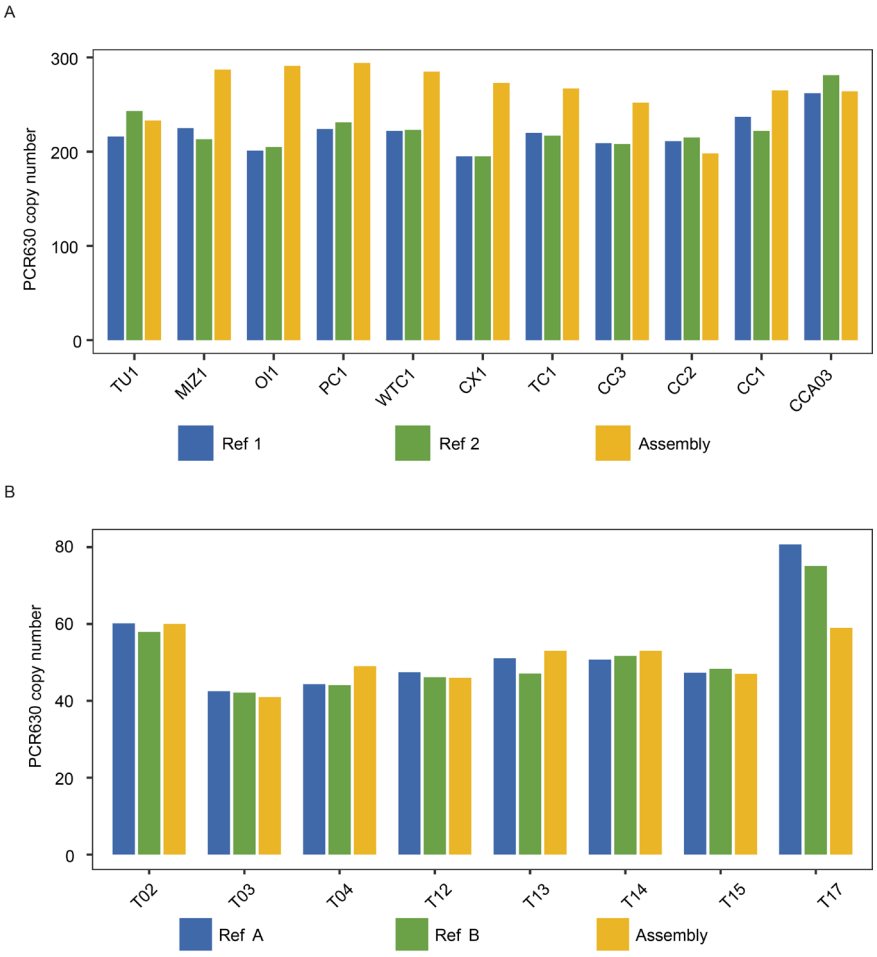

fig. S17. Digital PCR-based analysis of satellites.

Comparison of the copy number of satellite PCR630 in the 11 *B. rapa* (AA) (**A**) and 8 *B. oleracea* (CC) (**B**) genomes. Digital PCR-based estimation was obtained with single copy genes as reference (AA: Ref 1 and Ref 2; CC: Ref A and Ref B). The CC genomes are not complete, with high probability of missing satellite DNAs in their assemblies (*30*). This may result in overcalculating copy number changes in AA vs CC based on the in silico assay. We have thus re-examined the completeness and assembly quality of the published CC genomes (*30*) used for comparisons in our study. The total genome sizes of those CC assemblies range from 539.87 to 584.16 Mb with an average contig N50 of 19.18 Mb. On average, 98% contig sequences are anchored to the nine CC pseudochromosomes. The average BUSCO complete score is 98.70%, indicating high completeness and quality of the CC assemblies. We then performed digital PCRs on 11 AA (A) and 8 CC (B) (*30*) accessions to quantify satellite copy numbers. The PCR630 copy numbers measured by digital PCR vs in silico assay are close. The ratio between the PCR630 copy numbers obtained from digital PCR in AA vs CC is about 4.24. Unfortunately, digital PCR cannot be carried out to estimate the CenBr copy number due to that CentBr is of high sequence polymorphism, and no primers could be designed for digital PCR to capture all CenBrl variants. Nevertheless, both digital PCR and in silico assays show that AA genomes contain more CentBr and PCR630 than the CC counterparts.

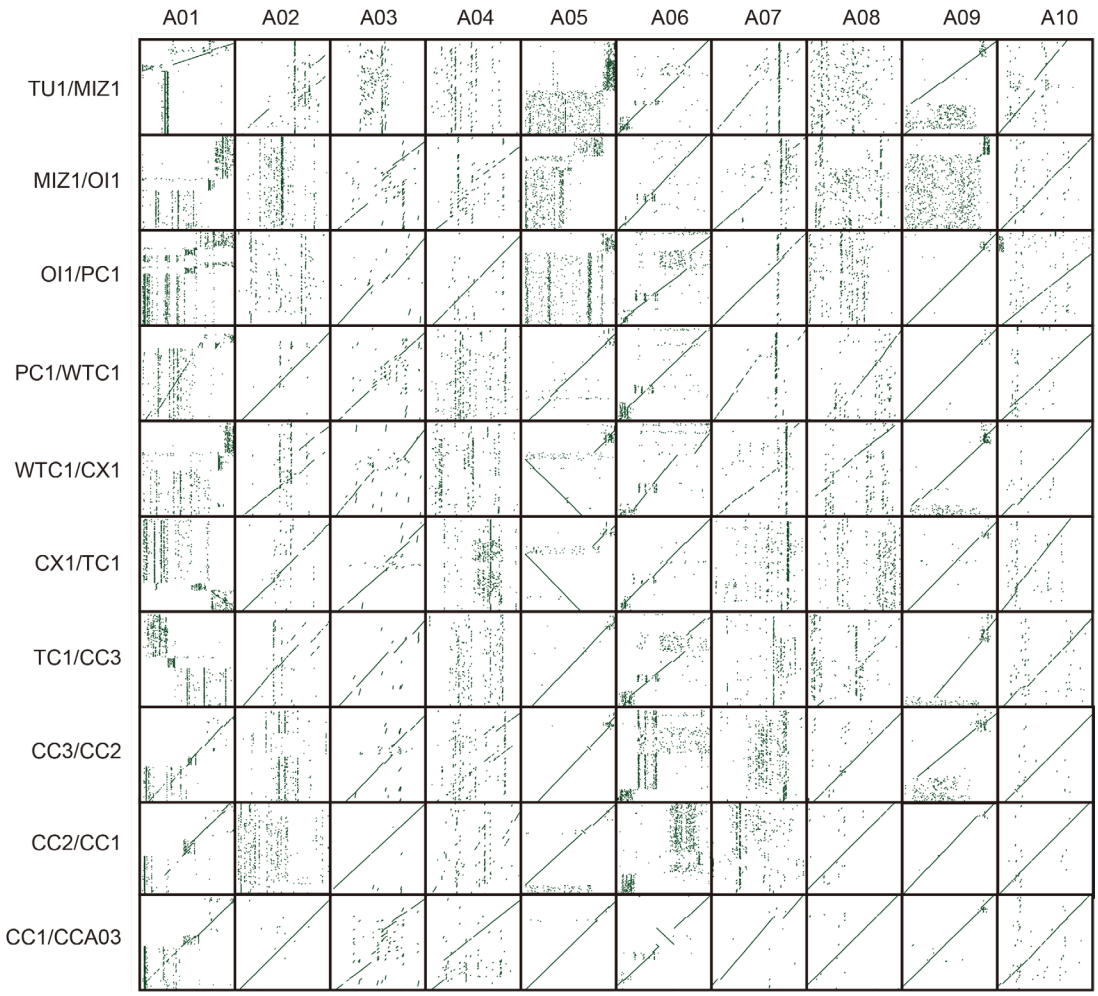

fig. S18. Dot-plots show sequence synteny in the (peri)centromeric regions of 10 chromosomes A01-A10 for each of 10 pairs of the 11 *B. rapa* accessions as indicated. Dot-plots were produced using the DGENIE software and alignments with mashmap (v2.0). The pair of relevant *B. rapa* accessions are indicated on the left of the graphics. These pairs were chosen based on the position on the phylogenetic tree (Fig. 1A).

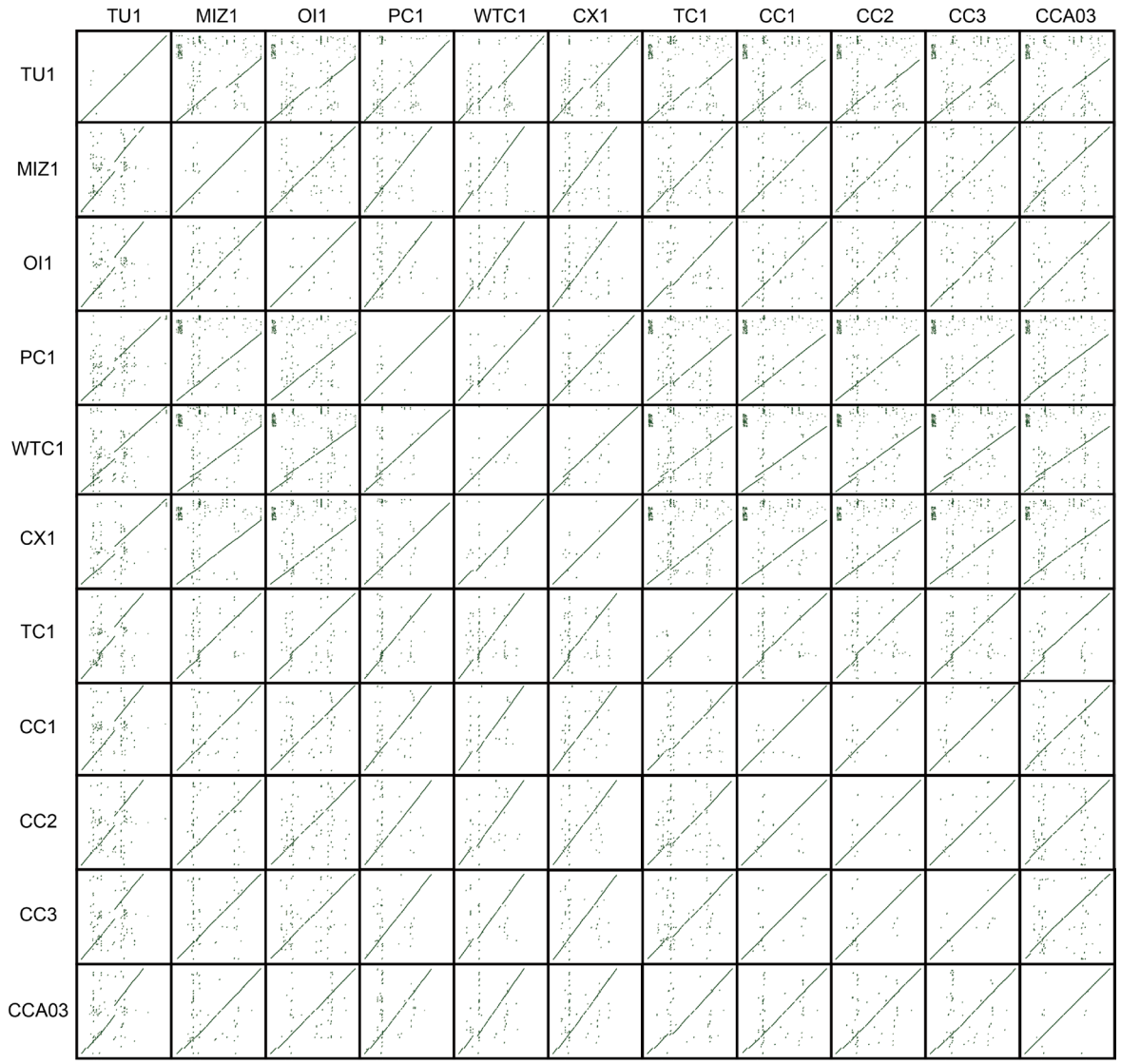

fig. S19. Dot-plots show sequence synteny in the (peri)centromeric regions of chromosome A10 for pairwise comparison between the 11 *B. rapa* accessions.
Accessions include TU1, MIZ1, OI1, PC1, WTC1, CX1, TC1, CC1, CC2, CC3 and CCA03.

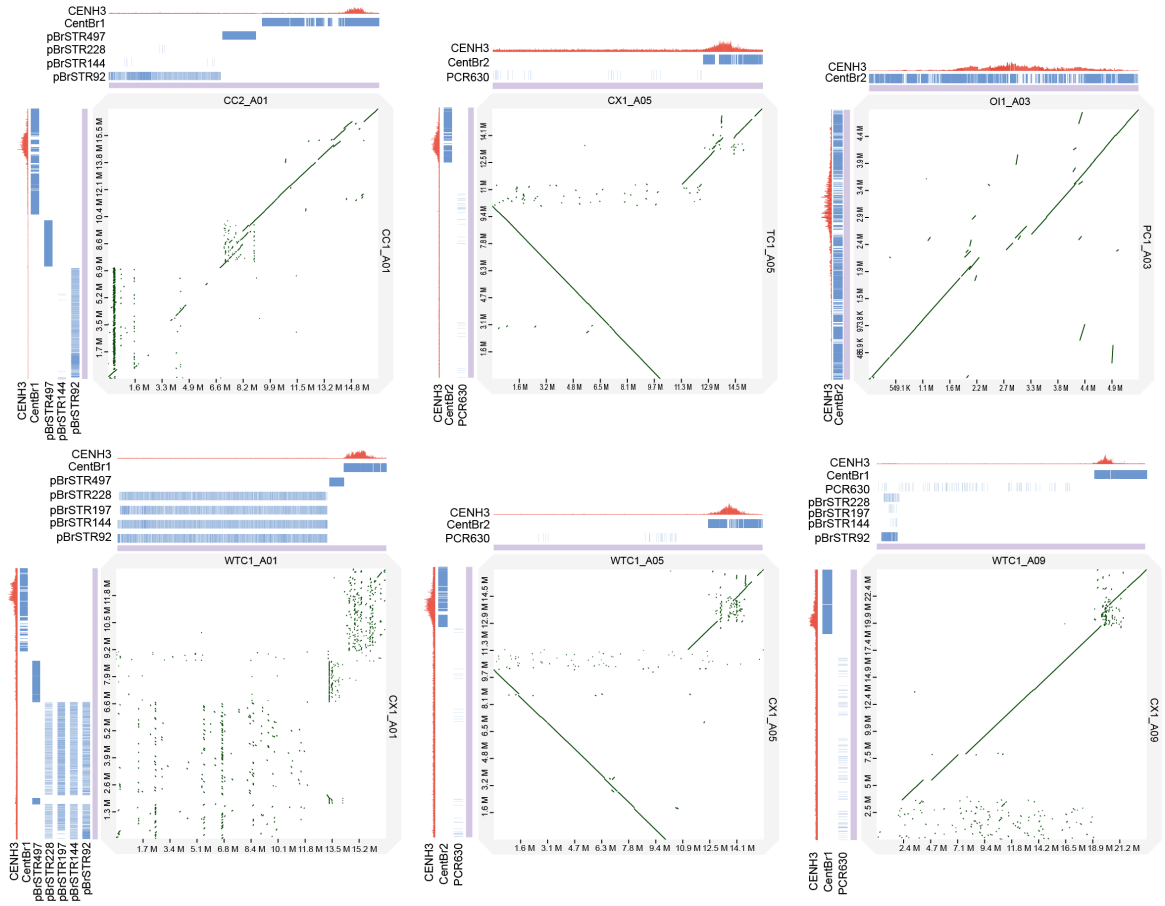

fig. S20. Association of subspecies-specific satellites with (peri)centromeric synteny. CENH3 peaks (red) and satellite coverage (blue) in chromosomes of different *B. rapa* accessions as indicated. Example dot-plots show sequence syntenies in the (peri)centromeric regions of chromosomes for six pairwise comparisons chromosome A01 of CC1 vs CC2, chromosome A05 of TC1 vs CX1, chromosome A03 of PC1 vs OI1, chromosome A01 of CX1 vs WTC1, chromosome A05 of CX1 vs WTC1, and chromosome A09 of CX1 vs WTC1. Horizontal vs vertical axis represents nucleotide positions at the scale of million (M) bases in chromosomes.

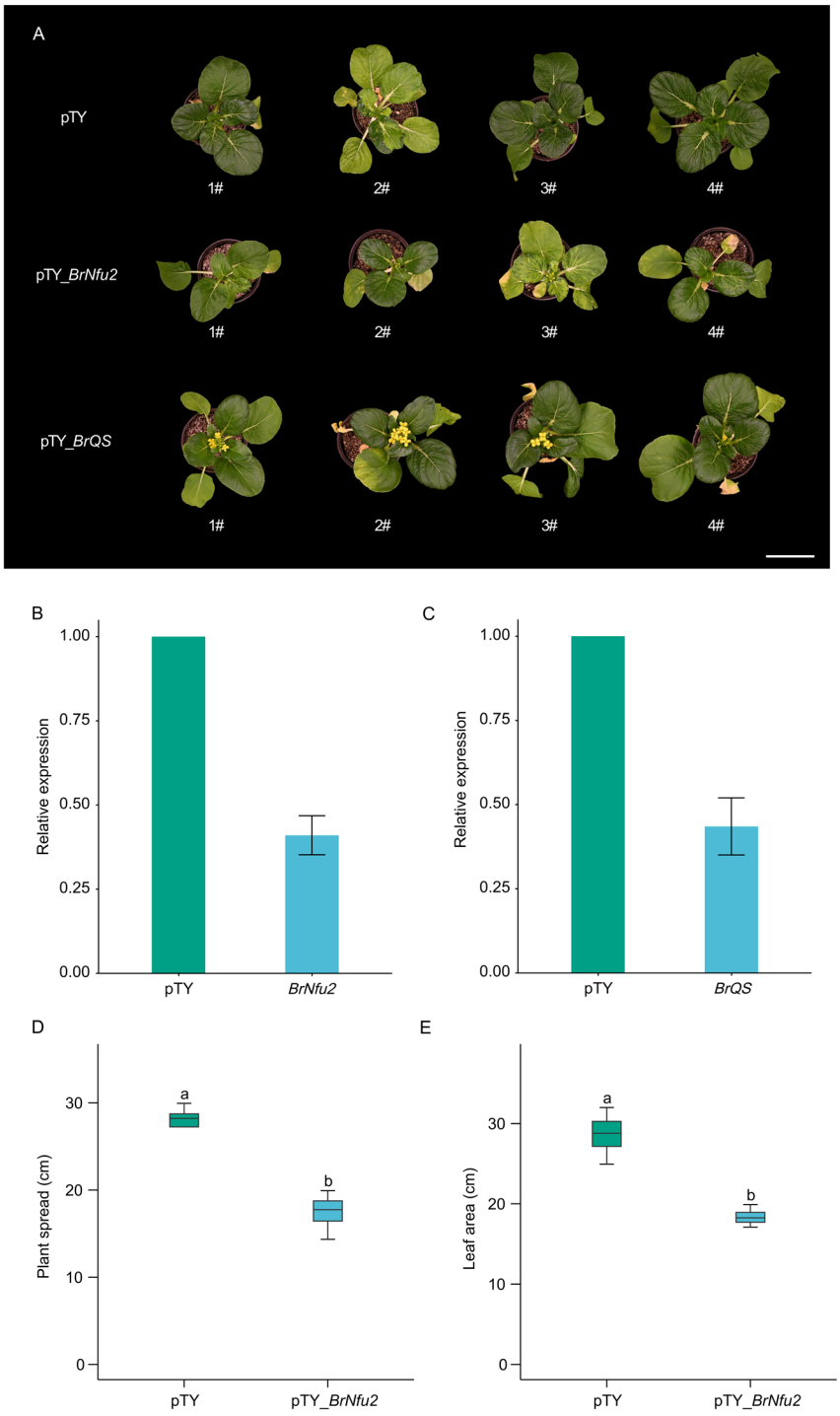

fig. S21. Knock-down of *BrNfu2* and *BrQS* by virus-induced gene silencing (VIGS) affects plant development in CX1.

(**A**) Phenotypic changes caused by *BrNfu2* (reduced size) and *BrQS* (early flowering) gene silencing in CX1 plants. Plants were photographed at 33 days post virus inoculation by bombardment. Relative expression of *BrNfu2* in pTY (empty vector) and gene silencing plants (**B**), plant spread (**C**) and leaf area (**D**). (**E**) Relative expression of *BrQS* in pTY (empty vector) and gene silencing plants. Different lowercase letters above the box plots represent significant differences ($P < 0.05$).

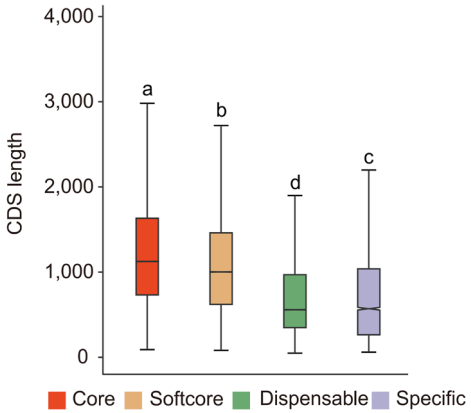

fig. S22. Distribution of protein coding-sequence (CDS) lengths for different types of genes.

The box-plots show the CDS lengths of genes in core, softcore, dispensable, and specific gene families. Different lowercase letters above the box plots represent significant differences ($P < 0.05$).

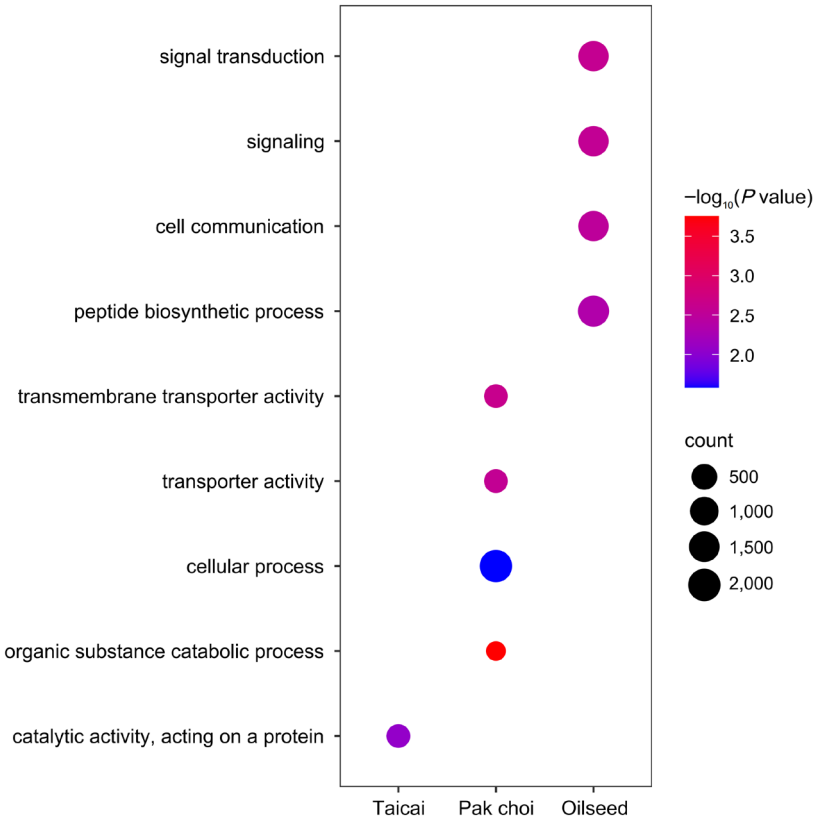

fig. S23. Functional analysis (Gene Ontology) of specific genes on different morphotype/subspecies Taicai, Pak choi and Oilseed.

The *P* value indicates the significance of enrichment for the GO terms; a lower *P* value corresponds to a more significant enrichment result. Morphotype/subspecies-specific genes that were not significantly enriched are not shown here.

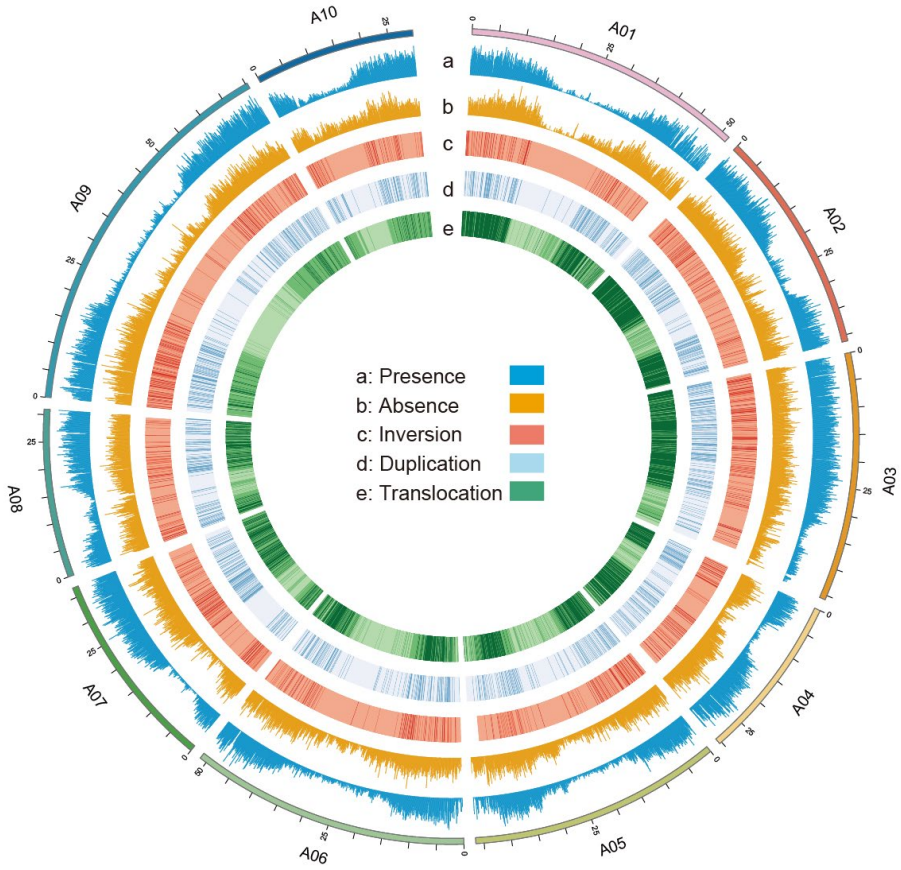

fig. S24. The SV component coverage map with a window of 100kb.
Each circle represents a different variation type in ten chromosomes.

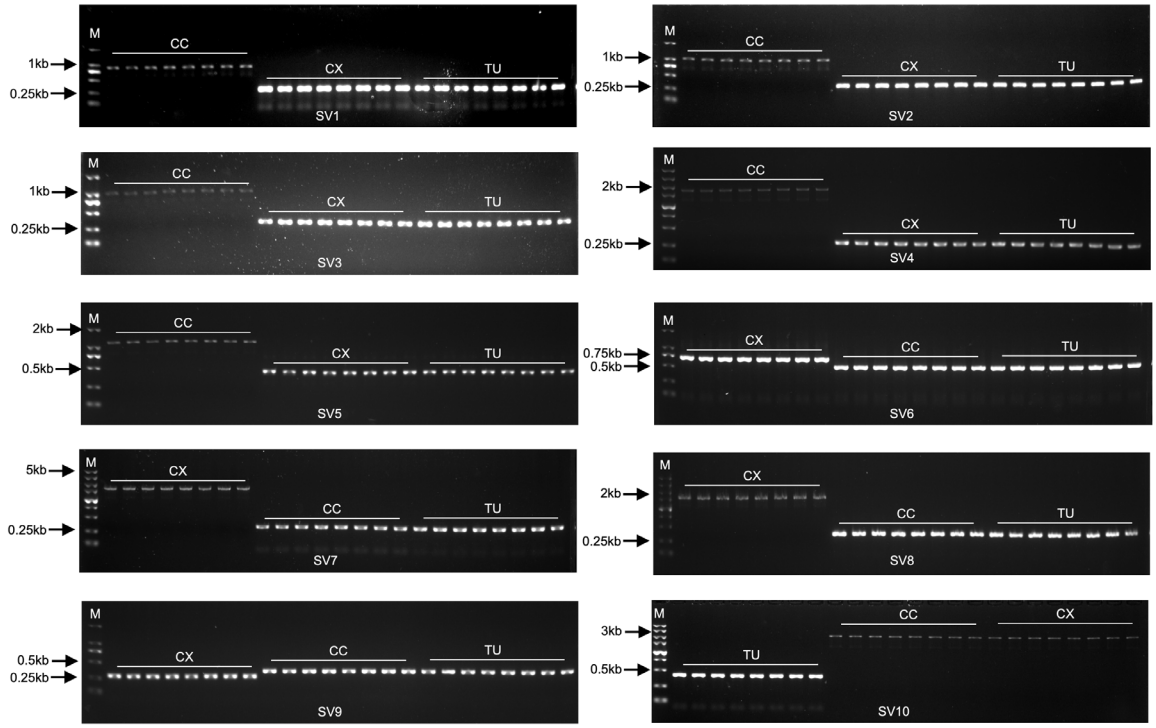

fig. S25. PCR amplification for SVs validation.

Ten PAVs were randomly selected for wet-experimental validation. Different bands show the presence or absence of 8 Chinese cabbage (CC), 8 Caixin (CX) and 8 Turnip (TU). SV1-5 is present in CC, but absent in other morphotypes. SV6-8 are present in CX, but not in other morphotypes. SV9 is absent in CX, but appears in other morphotypes. SV10 is absent in TU, and present in other morphotypes. Subspecies/morphotypes, SVs, as well as size and positions of DNA markers are indicated.

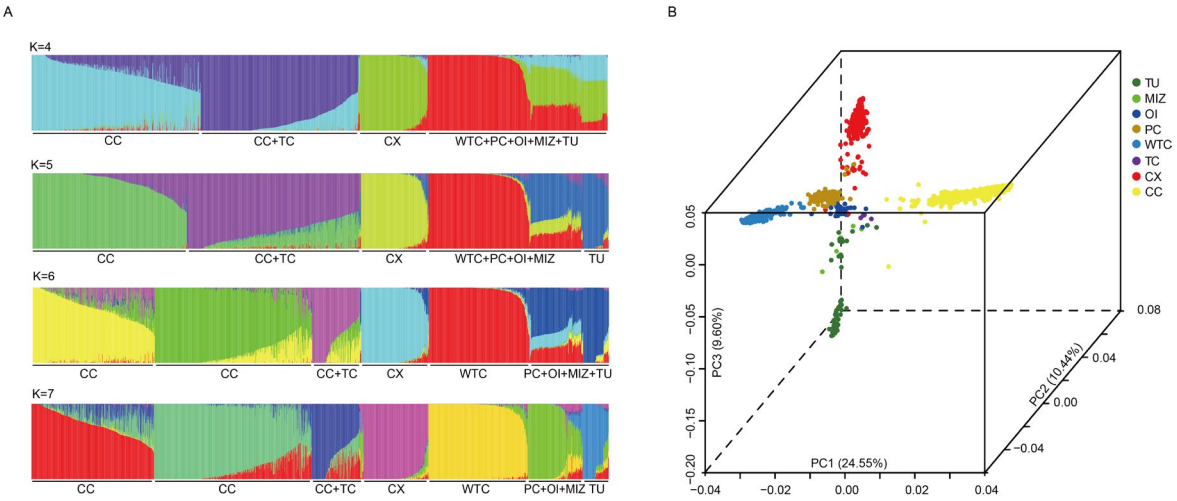

fig. S26. Population structure and principal component analysis (PCA) based on SVs in 1,720 *B. rapa* accessions.

(A) Structure of 1,720 *B. rapa* accessions based on SVs. Bar-plots showing the inferred ancestral components at K = 4 to 7. Each vertical bar represents a group of accessions. Colored segments within each bar indicate the proportional contributions from different ancestral population clusters. (B) Three-dimensional PCA of *B. rapa* accessions based on SVs. Each dot represents a group colored by morphotypes, including Turnip (TU), Mizuna (MIZ), Oilseed (OI), Pak choi (PC), Wutacai (WTC), Caixin (CX), Taicai (TC), and Chinese cabbage (CC). PC1, PC2, and PC3 explain 24.55%, 10.44%, and 9.60% of the total genetic variation, respectively.

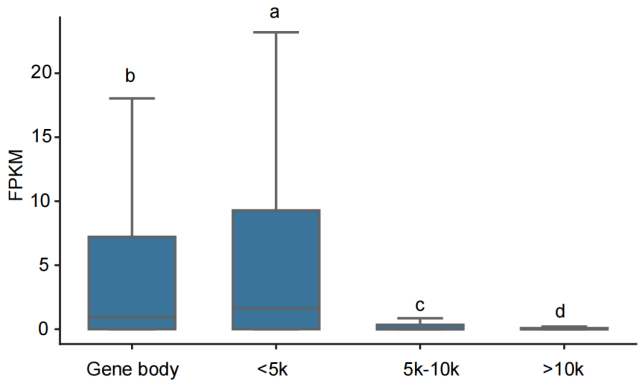

fig. S27. Gene expression corresponding to differential distances from SVs.
Significance testing between chromosomal regions were performed using Mann-Whitney U tests. The different lowercase letters above the box plots represent significant differences (P<0.05). FPKM: Fragments Per Kilobase of exon per Million mapped fragments.

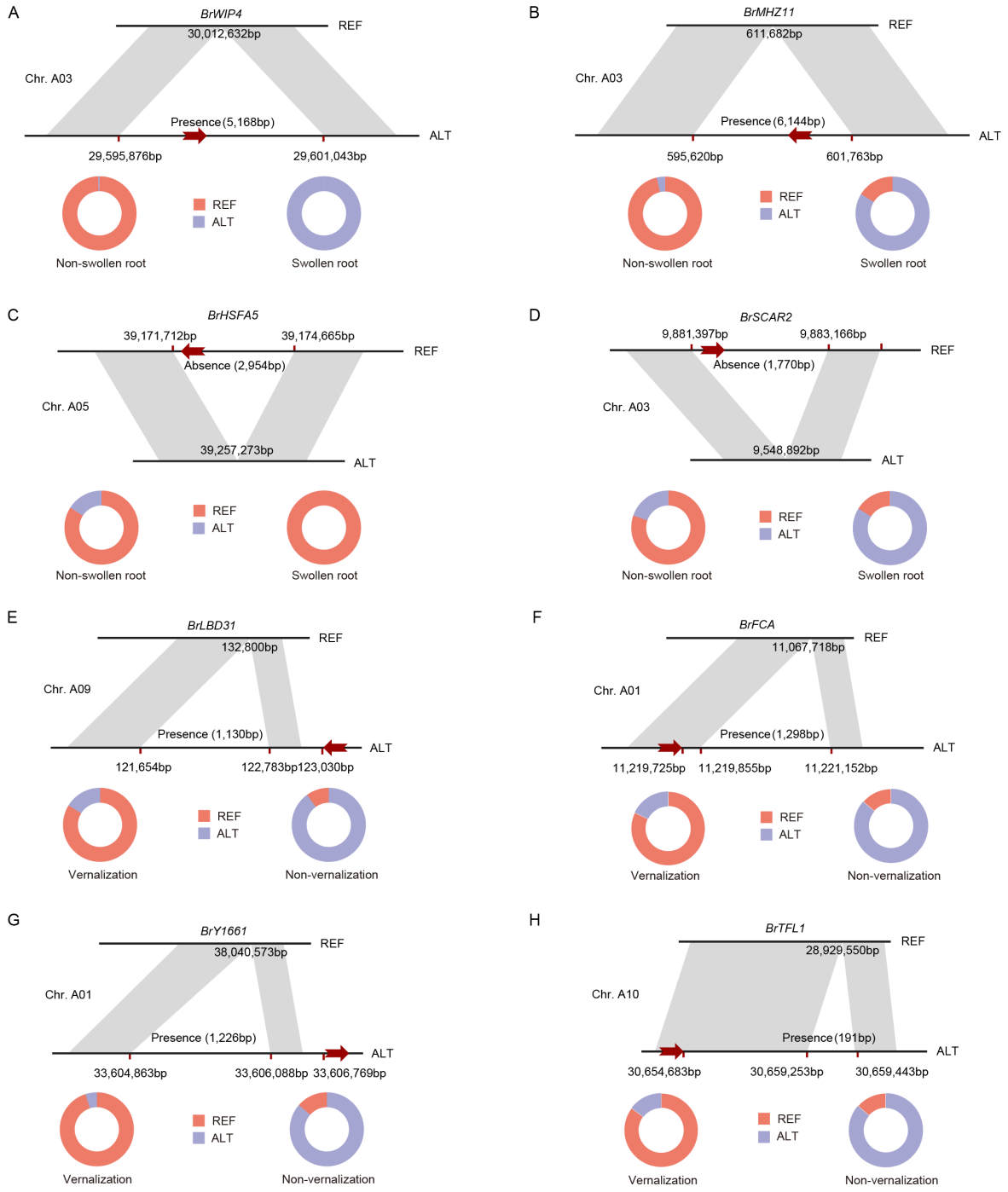

fig. S28. Presence-absence variation leads to gene function variation in different subspecies.

(**A**) In Turnip, a 5,168 bp fragment was identified, encompassing the entire coding region of *BrWIP4* gene. This fragment was present in 61/74 (82.43%) of Turnip accessions, but were only found in 9/1,642 (0.55%) non-Turnip accessions. (**B**) In Turnip, a 6,144 bp fragment was identified, encompassing the entire coding region of *BrMHZ11* gene. This fragment was present in 62/74 (83.78%) of Turnip accessions, but were only found in 59/1,642 (3.59%) non-Turnip accessions. (**C**) All 74 Turnip accessions did not contain a 2,954 bp fragment, whereas 1,381/1,642 (84.10%) of non-Turnip accessions contained this segment. This segment includes *BrHSFA5*. (**D**) 62/74 (83.78%) Turnip accessions did not

contain a 1,770 bp fragment, whereas 1,318/1,642 (80.33%) of non-Turnip accessions contained this segment. This segment includes *BrSCAR2*. (**E**) In Caixin, a 1,130 bp fragment was identified, encompassing the region of *BrLBD31* downstream. This fragment was present in 198/220 (90.00%) of Caixin accessions, but were only found in 242/1,496 (16.18%) non-Caixin accessions. (**F**) In Caixin, a 1,298 bp fragment was identified, encompassing the region of *BrFCA* downstream. This fragment was present in 190/220 (86.36%) of Caixin accessions, but were only found in 267/1,496 (17.85%) non-Caixin accessions. (**G)** In Caixin, a 1,226 bp fragment was identified, encompassing the region of *BrY1661* upstream. This fragment was present in 190/220 (86.36%) of Caixin accessions, but were only found in 74/1,496 (4.95%) non-Caixin accessions. (**H**) In Caixin, a 191 bp fragment was identified, encompassing the region of *BrTFL1* downstream. This fragment was present in 190/220 (86.36%) of Caixin accessions, but were only found in 220/1,496 (14.71%) non-Caixin accessions. REF represents the same sequence as the reference genome CCA03, and ALT indicates that the sequence is different from REF. Gray boxes represent the genomic collinearity region. Red arrows show related genes.

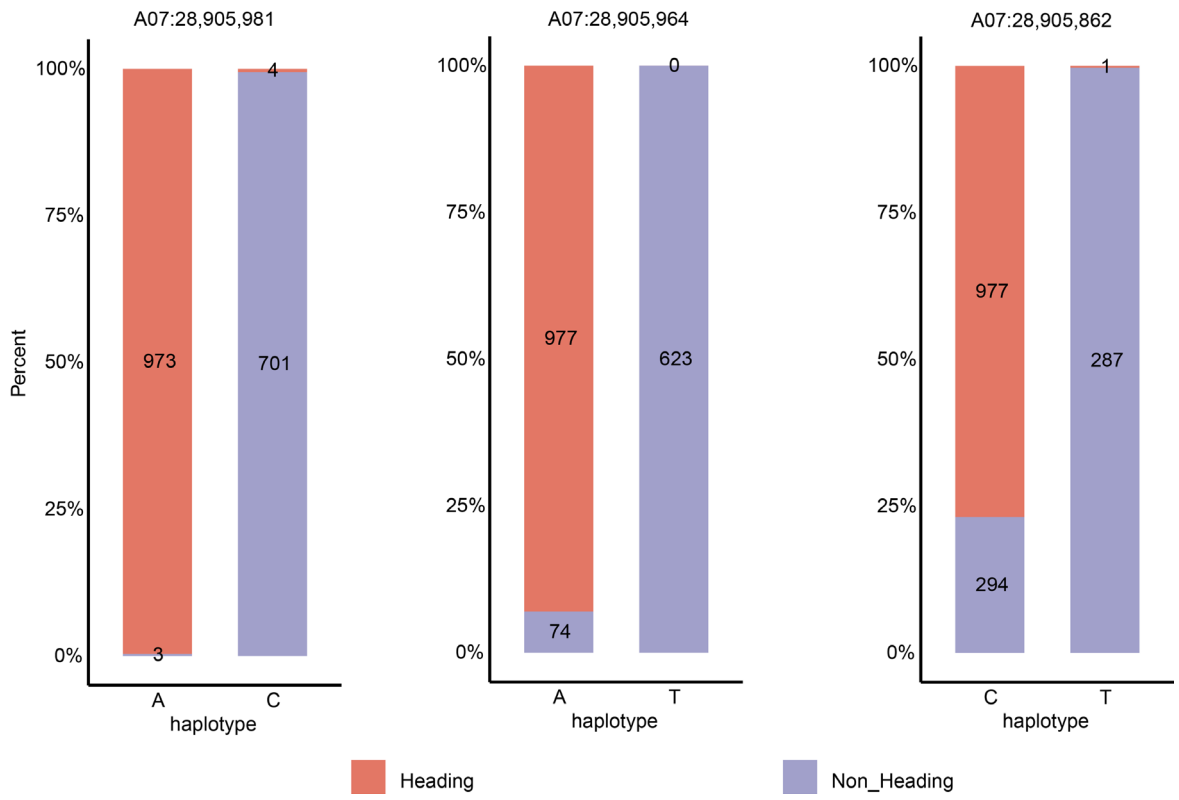

fig. S29. Haplotype analysis of three non-synonymous SNPs in *BrLH1*.
"Heading" denotes accessions forming leafy heads, whereas "Non-Heading" refers to those without head formation. The three panels display the genotype-to-phenotype associations for the three non-synonymous SNPs located at A07:28,905,981, A07:28,905,964, and A07:28,905,862 within the *BrLH1* gene. Each bar represents the proportion of accessions with or without heading in each haplotype. In our *B. rapa* population, the A-to-C SNP at A07:28,905,981, the A-to-T SNP at A07:28,905,964, and the C-to-T SNP at A07:28,905,862 reduces the proportion of heading accessions from 99.7% to 0.6%, 93.0% to 0%, and 96.9% to 0.3%, respectively. The three SNPs collectively exhibit substantial mutation effects and mutations at these SNPs are closely associated with the traits of heading and non-heading in *B. rapa*.

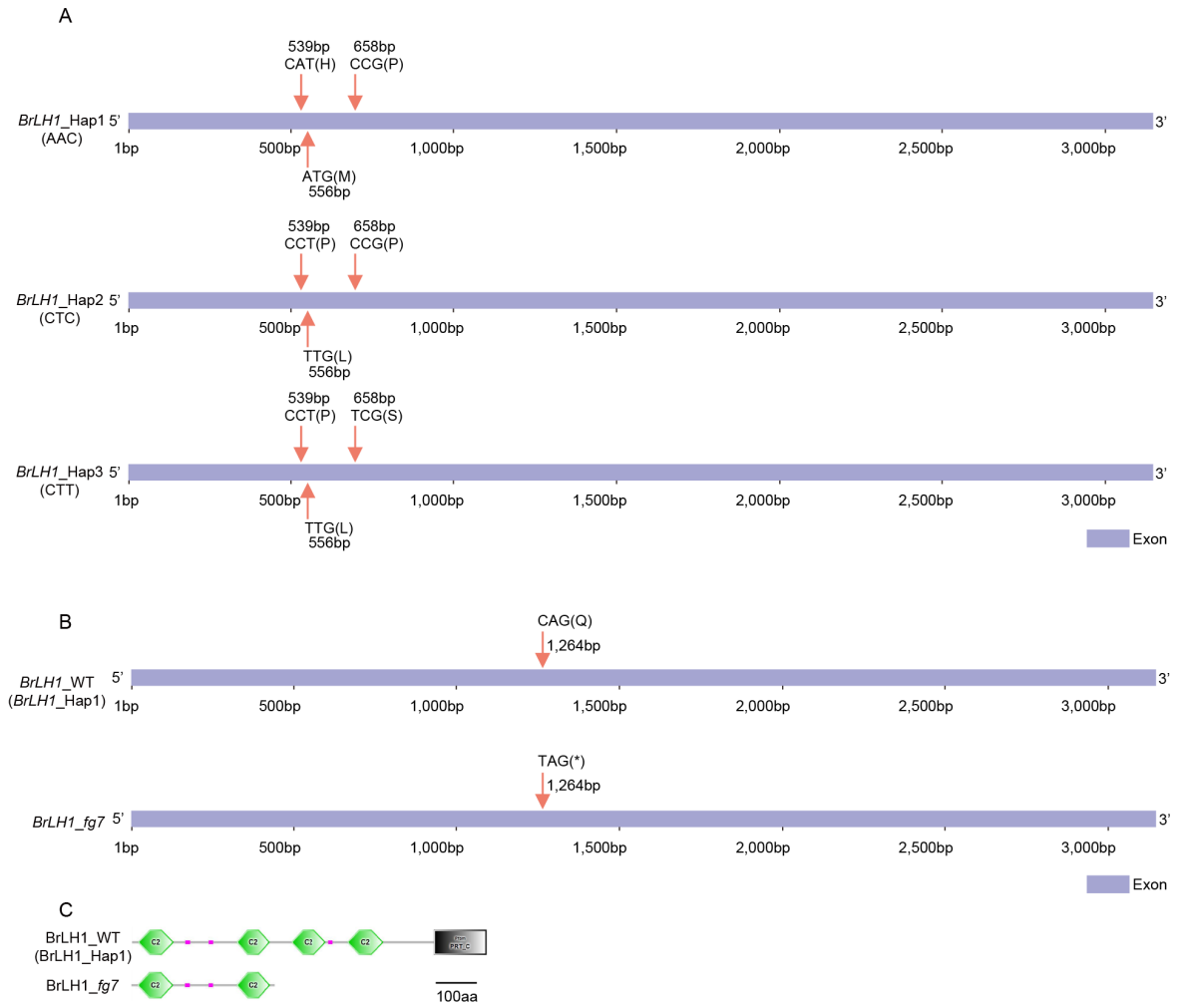

fig. S30. Identification of candidate gene at the loci for *fg7*.

(**A**) Pangenomic and genetic basis of heading vs non-heading in *B. rapa* subspecies. (**B, C**) Forward genetic analysis of candidate gene *BrLH1* responsible for non-heading phenotype in the Chinese cabbage *fg7* mutant. A C-to-T SNP was found in the *BrLH1* exon at nucleotide 1,264 bp. This SNP leads to introduce a premature stop codon in the *BrLH1* coding sequence (B), resulting in translational truncation of the wild-type 1,048 amino-acid (AA) BrLH1 protein to a 421-AA polypeptide (C). The codon for Q in wild-type *BrLH1*, the premature stop codon (*) in the *fg7* mutant *BrLH1* (*mBrLH1*), and relevant domains in BrLH1 and mBrLH1 proteins are indicated. C2 presents Protein kinase C conserved region 2. PRT_C is the functional domain Plant phosphoribosyltransferase C-terminal. Pink point represents the low complexity region. The domain was predicted in SMART (https://smart.embl.de/).

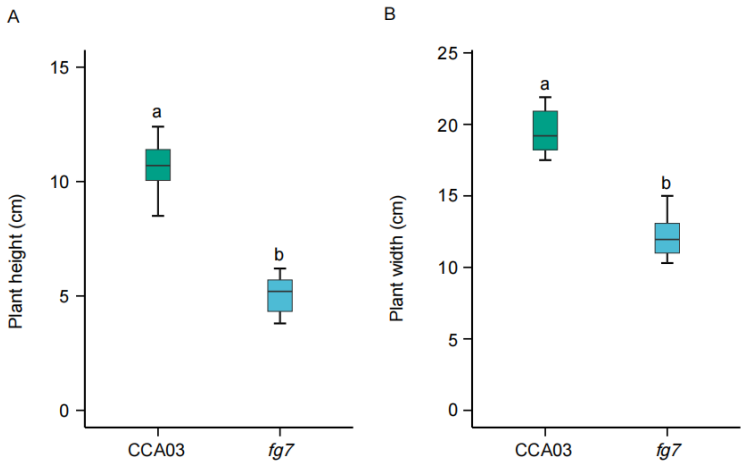

fig. S31. *BrLH1* genotype to phenotypes in *B. rapa*.
Plants height (**A**) and width (**B**) of wild type and mutant *fg7*. Different lowercase letters above the box plots represent significant differences ($P < 0.05$).

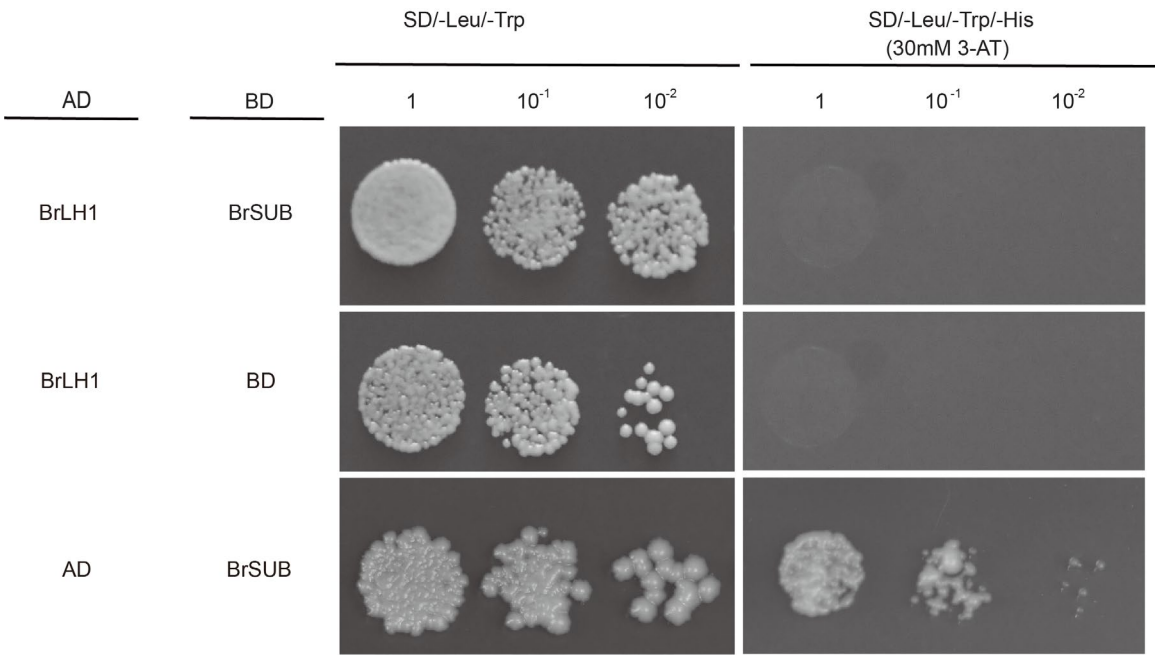

fig. S32. BrLH1 interacts directly with BrSUB in the yeast two-hybrid system.

The construct combinations were co-introduced into the yeast strain AH109. Transformants diluted to different concentrations were grown on the -Leu-Trp (lacking leucine and tryptophan) control plates and the -Leu-Trp-His (lacking leucine, tryptophan and histidine) with 30mM 3-AT (3-Amino-1,2,4-Triazole) selective plates for 3-4 days. The combination of BrLH1/pGBKT7 (empty vector) and pGADT7 (empty vector)/BrSUB as a negative control (BD: pGBKT7; AD: pGADT7).

Taken together, our results reveal how *BrLH1* and its protein product may genetically and biochemically modulate trait development in *B. rapa*.

(i) *BrLH1* belongs to the *SLM* gene family. It encodes a protein containing multiple C2 domains and transmembrane domains, known as MCTP (Multiple C2 domains and Transmembrane Region Proteins). In *B. rapa*, only a single copy of *BrLH1* exists and no other related homologs are found. The *BrLH1* homolog *QUIRKY* (*QKY*) in *Arabidopsis thaliana* is involved in regulating plant cell morphogenesis and cell patterning (*69*). *QKY* mutants exhibit various developmental defects, including disordered root epidermal cell patterns, abnormal floral organ development, twisted stems, and twisted leaves In *Arabidopsis* (*70,71*). QKY directly interacts with the STRUBBELIG (SUB) receptor-like kinase to stabilize SUB at the plasma membrane and maintain its level at the cell surface, which is essential for controlling how tissues develop. In additional, QKY also interacts with SCRAMBLED (SCM), which controls the CAPRICE protein movement to regulate root epidermal cell patterning. SUB mutants also display multiple developmental defects, such as twisted leaves and stems (*72*). Through yeast two-hybrid screening, we found that BrLH1 interacts with BrSUB (fig. S32). Thus, BrLH1 may involve BrSUB to modulate leaf heading in *B. rapa*.

(ii) *BrLH1* consists of 3,147 bp. The three non-synonymous SNPs locate at nucleotide 539, 556, and 658 in the gene, respectively. We notice that in the Chinese cabbage population, the A-to-C SNP at A07:28,905,981, the A-to-T SNP at A07:28,905,964, and the C-to-T SNP at A07:28,905,862 reduces the proportion of heading accessions from 99.7% to 0.6%, 93.0% to 0%, and 96.9% to 0.3%, respectively (fig. S29 and fig. S30A). The three SNPs exhibit substantial mutation effects and mutation at each SNP is closely associated with the traits of heading and non-heading in *B. rapa* (Fig. 5B, fig. S29 and fig. S30A).

(iii) The *fg7* mutant plants were dwarf (Fig. 5C). Why the accessions without AAC haplotype are not dwarf remains to be elucidated. *BrLH1* consists of 3,147 bp. Likely the C-to-T mutation at nucleotide 1,264 in *BrLH1* in *fg7* alters a sense codon to a non-sense stop codon (fig. S30, B to C), leading to premature termination of protein translation to produce a truncated 421-AA polypeptide rather than the wild-type 1,048-AA BrLH1 (fig. S30C). Such truncated polypeptide may completely lose its biological functions, leading to non-heading and plant growth reduction (i.e., the dwarf phenotypes) in *fg7*. In contrast, the three SNPs in *BrLH1* in natural populations without the AAC haplotype are all sense mutations, which cause only single amino-acid changes in BrLH1 protein. Such single-amino mutation may not impose any effect on BrLH1 to control plant growth but affects BrLH1 to modulate leaf heading. Consequently, these accessions cannot form leaf heads although they properly grow to normal plant sizes.

References and Notes

1. T. J. Davies, T. G. Barraclough, M. W. Chase, P. S. Soltis, D. E. Soltis, V. Savolainen, Darwin's abominable mystery: Insights from a supertree of the angiosperms. *Proc. Natl. Acad. Sci. U.S.A.* **101**, 1904–1909 (2004). 10.1073/pnas.0308127100 Medline

2. R. J. A. Buggs, The deepening of Darwin's abominable mystery. *Nat. Ecol. Evol.* **1**, 169 (2017). Medline

3. H. Yan, J. Han, S. Jin, Z. Han, Z. Si, S. Yan, L. Xuan, G. Yu, X. Guan, L. Fang, K. Wang, T. Zhang, Post-polyploidization centromere evolution in cotton. *Nat. Genet.* **57**, 1021–1030 (2025). 10.1038/s41588-025-02115-3 Medline

4. S. Secomandi, G. R. Gallo, R. Rossi, C. Rodríguez Fernandes, E. D. Jarvis, A. Bonisoli-Alquati, L. Gianfranceschi, G. Formenti, Pangenome graphs and their applications in biodiversity genomics. *Nat. Genet.* **57**, 13–26 (2025). 10.1038/s41588-024-02029-6 Medline

5. Y. Liu, H. Du, P. Li, Y. Shen, H. Peng, S. Liu, G. A. Zhou, H. Zhang, Z. Liu, M. Shi, X. Huang, Y. Li, M. Zhang, Z. Wang, B. Zhu, B. Han, C. Liang, Z. Tian, Pan-genome of wild and cultivated soybeans. *Cell* **182**, 162–176.e13 (2020). 10.1016/j.cell.2020.05.023 Medline

6. P. Qin, H. Lu, H. Du, H. Wang, W. Chen, Z. Chen, Q. He, S. Ou, H. Zhang, X. Li, X. Li, Y. Li, Y. Liao, Q. Gao, B. Tu, H. Yuan, B. Ma, Y. Wang, Y. Qian, S. Fan, W. Li, J. Wang, M. He, J. Yin, T. Li, N. Jiang, X. Chen, C. Liang, S. Li, Pan-genome analysis of 33 genetically diverse rice accessions reveals hidden genomic variations. *Cell* **184**, 3542–3558.e16 (2021). 10.1016/j.cell.2021.04.046 Medline

7. T. Shi, X. Zhang, Y. Hou, C. Jia, X. Dan, Y. Zhang, Y. Jiang, Q. Lai, J. Feng, J. Feng, T. Ma, J. Wu, S. Liu, L. Zhang, Z. Long, L. Chen, N. R. Street, P. K. Ingvarsson, J. Liu, T. Yin, J. Wang, The super-pangenome of *Populus* unveils genomic facets for its adaptation and diversification in widespread forest trees. *Mol. Plant* **17**, 725–746 (2024). 10.1016/j.molp.2024.03.009 Medline

8. Y. Zhang, M. Zhao, J. Tan, M. Huang, X. Chu, Y. Li, X. Han, T. Fang, Y. Tian, R. Jarret, D. Lu, Y. Chen, L. Xue, X. Li, G. Qin, B. Li, Y. Sun, X. W. Deng, Y. Deng, X. Zhang, H. He, Telomere-to-telomere Citrullus super-pangenome provides direction for watermelon breeding. *Nat. Genet.* **56**, 1750–1761 (2024). 10.1038/s41588-024-01823-6 Medline

9. Z. Liu, N. Wang, Y. Su, Q. Long, Y. Peng, L. Shangguan, F. Zhang, S. Cao, X. Wang, M. Ge, H. Xue, Z. Ma, W. Liu, X. Xu, C. Li, X. Cao, B. Ahmad, X. Su, Y. Liu, G. Huang, M. Du, Z. Liu, Y. Gan, L. Sun, X. Fan, C. Zhang, H. Zhong, X. Leng, Y. Ren, T. Dong, D. Pei, X. Wu, Z. Jin, Y. Wang, C. Liu, J. Chen, B. Gaut, S. Huang, J. Fang, H. Xiao, Y. Zhou, Grapevine pangenome

facilitates trait genetics and genomic breeding. *Nat. Genet.* **56**, 2804–2814 (2024). 10.1038/s41588-024-01967-5 Medline

10. F. Cheng, R. Sun, X. Hou, H. Zheng, F. Zhang, Y. Zhang, B. Liu, J. Liang, M. Zhuang, Y. Liu, D. Liu, X. Wang, P. Li, Y. Liu, K. Lin, J. Bucher, N. Zhang, Y. Wang, H. Wang, J. Deng, Y. Liao, K. Wei, X. Zhang, L. Fu, Y. Hu, J. Liu, C. Cai, S. Zhang, S. Zhang, F. Li, H. Zhang, J. Zhang, N. Guo, Z. Liu, J. Liu, C. Sun, Y. Ma, H. Zhang, Y. Cui, M. R. Freeling, T. Borm, G. Bonnema, J. Wu, X. Wang, Subgenome parallel selection is associated with morphotype diversification and convergent crop domestication in *Brassica rapa* and *Brassica oleracea*. *Nat. Genet.* **48**, 1218–1224 (2016). 10.1038/ng.3634 Medline

11. X. Cai, L. Chang, T. Zhang, H. Chen, L. Zhang, R. Lin, J. Liang, J. Wu, M. Freeling, X. Wang, Impacts of allopolyploidization and structural variation on intraspecific diversification in *Brassica rapa*. *Genome Biol.* **22**, 166–190 (2021). 10.1186/s13059-021-02383-2 Medline

12. A. C. McAlvay, A. P. Ragsdale, M. E. Mabry, X. Qi, K. A. Bird, P. Velasco, H. An, J. C. Pires, E. Emshwiller, *Brassica rapa* domestication: Untangling wild and feral forms and convergence of crop morphotypes. *Mol. Biol. Evol.* **38**, 3358–3372 (2021). 10.1093/molbev/msab108 Medline

13. X. Qi, H. An, A. P. Ragsdale, T. E. Hall, R. N. Gutenkunst, J. Chris Pires, M. S. Barker, Genomic inferences of domestication events are corroborated by written records in *Brassica rapa*. *Mol. Ecol.* **26**, 3373–3388 (2017). 10.1111/mec.14131 Medline

14. Y. Zhou, H. Ye, E. Liu, J. Tian, L. Song, Z. Ren, M. Wang, Z. Sun, L. Tang, Z. Ren, J. Li, Q. Nie, A. Wang, K. Wang, The complexity of structural variations in *Brassica rapa* revealed by assembly of two complete T2T genomes. *Sci. Bull.* **69**, 2346–2351 (2024). 10.1016/j.scib.2024.03.030 Medline

15. L. Zhang, J. Liang, H. Chen, Z. Zhang, J. Wu, X. Wang, A near-complete genome assembly of *Brassica rapa* provides new insights into the evolution of centromeres. *Plant Biotechnol. J.* **21**, 1022–1032 (2023). 10.1111/pbi.14015 Medline

16. A. Rhie, B. P. Walenz, S. Koren, A. M. Phillippy, Merqury: Reference-free quality, completeness, and phasing assessment for genome assemblies. *Genome Biol.* **21**, 245–272 (2020). 10.1186/s13059-020-02134-9 Medline

17. S. Ou, J. Chen, N. Jiang, Assessing genome assembly quality using the LTR Assembly Index (LAI). *Nucleic Acids Res.* **46**, e126 (2018). 10.1093/nar/gky730 Medline

18. K. L. McKinley, I. M. Cheeseman, The molecular basis for centromere identity and function. *Nat. Rev. Mol. Cell Biol.* **17**, 16–29 (2016). 10.1038/nrm.2015.5

Medline

19. M. Han, Y. Yang, M. Zhang, K. Wang, Considerations regarding centromere assembly in plant whole-genome sequencing. *Methods* **187**, 54–56 (2021). 10.1016/j.ymeth.2020.09.006 Medline

20. K. B. Lim, H. de Jong, T. J. Yang, J. Y. Park, S. J. Kwon, J. S. Kim, M. H. Lim, J. A. Kim, M. Jin, Y. M. Jin, S. H. Kim, Y. P. Lim, J. W. Bang, H. I. Kim, B. S. Park, Characterization of rDNAs and tandem repeats in the heterochromatin of *Brassica rapa*. *Mol. Cells* **19**, 436–444 (2005). 10.1016/S1016-8478(23)13190-6 Medline

21. J. M. Song, W. Z. Xie, S. Wang, Y. X. Guo, D. H. Koo, D. Kudrna, C. Gong, Y. Huang, J. W. Feng, W. Zhang, Y. Zhou, A. Zuccolo, E. Long, S. Lee, J. Talag, R. Zhou, X. T. Zhu, D. Yuan, J. Udall, W. Xie, R. A. Wing, Q. Zhang, J. Poland, J. Zhang, L. L. Chen, Two gap-free reference genomes and a global view of the centromere architecture in rice. *Mol. Plant* **14**, 1757–1767 (2021). 10.1016/j.molp.2021.06.018 Medline

22. X. Chang, X. He, J. Li, Z. Liu, R. Pi, X. Luo, R. Wang, X. Hu, S. Lu, X. Zhang, M. Wang, High-quality *Gossypium hirsutum* and *Gossypium barbadense* genome assemblies reveal the landscape and evolution of centromeres. *Plant Commun.* **5**, 100722–100735 (2024). 10.1016/j.xplc.2023.100722 Medline

23. H. Zhao, X. Zhu, K. Wang, J. I. Gent, W. Zhang, R. K. Dawe, J. Jiang, Gene expression and chromatin modifications associated with maize centromeres. *G3* **6**, 183–192 (2015). 10.1534/g3.115.022764 Medline

24. J. Chen, Z. Wang, K. Tan, W. Huang, J. Shi, T. Li, J. Hu, K. Wang, C. Wang, B. Xin, H. Zhao, W. Song, M. B. Hufford, J. C. Schnable, W. Jin, J. Lai, A complete telomere-to-telomere assembly of the maize genome. *Nat. Genet.* **55**, 1221–1231 (2023). 10.1038/s41588-023-01419-6 Medline

25. G. Hu, Z. Wang, Z. Tian, K. Wang, G. Ji, X. Wang, X. Zhang, Z. Yang, X. Liu, R. Niu, D. Zhu, Y. Zhang, L. Duan, X. Ma, X. Xiong, J. Kong, X. Zhao, Y. Zhang, J. Zhao, S. He, C. E. Grover, J. Su, K. Feng, G. Yu, J. Han, X. Zang, Z. Wu, W. Pan, J. F. Wendel, X. Ma, A telomere-to-telomere genome assembly of cotton provides insights into centromere evolution and short-season adaptation. *Nat. Genet.* **57**, 1031–1043 (2025). 10.1038/s41588-025-02130-4 Medline

26. Y. Wang, L. Zhao, D. Wang, K. Chen, T. Luo, J. Luo, C. Jiang, Z. He, H. Huang, J. Xie, Y. Jiang, J. Liu, T. Ma, Four near-complete genome assemblies reveal the landscape and evolution of centromeres in Salicaceae. *Genome Biol.* **26**, 111–137 (2025). 10.1186/s13059-025-03578-7 Medline

27. W. Wang, R. Guan, X. Liu, H. Zhang, B. Song, Q. Xu, G. Fan, W. Chen, X. Wu, X. Liu, J. Wang, Chromosome level comparative analysis of *Brassica*

genomes. *Plant Mol. Biol.* **99**, 237–249 (2019). 10.1007/s11103-018-0814-x Medline

28. S. Perumal, C. S. Koh, L. Jin, M. Buchwaldt, E. E. Higgins, C. Zheng, D. Sankoff, S. J. Robinson, S. Kagale, Z. K. Navabi, L. Tang, K. N. Horner, Z. He, I. Bancroft, B. Chalhoub, A. G. Sharpe, I. A. P. Parkin, A high-contiguity *Brassica nigra* genome localizes active centromeres and defines the ancestral *Brassica* genome. *Nat. Plants* **6**, 929–941 (2020). 10.1038/s41477-020-0735-y Medline

29. K. Paritosh, A. K. Pradhan, D. Pental, A highly contiguous genome assembly of *Brassica nigra* (BB) and revised nomenclature for the pseudochromosomes. *BMC Genomics* **21**, 887–899 (2020). 10.1186/s12864-020-07271-w Medline

30. X. Li, Y. Wang, C. Cai, J. Ji, F. Han, L. Zhang, S. Chen, L. Zhang, Y. Yang, Q. Tang, J. Bucher, X. Wang, L. Yang, M. Zhuang, K. Zhang, H. Lv, G. Bonnema, Y. Zhang, F. Cheng, Large-scale gene expression alterations introduced by structural variation drive morphotype diversification in *Brassica oleracea*. *Nat. Genet.* **56**, 517–529 (2024). 10.1038/s41588-024-01655-4 Medline

31. J. Yang, D. Liu, X. Wang, C. Ji, F. Cheng, B. Liu, Z. Hu, S. Chen, D. Pental, Y. Ju, P. Yao, X. Li, K. Xie, J. Zhang, J. Wang, F. Liu, W. Ma, J. Shopan, H. Zheng, S. A. Mackenzie, M. Zhang, The genome sequence of allopolyploid *Brassica juncea* and analysis of differential homoeolog gene expression influencing selection. *Nat. Genet.* **48**, 1225–1232 (2016). 10.1038/ng.3657 Medline

32. J. Yang, J. Wang, Z. Li, X. Li, Z. He, L. Zhang, T. Sha, X. Lyu, S. Chen, Y. Gu, Z. Li, Z. Hu, H. He, I. Bancroft, M. Zhang, Genomic signatures of vegetable and oilseed allopolyploid *Brassica juncea* and genetic loci controlling the accumulation of glucosinolates. *Plant Biotechnol. J.* **19**, 2619–2628 (2021). 10.1111/pbi.13687 Medline

33. K. Paritosh, S. K. Yadava, P. Singh, L. Bhayana, A. Mukhopadhyay, V. Gupta, N. C. Bisht, J. Zhang, D. A. Kudrna, D. Copetti, R. A. Wing, V. B. Reddy Lachagari, A. K. Pradhan, D. Pental, A chromosome-scale assembly of allotetraploid *Brassica juncea* (AABB) elucidates comparative architecture of the A and B genomes. *Plant Biotechnol. J.* **19**, 602–614 (2021). 10.1111/pbi.13492 Medline

34. K. B. Lim, T. J. Yang, Y. J. Hwang, J. S. Kim, J. Y. Park, S. J. Kwon, J. Kim, B. S. Choi, M. H. Lim, M. Jin, H. I. Kim, H. de Jong, I. Bancroft, Y. Lim, B. S. Park, Characterization of the centromere and peri-centromere retrotransposons in *Brassica rapa* and their distribution in related *Brassica* species. *Plant J.* **49**, 173–183 (2007). 10.1111/j.1365-313X.2006.02952.x Medline

35. J. M. Song, Z. Guan, J. Hu, C. Guo, Z. Yang, S. Wang, D. Liu, B. Wang, S. Lu, R. Zhou, W. Z. Xie, Y. Cheng, Y. Zhang, K. Liu, Q. Y. Yang, L. L. Chen, L. Guo, Eight high-quality genomes reveal pan-genome architecture and ecotype differentiation of *Brassica napus*. *Nat. Plants* **6**, 34–45 (2020). 10.1038/s41477-019-0577-7 Medline

36. X. Song, Y. Wei, D. Xiao, K. Gong, P. Sun, Y. Ren, J. Yuan, T. Wu, Q. Yang, X. Li, F. Nie, N. Li, S. Feng, Q. Pei, T. Yu, C. Zhang, T. Liu, X. Wang, J. Yang, *Brassica carinata* genome characterization clarifies U's triangle model of evolution and polyploidy in *Brassica*. *Plant Physiol.* **186**, 388–406 (2021). 10.1093/plphys/kiab048 Medline

37. W. C. Yim, M. L. Swain, D. Ma, H. An, K. A. Bird, D. D. Curdie, S. Wang, H. D. Ham, A. Luzuriaga-Neira, J. S. Kirkwood, M. Hur, J. K. Q. Solomon, J. F. Harper, D. K. Kosma, D. Alvarez-Ponce, J. C. Cushman, P. P. Edger, A. S. Mason, J. C. Pires, H. Tang, X. Zhang, The final piece of the Triangle of U: Evolution of the tetraploid *Brassica carinata* genome. *Plant Cell* **34**, 4143–4172 (2022). 10.1093/plcell/koac249 Medline

38. Y. Niu, Q. Liu, Z. He, R. Raman, H. Wang, X. Long, H. Qin, H. Raman, I. A. P. Parkin, I. Bancroft, J. Zou, A *Brassica carinata* pan-genome platform for *Brassica* crop improvement. *Plant Commun.* **5**, 100725 (2024). 10.1016/j.xplc.2023.100725 Medline

39. X. Hou, D. Wang, Z. Cheng, Y. Wang, Y. Jiao, A near-complete assembly of an *Arabidopsis thaliana* genome. *Mol. Plant* **15**, 1247–1250 (2022). 10.1016/j.molp.2022.05.014 Medline

40. E. Janková Drdová, M. Klejchová, K. Janko, M. Hála, H. Soukupová, F. Cvrčková, V. Žárský, Developmental plasticity of Arabidopsis hypocotyl is dependent on exocyst complex function. *J. Exp. Bot.* **70**, 1255–1265 (2019). 10.1093/jxb/erz005 Medline

41. D. Safavian, Y. Zayed, E. Indriolo, L. Chapman, A. Ahmed, D. R. Goring, RNA silencing of exocyst genes in the stigma impairs the acceptance of compatible pollen in Arabidopsis. *Plant Physiol.* **169**, 2526–2538 (2015). 10.1104/pp.15.00635 Medline

42. M. Fendrych, L. Synek, T. Pecenková, H. Toupalová, R. Cole, E. Drdová, J. Nebesárová, M. Sedinová, M. Hála, J. E. Fowler, V. Zársky, The Arabidopsis exocyst complex is involved in cytokinesis and cell plate maturation. *Plant Cell* **22**, 3053–3065 (2010). 10.1105/tpc.110.074351 Medline

43. B. Touraine, J. P. Boutin, A. Marion-Poll, J. F. Briat, G. Peltier, S. Lobréaux, Nfu2: A scaffold protein required for [4Fe-4S] and ferredoxin iron-sulphur cluster assembly in *Arabidopsis* chloroplasts. *Plant J.* **40**, 101–111 (2004). 10.1111/j.1365-313X.2004.02189.x Medline

44. J. H. M. Schippers, A. Nunes-Nesi, R. Apetrei, J. Hille, A. R. Fernie, P. P. Dijkwel, The *Arabidopsis* onset of leaf death5 mutation of quinolinate synthase affects nicotinamide adenine dinucleotide biosynthesis and causes early ageing. *Plant Cell* **20**, 2909–2925 (2008). 10.1105/tpc.107.056341 Medline

45. K. Chapman, A. Ivanovici, M. Taleski, C. J. Sturrock, J. L. P. Ng, N. A. Mohd-Radzman, F. Frugier, M. J. Bennett, U. Mathesius, M. A. Djordjevic, CEP receptor signalling controls root system architecture in *Arabidopsis* and Medicago. *New Phytol.* **226**, 1809–1821 (2020). 10.1111/nph.16483 Medline

46. A. C. Bryan, A. Obaidi, M. Wierzba, F. E. Tax, XYLEM INTERMIXED WITH PHLOEM1, a leucine-rich repeat receptor-like kinase required for stem growth and vascular development in *Arabidopsis thaliana*. *Planta* **235**, 111–122 (2012). 10.1007/s00425-011-1489-6 Medline

47. D. R. Gallie, Z. Chen, Chloroplast-localized iron superoxide dismutases FSD2 and FSD3 are functionally distinct in *Arabidopsis*. *PLOS ONE* **14**, e0220078 (2019). 10.1371/journal.pone.0220078 Medline

48. F. Myouga, C. Hosoda, T. Umezawa, H. Iizumi, T. Kuromori, R. Motohashi, Y. Shono, N. Nagata, M. Ikeuchi, K. Shinozaki, A heterocomplex of iron superoxide dismutases defends chloroplast nucleoids against oxidative stress and is essential for chloroplast development in *Arabidopsis*. *Plant Cell* **20**, 3148–3162 (2008). 10.1105/tpc.108.061341 Medline

49. M. Šustr, H. Konrádová, M. Martinčová, A. Soukup, E. Tylová, Potassium transporter KUP9 regulates plant response to K^+ deficiency and affects carbohydrate allocation in *A.thaliana*. *J. Plant Physiol.* **292**, 154147 (2024). 10.1016/j.jplph.2023.154147 Medline

50. M. Okamoto, A. Kumar, W. Li, Y. Wang, M. Y. Siddiqi, N. M. Crawford, A. D. Glass, High-affinity nitrate transport in roots of *Arabidopsis* depends on expression of the *NAR2*-like gene *AtNRT3.1*. *Plant Physiol.* **140**, 1036–1046 (2006). 10.1104/pp.105.074385 Medline

51. M. Kang, H. Wu, H. Liu, W. Liu, M. Zhu, Y. Han, W. Liu, C. Chen, Y. Song, L. Tan, K. Yin, Y. Zhao, Z. Yan, S. Lou, Y. Zan, J. Liu, The pan-genome and local adaptation of *Arabidopsis thaliana*. *Nat. Commun.* **14**, 6259 (2023). 10.1038/s41467-023-42029-4 Medline

52. J. Du, M. Li, D. Kong, L. Wang, Q. Lv, J. Wang, F. Bao, Q. Gong, J. Xia, Y. He, Nitric oxide induces cotyledon senescence involving co-operation of the *NES1*/*MAD1* and *EIN2*-associated *ORE1* signalling pathways in *Arabidopsis*. *J. Exp. Bot.* **65**, 4051–4063 (2014). 10.1093/jxb/ert429 Medline

53. C. Belser, B. Istace, E. Denis, M. Dubarry, F. C. Baurens, C. Falentin, M. Genete, W. Berrabah, A. M. Chèvre, R. Delourme, G. Deniot, F. Denoeud, P. Duffé, S.

Engelen, A. Lemainque, M. Manzanares-Dauleux, G. Martin, J. Morice, B. Noel, X. Vekemans, A. D'Hont, M. Rousseau-Gueutin, V. Barbe, C. Cruaud, P. Wincker, J. M. Aury, Chromosome-scale assemblies of plant genomes using nanopore long reads and optical maps. *Nat. Plants* **4**, 879–887 (2018). 10.1038/s41477-018-0289-4 Medline

54. K. Yue, P. Sandal, E. L. Williams, E. Murphy, E. Stes, N. Nikonorova, P. Ramakrishna, N. Czyzewicz, L. Montero-Morales, R. Kumpf, Z. Lin, B. van de Cotte, M. Iqbal, M. Van Bel, E. Van De Slijke, M. R. Meyer, A. Gadeyne, C. Zipfel, G. De Jaeger, M. Van Montagu, D. Van Damme, K. Gevaert, A. G. Rao, T. Beeckman, I. De Smet, PP2A-3 interacts with ACR4 and regulates formative cell division in the *Arabidopsis* root. *Proc. Natl. Acad. Sci. U.S.A.* **113**, 1447–1452 (2016). 10.1073/pnas.1525122113 Medline

55. E. Ramireddy, L. Chang, T. Schmülling, Cytokinin as a mediator for regulating root system architecture in response to environmental cues. *Plant Signal. Behav.* **9**, e27771 (2014). 10.4161/psb.27771 Medline

56. J. R. Haag, O. Pontes, C. S. Pikaard, Metal A and metal B sites of nuclear RNA polymerases Pol IV and Pol V are required for siRNA-dependent DNA methylation and gene silencing. *PLOS ONE* **4**, e4110 (2009). 10.1371/journal.pone.0004110 Medline

57. N. Dharmasiri, S. Dharmasiri, D. Weijers, N. Karunarathna, G. Jurgens, M. Estelle, *AXL* and *AXR1* have redundant functions in RUB conjugation and growth and development in Arabidopsis. *Plant J.* **52**, 114–123 (2007). 10.1111/j.1365-313X.2007.03211.x Medline

58. J. O. Narciso, W. Zeng, K. Ford, E. R. Lampugnani, J. Humphries, I. Austarheim, A. van de Meene, A. Bacic, M. S. Doblin, Biochemical and functional characterization of GALT8, an *Arabidopsis* GT31 β-(1,3)-galactosyltransferase that influences seedling development. *Front. Plant Sci.* **12**, 678564 (2021). 10.3389/fpls.2021.678564 Medline

59. Q. Li, X. Qiao, L. Li, C. Gu, H. Yin, K. Qi, Z. Xie, S. Yang, Q. Zhao, Z. Wang, Y. Yang, J. Pan, H. Li, J. Wang, C. Wang, L. H. Rieseberg, S. Zhang, S. Tao, Haplotype-resolved T2T genome assemblies and pangenome graph of pear reveal diverse patterns of allele-specific expression and the genomic basis of fruit quality traits. *Plant Commun.* **5**, 101000–101021 (2024). 10.1016/j.xplc.2024.101000 Medline

60. X. Yu, M. Qu, P. Wu, M. Zhou, E. Lai, H. Liu, S. Guo, S. Li, X. Yao, L. Gao, Super pan-genome reveals extensive genomic variations associated with phenotypic divergence in Actinidia. *Mol. Hortic.* **5**, 4–20 (2025). 10.1186/s43897-024-00123-1 Medline

61. N. Li, Q. He, J. Wang, B. Wang, J. Zhao, S. Huang, T. Yang, Y. Tang, S. Yang, P.

Aisimutuola, R. Xu, J. Hu, C. Jia, K. Ma, Z. Li, F. Jiang, J. Gao, H. Lan, Y. Zhou, X. Zhang, S. Huang, Z. Fei, H. Wang, H. Li, Q. Yu, Super-pangenome analyses highlight genomic diversity and structural variation across wild and cultivated tomato species. *Nat. Genet.* **55**, 852–860 (2023). 10.1038/s41588-023-01340-y Medline

62. Z. Wu, D. Zhu, X. Lin, J. Miao, L. Gu, X. Deng, Q. Yang, K. Sun, D. Zhu, X. Cao, T. Tsuge, C. Dean, T. Aoyama, H. Gu, L. J. Qu, RNA binding proteins RZ-1B and RZ-1C play critical roles in regulating pre-mRNA splicing and gene expression during development in *Arabidopsis*. *Plant Cell* **28**, 55–73 (2016). 10.1105/tpc.15.00949 Medline

63. B. C. W. Crawford, J. Sewell, G. Golembeski, C. Roshan, J. A. Long, M. F. Yanofsky, Genetic control of distal stem cell fate within root and embryonic meristems. *Science* **347**, 655–659 (2015). 10.1126/science.aaa0196 Medline

64. M. Cerise, V. da Silveira Falavigna, G. Rodríguez-Maroto, A. Signol, E. Severing, H. Gao, A. van Driel, C. Vincent, S. Wilkens, F. R. Iacobini, P. Formosa-Jordan, A. Pajoro, G. Coupland, Two modes of gene regulation by TFL1 mediate its dual function in flowering time and shoot determinacy of *Arabidopsis*. *Development* **150**, dev202089 (2023). 10.1242/dev.202089 Medline

65. Y. Wang, Z. Tao, W. Wang, D. Filiault, C. Qiu, C. Wang, H. Wang, S. Rehman, J. Shi, Y. Zhang, P. Li, Molecular variation in a functionally divergent homolog of FCA regulates flowering time in *Arabidopsis thaliana*. *Nat. Commun.* **11**, 5830–5844 (2020). 10.1038/s41467-020-19666-0 Medline

66. X. Zhang, W. Ma, M. Liu, X. Li, J. Li, Y. Lu, G. Li, S. Zhang, D. Feng, Y. Wang, H. Liang, S. Luo, N. Li, A. Gu, S. Xuan, X. Chen, S. Shen, J. Zhao, OCTOPUS regulates BIN2 to control leaf curvature in Chinese cabbage. *Proc. Natl. Acad. Sci. U.S.A.* **119**, e2208978119 (2022). 10.1073/pnas.2208978119 Medline

67. X. Sun, X. Li, Y. Lu, S. Wang, X. Zhang, K. Zhang, X. Su, M. Liu, D. Feng, S. Luo, A. Gu, Y. Fu, X. Chen, S. Xuan, Y. Wang, D. Xu, S. Chen, W. Ma, S. Shen, F. Cheng, J. Zhao, Construction of a high-density mutant population of Chinese cabbage facilitates the genetic dissection of agronomic traits. *Mol. Plant* **15**, 913–924 (2022). 10.1016/j.molp.2022.02.006 Medline

68. W. Ma, P. Zhang, J. Zhao, Y. Hong, Chinese cabbage: An emerging model for functional genomics in leafy vegetable crops. *Trends Plant Sci.* **28**, 515–518 (2023). 10.1016/j.tplants.2023.02.008 Medline

69. C. Trehin, S. Schrempp, A. Chauvet, A. Berne-Dedieu, A. M. Thierry, J. E. Faure, I. Negrutiu, P. Morel, *QUIRKY* interacts with *STRUBBELIG* and *PAL OF QUIRKY* to regulate cell growth anisotropy during *Arabidopsis* gynoecium

development. *Development* **140**, 4807–4817 (2013). 10.1242/dev.091868 Medline

70. L. Fulton, M. Batoux, P. Vaddepalli, R. K. Yadav, W. Busch, S. U. Andersen, S. Jeong, J. U. Lohmann, K. Schneitz, *DETORQUEO, QUIRKY*, and *ZERZAUST* represent novel components involved in organ development mediated by the receptor-like kinase STRUBBELIG in *Arabidopsis thaliana*. *PLOS Genet.* **5**, e1000355 (2009). 10.1371/journal.pgen.1000355 Medline

71. J. H. Song, S. H. Kwak, K. H. Nam, J. Schiefelbein, M. M. Lee, QUIRKY regulates root epidermal cell patterning through stabilizing SCRAMBLED to control CAPRICE movement in *Arabidopsis*. *Nat. Commun.* **10**, 1744–1756 (2019). 10.1038/s41467-019-09715-8 Medline

72. P. Vaddepalli, L. Fulton, M. Batoux, R. K. Yadav, K. Schneitz, Structure-function analysis of STRUBBELIG, an Arabidopsis atypical receptor-like kinase involved in tissue morphogenesis. *PLOS ONE* **6**, e19730 (2011). 10.1371/journal.pone.0019730 Medline

73. P. Wlodzimierz, F. A. Rabanal, R. Burns, M. Naish, E. Primetis, A. Scott, T. Mandáková, N. Gorringe, A. J. Tock, D. Holland, K. Fritschi, A. Habring, C. Lanz, C. Patel, T. Schlegel, M. Collenberg, M. Mielke, M. Nordborg, F. Roux, G. Shirsekar, C. Alonso-Blanco, M. A. Lysak, P. Y. Novikova, A. Bousios, D. Weigel, I. R. Henderson, Cycles of satellite and transposon evolution in *Arabidopsis* centromeres. *Nature* **618**, 557–565 (2023). 10.1038/s41586-023-06062-z Medline

74. B. G. Mellone, D. Fachinetti, Diverse mechanisms of centromere specification. *Curr. Biol.* **31**, R1491–R1504 (2021). 10.1016/j.cub.2021.09.083 Medline

75. Q. Hou, X. An, B. Ma, S. Wu, X. Wei, T. Yan, Y. Zhou, T. Zhu, K. Xie, D. Zhang, Z. Li, L. Zhao, C. Niu, Y. Long, C. Liu, W. Zhao, F. Ni, J. Li, D. Fu, Z. N. Yang, X. Wan, ZmMS1/ZmLBD30-orchestrated transcriptional regulatory networks precisely control pollen exine development. *Mol. Plant* **16**, 1321–1338 (2023). 10.1016/j.molp.2023.07.010 Medline

76. Z. Gompert, J. L. Feder, T. L. Parchman, N. P. Planidin, F. J. H. Whiting, P. Nosil, Adaptation repeatedly uses complex structural genomic variation. *Science* **388**, eadp3745 (2025). 10.1126/science.adp3745 Medline

77. Q. He, W. Li, Y. Miao, Y. Wang, N. Liu, J. Liu, T. Li, Y. Xiao, H. Zhang, Y. Wang, H. Liang, Y. Yun, S. Wang, Q. Sun, H. Wang, Z. Gong, H. Du, The near-complete genome assembly of hexaploid wild oat reveals its genome evolution and divergence with cultivated oats. *Nat. Plants* **10**, 2062–2078 (2024). 10.1038/s41477-024-01866-x Medline

78. P. Lou, S. Woody, K. Greenham, R. VanBuren, M. Colle, P. P. Edger, R. Sartor, Y. Zheng, N. Levendoski, J. Lim, C. So, B. Stoveken, T. Woody, J. Zhao, S.

Shen, R. M. Amasino, C. R. McClung, Genetic and genomic resources to study natural variation in *Brassica rapa*. *Plant Direct* **4**, e00285 (2020). 10.1002/pld3.285 Medline

79. D. Dimitrov, X. Xu, X. Su, N. Shrestha, Y. Liu, J. D. Kennedy, L. Lyu, D. Nogués-Bravo, J. Rosindell, Y. Yang, J. Fjeldså, J. Liu, B. Schmid, J. Fang, C. Rahbek, Z. Wang, Diversification of flowering plants in space and time. *Nat. Commun.* **14**, 7609–7625 (2023). 10.1038/s41467-023-43396-8 Medline

80. K. A. Simonin, A. B. Roddy, Genome downsizing, physiological novelty, and the global dominance of flowering plants. *PLOS Biol.* **16**, e2003706 (2018). 10.1371/journal.pbio.2003706 Medline

81. Z. Zhou, H. Feng, B. R. Zhou, R. Ghirlando, K. Hu, A. Zwolak, L. M. Miller Jenkins, H. Xiao, N. Tjandra, C. Wu, Y. Bai, Structural basis for recognition of centromere histone variant CenH3 by the chaperone Scm3. *Nature* **472**, 234–237 (2011). 10.1038/nature09854 Medline

82. J. Han, R. E. Masonbrink, W. Shan, F. Song, J. Zhang, W. Yu, K. Wang, Y. Wu, H. Tang, J. F. Wendel, K. Wang, Rapid proliferation and nucleolar organizer targeting centromeric retrotransposons in cotton. *Plant J.* **88**, 992–1005 (2016). 10.1111/tpj.13309 Medline

83. H. Cheng, G. T. Concepcion, X. Feng, H. Zhang, H. Li, Haplotype-resolved de novo assembly using phased assembly graphs with hifiasm. *Nat. Methods* **18**, 170–175 (2021). 10.1038/s41592-020-01056-5 Medline

84. M. Rautiainen, S. Nurk, B. P. Walenz, G. A. Logsdon, D. Porubsky, A. Rhie, E. E. Eichler, A. M. Phillippy, S. Koren, Telomere-to-telomere assembly of diploid chromosomes with Verkko. *Nat. Biotechnol.* **41**, 1474–1482 (2023). 10.1038/s41587-023-01662-6 Medline

85. H. Li, New strategies to improve minimap2 alignment accuracy. *Bioinformatics* **37**, 4572–4574 (2021). 10.1093/bioinformatics/btab705 Medline

86. X. Zeng, Z. Yi, X. Zhang, Y. Du, Y. Li, Z. Zhou, S. Chen, H. Zhao, S. Yang, Y. Wang, G. Chen, Chromosome-level scaffolding of haplotype-resolved assemblies using Hi-C data without reference genomes. *Nat. Plants* **10**, 1184–1200 (2024). 10.1038/s41477-024-01755-3 Medline

87. M. Goel, H. Sun, W. B. Jiao, K. Schneeberger, SyRI: Finding genomic rearrangements and local sequence differences from whole-genome assemblies. *Genome Biol.* **20**, 277–290 (2019). 10.1186/s13059-019-1911-0 Medline

88. J. Hu, Z. Wang, F. Liang, S. L. Liu, K. Ye, D. P. Wang, Nextpolish2: A repeat-aware polishing tool for genomes assembled using hifi long reads. *Genomics Proteomics Bioinformatics* **22**, qzad009 (2024). 10.1093/gpbjnl/qzad009 Medline

89. H. Li, Aligning sequence reads, clone sequences and assembly contigs with BWA-MEM. *Bioinformatics* **00**, 1–2 (2013). 10.48550/arXiv.1303.3997

90. H. Li, B. Handsaker, A. Wysoker, T. Fennell, J. Ruan, N. Homer, G. Marth, G. Abecasis, R. Durbin; 1000 Genome Project Data Processing Subgroup, The sequence alignment/map format and samtools. *Bioinformatics* **25**, 2078–2079 (2009). 10.1093/bioinformatics/btp352 Medline

91. J. Wolff, L. Rabbani, R. Gilsbach, G. Richard, T. Manke, R. Backofen, B. A. Grüning, Galaxy HiCExplorer 3: A web server for reproducible Hi-C, capture Hi-C and single-cell Hi-C data analysis, quality control and visualization. *Nucleic Acids Res.* **48** (W1), W177–W184 (2020). 10.1093/nar/gkaa220 Medline

92. H. Thorvaldsdóttir, J. T. Robinson, J. P. Mesirov, Integrative Genomics Viewer (IGV): High-performance genomics data visualization and exploration. *Brief. Bioinform.* **14**, 178–192 (2013). 10.1093/bib/bbs017 Medline

93. S. Ou, W. Su, Y. Liao, K. Chougule, J. R. A. Agda, A. J. Hellinga, C. S. B. Lugo, T. A. Elliott, D. Ware, T. Peterson, N. Jiang, C. N. Hirsch, M. B. Hufford, Benchmarking transposable element annotation methods for creation of a streamlined, comprehensive pipeline. *Genome Biol.* **20**, 275–293 (2019). 10.1186/s13059-019-1905-y Medline

94. A. Dobin, C. A. Davis, F. Schlesinger, J. Drenkow, C. Zaleski, S. Jha, P. Batut, M. Chaisson, T. R. Gingeras, STAR: Ultrafast universal RNA-seq aligner. *Bioinformatics* **29**, 15–21 (2013). 10.1093/bioinformatics/bts635 Medline

95. M. Pertea, D. Kim, G. M. Pertea, J. T. Leek, S. L. Salzberg, Transcript-level expression analysis of RNA-seq experiments with HISAT, StringTie and Ballgown. *Nat. Protoc.* **11**, 1650–1667 (2016). 10.1038/nprot.2016.095 Medline

96. J. Keilwagen, F. Hartung, J. Grau, GeMoMa: Homology-based gene prediction utilizing intron position conservation and RNA-seq data. *Methods Mol. Biol.* **1962**, 161–177 (2019). 10.1007/978-1-4939-9173-0_9 Medline

97. B. J. Haas, S. L. Salzberg, W. Zhu, M. Pertea, J. E. Allen, J. Orvis, O. White, C. R. Buell, J. R. Wortman, Automated eukaryotic gene structure annotation using EVidenceModeler and the Program to Assemble Spliced Alignments. *Genome Biol.* **9**, R7 (2008). 10.1186/gb-2008-9-1-r7 Medline

98. M. Goel, K. Schneeberger, plotsr: Visualizing structural similarities and rearrangements between multiple genomes. *Bioinformatics* **38**, 2922–2926 (2022). 10.1093/bioinformatics/btac196 Medline

99. Y. Zhang, T. Liu, C. A. Meyer, J. Eeckhoute, D. S. Johnson, B. E. Bernstein, C. Nusbaum, R. M. Myers, M. Brown, W. Li, X. S. Liu, Model-based analysis of ChIP-Seq (MACS). *Genome Biol.* **9**, R137 (2008). 10.1186/gb-2008-9-9-r137

Medline

100. Y. Zhang, J. Chu, H. Cheng, H. Li, De novo reconstruction of satellite repeat units from sequence data. *Genome Res.* **33**, 1994–2001 (2023). 10.1101/gr.278005.123 Medline

101. G. Pertea, M. Pertea, GFF utilities: Gffread and gffcompare. *F1000Res.* **9**, 304–323 (2020). 10.12688/f1000research.23297.1 Medline

102. D. M. Emms, S. Kelly, OrthoFinder: Phylogenetic orthology inference for comparative genomics. *Genome Biol.* **20**, 238–252 (2019). 10.1186/s13059-019-1832-y Medline

103. M. Smolka, L. F. Paulin, C. M. Grochowski, D. W. Horner, M. Mahmoud, S. Behera, E. Kalef-Ezra, M. Gandhi, K. Hong, D. Pehlivan, S. W. Scholz, C. M. B. Carvalho, C. Proukakis, F. J. Sedlazeck, Detection of mosaic and population-level structural variants with Sniffles2. *Nat. Biotechnol.* **42**, 1571–1580 (2024). 10.1038/s41587-023-02024-y Medline

104. T. Jiang, Y. Liu, Y. Jiang, J. Li, Y. Gao, Z. Cui, Y. Liu, B. Liu, Y. Wang, Long-read-based human genomic structural variation detection with cuteSV. *Genome Biol.* **21**, 189–213 (2020). 10.1186/s13059-020-02107-y Medline

105. L. Yin, H. Zhang, Z. Tang, J. Xu, D. Yin, Z. Zhang, X. Yuan, M. Zhu, S. Zhao, X. Li, X. Liu, rMVP: A memory-efficient, visualization-enhanced, and parallel-accelerated tool for genome-wide association study. *Genomics Proteomics Bioinformatics* **19**, 619–628 (2021). 10.1016/j.gpb.2020.10.007 Medline

106. Z. Yu, X. Chen, Y. Li, S. H. A. Shah, D. Xiao, J. Wang, X. Hou, T. Liu, Y. Li, ETHYLENE RESPONSE FACTOR 070 inhibits flowering in Pak-choi by indirectly impairing *BcLEAFY* expression. *Plant Physiol.* **195**, 986–1004 (2024). 10.1093/plphys/kiae021 Medline

107. W. Ma, Y. Liu, X. Wei, X. Zhang, X. Li, Z. Liu, L. Yuan, G. Li, J. Zhao, *Brassica rapa* pan-genome publication prerelease, Zenodo (2025); https://doi.org/10.5281/zenodo.17000216.

108. J. Thakur, J. Packiaraj, S. Henikoff, Sequence, chromatin and evolution of satellite DNA. *Int. J. Mol. Sci.* **22**, 4309–4337 (2021). 10.3390/ijms22094309 Medline